AD-A041 213 MICHIGAN UNIV ANN ARBOR DEPT OF ELECTRICAL AND COMPU--ETC F/G 9/1
INVESTIGATION OF INTERFEROMETRIC WAVEGUIDES.(U)
MAY 77 E N LEITH, G C KUNG, S K CASE N00014-67-A-0181-0058

UNCLASSIFIED NL

1 OF 2
AD A041213

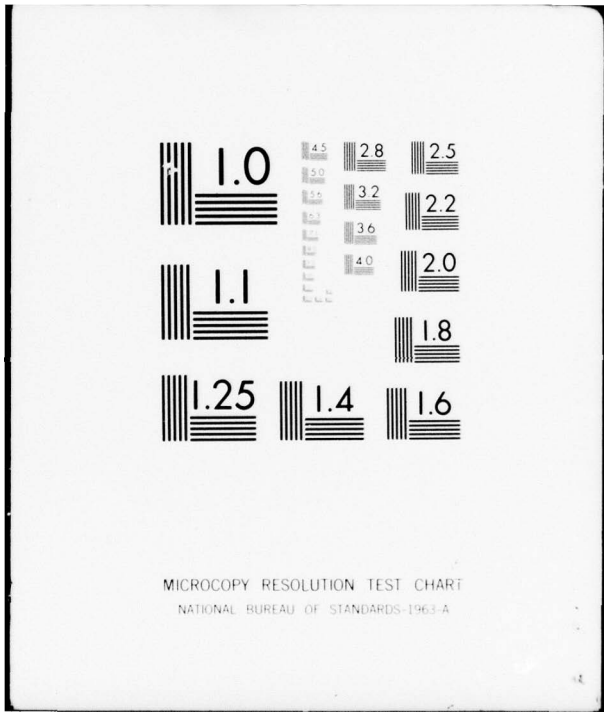
1.0
1.1
1.25
1.4
1.6
1.8
2.0
2.2
2.5
2.8
3.2
3.6
4.0
4.5
5.0
5.6
MICROCOPY RESOLUTION TEST CHART
NATIONAL BUREAU OF STANDARDS-1963-A

Report No. 2

Final Report

Investigation of Interferometric Waveguides

Period: April 1, 1974 - March 31, 1977

Contributors:

E. N. LEITH

G. KUNG

S. CASE

W. WANG

T. DILAURA

May 1977

Under contract with:
U. S. Department of the Navy
Office of Naval Research
Contract No. N00014-67-A-0181-0058
Arlington, Virginia

Department of Electrical and Computer Engineering
THE UNIVERSITY OF MICHIGAN 1817

UNCLASSIFIED

SECURITY CLASSIFICATION OF THIS PAGE *(When Data Entered)*

REPORT DOCUMENTATION PAGE

READ INSTRUCTIONS BEFORE COMPLETING FORM

1. REPORT NUMBER: 2
2. GOVT ACCESSION NO.:
3. RECIPIENT'S CATALOG NUMBER:

4. TITLE *(and Subtitle)*: Investigation of Interferometric Waveguides.

5. TYPE OF ~~REPORT & PERIOD COVERED~~: Final Rept. no. 2 (Final)
April 1974 — March 1977

6. ~~PERFORMING ORG. REPORT NUMBER~~:

7. AUTHOR(s): E. N. Leith, G. Kung, S. Case, W. Wang, T. DiLaura

8. CONTRACT OR GRANT NUMBER(s): N00014-67-A-0181-0058

9. ~~PERFORMING ORGANIZATION NAME AND ADDRESS~~:
The Regents of The University of Michigan
Ann Arbor, Michigan 48109

10. PROGRAM ELEMENT, PROJECT, TASK AREA & WORK UNIT NUMBERS:

11. CONTROLLING OFFICE NAME AND ADDRESS:
Office of Naval Research
Arlington, Virginia

12. REPORT DATE: May 1977

13. NUMBER OF PAGES: 126 + 129p.

14. MONITORING AGENCY NAME & ADDRESS *(if different from Controlling Office)*:
NEL, Arlington, Virginia

15. SECURITY CLASS. *(of this report)*: Unclassified

15a. DECLASSIFICATION/DOWNGRADING SCHEDULE:

16. DISTRIBUTION STATEMENT *(of this Report)*:

17. DISTRIBUTION STATEMENT *(of the abstract entered in Block 20, if different from Report)*:

18. SUPPLEMENTARY NOTES:

19. KEY WORDS *(Continue on reverse side if necessary and identify by block number)*:

Bragg Diffraction
Coupling
Waveguides
Interference

20. ABSTRACT *(Continue on reverse side if necessary and identify by block number)*:

The guiding of waves in interferometrically produced waveguides is investigated. A very general technique of analysis was developed. Computer calculations based on this approach were used to study leakage from guiding channels and the effect of pulse shape. Experimental devices were constructed. A new concept, modular optics, was conceived.

DD FORM 1 JAN 73 1473 EDITION OF 1 NOV 65 IS OBSOLETE

UNCLASSIFIED

SECURITY CLASSIFICATION OF THIS PAGE *(When Data Entered)*

TABLE OF CONTENTS

ABSTRACT

The guiding of waves in interferometrically produced waveguides is investigated. A very general technique of analysis was developed. Computer calculations based on this approach were used to study leakage from guiding channels and the effect of pulse shape. Experimental devices were constructed. A new concept, modular optics, was conceived.

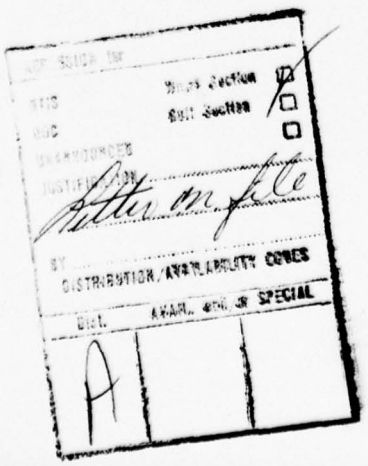

SUMMARY AND ACCOMPLISHMENTS

During the course of this contract, we pursued the following objectives, as stated in our plan of work in our initial proposal:

1. We will adapt the techniques of volume holography to the development of multichannel optical waveguiding structures. We will experiment with a number of the most successful materials, such as dichromated gelatin, thick plastics (e.g., polymethyl methacrylate, and various photopolymers.

2. We will develop methods for controlling the characteristics of these guiding channels through appropriate modulations of the interfacing beams. In particular, we will form cylindrical lenses within these channels, and will explore methods to permit these lenses to have focal lengths different for each channel.

3. We will develop methods for efficient coupling of light beams into these channels.

4. On the basis of what our studies indicate is realiziable, we will explore the feasibility of various forms of optical processing devices.

Some of these proved quite attainable, whereas others were found to be difficult and success was only partial. In addition, various new ideas, not anticipated in the original statement, but broadly falling within its scope, were conceived.

We list our various accomplishments, as they relate to the four items of our work plan.

Our principle effort was directed toward item 1. Our investigation of applying the techniques of volume holography to the development of multichannel guiding structures was done mostly on an analysis basis.

A major problem, recognized at the outset, was to find a theory to aid in the analysis of guiding in closely spaced channels having index profiles of the sort attainable with interferometric construction. Since the channels are to be constructed by recording interference fringes, and since the intensity profile is normally sinusoidal, we expect that the resulting channels will exhibit a sinusoidal index profile. The analysis of the waveguiding properties of such channels is not easy, and we felt that the conventional means were not very satisfactory. To this end, we developed a new and essentially different approach, which is highly versatile and quite simple to apply. This is the thin grating decomposition technique (hereafter, TGD) developed originally for analysis of diffraction from volume gratings, but readily adapted to the multichannel waveguide problem. This technique, as it applies to waveguiding, is described in appended paper No. 1, by Leith, et al.

We desired a theory which would, without more than a change of parameters,

describe both Bragg diffraction from thin gratings, and the guiding effects that occur with thick materials and high index modulations. We desired a theory that would describe the transition region, when partial guiding effects are observed, and which would also describe all the effects of the various elements that we wish to introduce into the guiding channels.

The TGD method fulfills all of these requirements, and we have used it extensively.

In our first report (Report No. 1, Annual Report, April 1974 - March 1975) we used the TGD method to examine leakage between channels and pulse shaping. The bulk of this work was published in Applied Optics; the paper is appended as paper No. 2.

This work has been continued, resulting in another paper, submitted for publication in Applied Optics (appended paper No. 3). We summarize the results of that paper as follows: We assumed a sinusoidal index profile throughout, and we generally assumed the input energy to have a shape, in the direction transverse to the channel, of one cycle of a sinusoid. We found that the index modulation required of the guiding structure to rise rapidly with decreasing channel spacing, being roughly quadratic in the region of 50-150 channel/mm, and to rise much more rapidly above 150/mm, so that as a practical matter channel densities above about 200/mm are not feasible.

We examined the guiding characteristics of various pulse profiles, other than the sinusoidal one previously noted. One interesting observation is that, regardless of the spatial width or shape of the input pulse, the output pulse tended to converge to one of sinusoidal profile matching in scale to that of the guiding channel, that is, if the channel profile is of the form

$$n = n_0 + n_1 \cos 2\pi \frac{x}{d}$$

where n_0 = averaged refractive index

n_1 = maximum deviation from n_0

d = channel periodicity

then the pulse profile, as a function propagation distance, tends to converge to

$$\tau(x) = \left(1 \quad \cos 2\pi \frac{x}{d}\right) \text{rect}\left(\frac{x}{d}\right)$$

This interesting phenomenon can be explained in terms of the basic mode equations for the sinusoidally profiled waveguide.

These are a few examples of results from our extensive study of guiding characteristics using the TGD method.

In addition to the theoretical study, we carried out a continuous experimental investigation of materials. We first used polymethyl methacrylate and various photopolymers, then tried dichromated gelatin. The latter is desirable because of the large refractive index changes that can be induced in it,

at least 10 X that inducible in polymethyl methacrylate. Dichromated gelatin, however, has its own special problem, the principle one being that samples of thickness greater than 50 to 100 microns are not feasible.

We first explored commercial plates which came in thicknesses of 15 to 30 microns. These were Kodak 649 photographic plates, and we prepared them for our purpose by removing the silver and sensitizing the gelatin with ammonium dichromate. This is a standard procedure. We then proceeded to prepare our own plates by mixing our own emulsion and applying it to glass plates. We could thus make gelatin films of any thickness we chose. This became a complicated experimental program; we had to cope with many problems, such as bonding of the gelatin to the substrate; drying of the gelatin without cracking or peeling, sensitizing the gelatin uniformly throughout its depth, and preparation of specimens which would remain bonded to the glass substrate throughout the entire procedure, including sensitization, development, washing, and drying.

Our goals were to try to form dichromated gelatin plates as thick as possible, while still achieving index modulation sufficient to produce waveguides. We succeeded in achieving thicknesses of about 50 microns while still achieving the required index modulation. This thickness is adequate for some of our purposes, but not for others.

The advancement of dichromated gelatin technology is a long-term project which is important to many of the activities of our laboratory. We expect our research efforts in this area to continue, with progress being rather gradual. Similarly, progress elsewhere is continuing, with gradual improvement in the technology.

Our effort on item 2 of the work plan was also extensive, although restricted to single channels.

Principally, we developed the concept of modular optics, which, while falling within the scope of that item, is we believe a worthwhile concept in its own right and goes beyond the scope of the work statement. This concept, stated briefly, is that one may form (in our case, interferometrically) optical elements of various sorts which can be attached by index-matching fluid coupling to a slab waveguide whereupon a guided wave is pulled out of the slab, is operated upon by the modular element, and then in its modified form is coupled back into the waveguide.

The modular element can be a beam splitter, a lens, a mode converter, or any other element that can be fabricated as an integrated optics structure. In this manner optical systems can be constructed that are in fact integrated optics systems, having the ruggedness, stability, and compactness of such systems, but also having the adjustability of conventional optical systems.

This concept has been disclosed in a patent application, and at present, four papers have been published or submitted on various aspects of this concept. To date, we have constructed a modular optics interferometer, and a double mode coupler.

On the third item of the work plan, the coupling into the guides, we made considerable progress. Of course, the modular optics devices just cited, come under this item also. In addition, we conceived a technique for producing a high efficiency grating coupler within the waveguide. We analyzed this structure using the TGD method, and found from computer analyses that the coupling efficiency could be high, nearly 100%. This work is described in the appended paper by Wang & DiLaura, submitted to Applied Optics.

At the basis of all of our analysis is the TGD method. Developed by Alferness to analyze third transmission gratings, the scope of its applicability has subsequently been enlarged, having been used to analyze grating couplers, reflection gratings, diffraction at the third Bragg angle of non-linear grating, and distributed feedback lasers where the modulation index of the active medium varies sinusoidally rather than in discrete steps.

Finally, much of our device analysis falls within the scope of item 4, the final item, of our work plan.

A total of 11 papers were proposed for publication from work supported either entirely or in part by this grant. Five of these are now in print and the remaining six are pending. In addition, two doctoral dissertations (G. Kung and W. Wang) were supported by this work. The papers are presented in the Appendix.

The principle obstacle to the fullest realization of our objectives is the materials problem; materials having the ideal characteristics (i.e., very thick, high transmittance before development for the exposed stage) and high index modulation are not available. We therefore (a) worked within the materials limitation; (b) performed, on a modest scale, materials development; and (c) carried out analysis and design on the basis of material characteristics not yet available. In addition, some of our results (i.e., the TGD analysis and the modular optics technique) have, we believe, import well beyond the scope of our grant objectives.

APPENDIX

PAPERS PREPARED WITH SUPPORT FROM THIS CONTRACT

THICK GRATING ANALYSIS OF INTERFEROMETRICALLY PRODUCED WAVEGUIDES

E. LEITH, G. KUNG, R. ALFERNESS and B. HANSCHE
Dept. of Electrical and Comp. Engineering, University of Michigan, Ann Arbor, Michigan, USA

Received 18 February 1975, revised manuscript received 10 April 1975

The thin-grating decomposition method of thick grating analysis is used to analyze guiding effects in thick phase gratings having sinusoidal refractive index modulation.

Interferometrically-produced phase gratings can be used as wave-guiding structures, as demonstrated by Rosenberg and Chandross [1]. Rosenberg gives an analysis of this phenomenon by ray tracing methods [2]. We note that the structure that produces Bragg diffraction is the same one that produces guiding, except that for guiding to be manifested, both the thickness and index modulation must be relatively large. We also note that the basic Bragg diffraction equation and the basic equation describing guiding in a slab waveguide are similar. We have therefore sought a single analysis, preferably a grating analysis based on physical optics, that describes both phenomena, and that will give insight into the transition region, when, with increasing refractive index modulation, the Bragg diffraction process produces confinement.

In the diffraction process, a plane wave impinges on the thick grating at the Bragg angle (fig. 1). When the wave enters the structure, a diffracted wave is formed; as the two waves propagate through the structure, there is a continuing exchange of energy between them. Continuing with this heuristic approach, we expect that when most or all of the energy in a plane wave is reflected from the first Bragg plane encountered, energy initially contained between two Bragg planes is confined between these planes until the wave emerges from the structure. Unfortunately, the usual analyses for diffraction from thick gratings assume uniform plane waves. The analyses predict the intensity of the emerging waves, but give no insight into the paths that the light traveled. In addition, the closed-form solutions are restrictive;

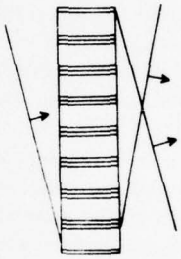

Fig. 1. Sinusoidal thick grating, showing incident and diffracted waves.

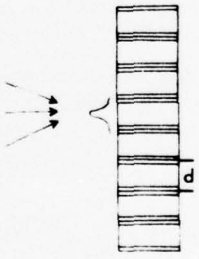

Fig. 2. Spatial light pulse incident on grating surface.

Kogelnik's coupled wave analysis [3], for example, allows for only two plane waves, and these must each be at or near the Bragg angles. We require an analysis that enables us to propagate a small spot of light (a spatial pulse) through the structure.

Alferness [4] has described an extremely general method, which allows the plane waves to be incident at any angle. It is, however, a plane-wave analysis, but it can be modified for our requirement. This method is called the thin grating decomposition method, and is conceptually quite simple, yet in all tests

that have been made, both by way of experiment and by comparison with special cases that can be analysed by other methods, the Alferness method has proved accurate. The method involves decomposing a thick grating into a stack of thin gratings, each of which is sufficiently thin that thin grating theory holds. Each thin grating diffracts the incident plane waves into various orders, depending on the grating structure. These diffracted waves are the input for the next thin layer. Typically, the decomposition involves about 30 to 100 thin gratings; thus, the analysis requires a computer.

In our procedure (fig. 2), a spatial pulse impinges on the source-side surface of the grating. The pulse is Fourier-decomposed into a spectrum of plane waves at various angles. The Alferness theory permits us to propagate each one through the structure, and to combine all of the emerging waves, both direct and diffracted, to find the resultant intensity distribution.

Since for calculational purposes we are restricted to a finite number of plane waves, we should choose an amplitude profile for the pulse which is not only realistic, but which can also be described without an excessive number of components. A suitable waveform is

$$f(x) = (\tfrac{1}{2} + \tfrac{1}{2}\cos 2\pi x/d)\ \mathrm{rect}\ x/d\ , \qquad (1)$$

where d is the grating period, and rect $x/d = 1$ for $|x| \leqslant \frac{1}{2}\,d$, and is zero otherwise. This waveform has the advantage that not only is it confined between the limits $|x| = \frac{1}{2}\,d$, but also that its spatial-frequency spectrum

$$F(f_x) = \tfrac{1}{2}\,d\ \mathrm{sinc}\ df_x + \tfrac{1}{4}\,d\ \mathrm{sinc}\ d(f_x + 1/d) + \tfrac{1}{4}\,d\ \mathrm{sinc}\ d(f_x - 1/d)\ , \qquad (2)$$

is very nearly confined between the values $f_x = 2/d$. [Note that sinc $x = (\sin \pi x)/\pi x$].

We sample this spectrum at intervals $1/Pd$, giving $4P - 1$ samples between the limits $\pm 2/d$ (fig. 3), giving a sampled spectrum

$$F_s(f_x) = F(f_x)\ \mathrm{comb}\ Pdf_x\ , \qquad (3)$$

where comb $af_x = \Sigma\,\delta(f_x - n/a)$ and δ is the Dirac delta function. The sampling results in a modified input function

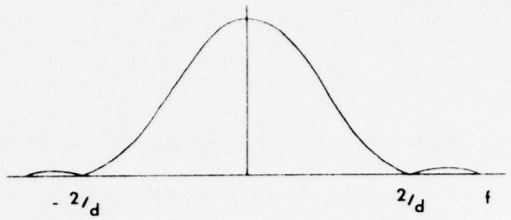

Fig. 3. Spatial frequency spectrum of pulse. Only the envelope is shown; 63 discrete frequencies reside under the envelope.

$$f_s(x) = [(\tfrac{1}{2} + \tfrac{1}{2}\cos 2\pi x/d)\ \mathrm{rect}\ x/d] * \mathrm{comb}\ x/Pd = \sum_{-2P}^{2P} a_n \cos 2\pi n x/d\ . \qquad (4)$$

This function, being composed of a finite number of harmonically-related spatial frequencies, thus physically corresponds to a set of $4P - 1$ plane waves, with incidence angles $\theta = \sin^{-1} n\lambda/d$. These we propagate through the grating structure, using the Alferness method. Some of these components satisfy nearly or exactly the Bragg condition and produce diffracted waves at the output; others do not. At the output plane, or exiting surface, all incident components, along with the new components generated by diffraction, are combined, thus forming the output waveform.

Some precautions should be observed in designing the experiment. The sampling process forms a periodic function f_s from the single pulse f; thus, the input is a sequence of pulses of the form f, separated by intervals Pd. We should choose P sufficiently large, i.e., take sufficient samples, that, over the propagation distance, the pulse spreading due to diffraction does not result in an overlap of adjacent pulses. The greater the number of samples, $4P - 1$, the greater the separation distance between pulses.

The calculated results are shown in fig. 4. We have assumed a grating with a sinusoidal variation of refractive index, with index variation along the x direction only (the unslanted fringe case). The pertinent parameters are: grating spacing $d = 1/100$ mm, grating thickness = 0.54 mm, wavelength $\lambda = 6328$ Å, and a refractive index of 1.50. The program broke this into 18 thin gratings of thickness 0.03 mm; such gratings satisfy Kogelnik's Q-factor criterion for a thin grating [3]. The output pulse is shown in a to d for various

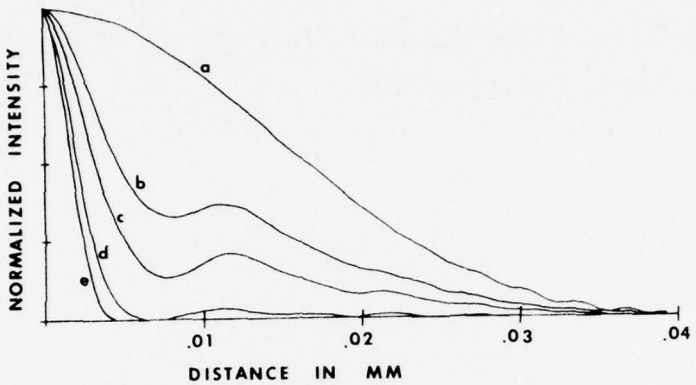

Fig. 4. Intensity distribution at output surface, for various values of Δn: (a) $\Delta n = 0$ (no grating); (b) $\Delta n = 10^{-4}$; (c) $\Delta n = 2 \times 10^{-4}$; (d) $\Delta n = 6 \times 10^{-4}$; (e) pulse incident at input surface.

index variations. Curve e shows, for comparison, the incident pulse. Curve a shows the output pulse for $\Delta n = 0$; this is just the diffraction spreading that occurs in the absence of a grating. Curve b, c, and d show the output for increasing values of Δn; as Δn increases, the pulse becomes increasingly confined. However, the greatest confinement appears to be of the energy that, in the absence of the grating structure, falls in the middle regions of the spread-out pulse. The energy in the outer portions, corresponding to the most oblique plane wave components, shows a lesser tendency to confinement.

The plane waves satisfying the Bragg condition are represented by the spatial frequency components $\pm 1/2d$, which is only $\frac{1}{4}$ of the maximum spatial frequency $2/d$. Also, we note that the value of Δn reported by Rosenberg and Chandross in their experiments was 6.4×10^{-4}; this is close to the value of Δn (6×10^{-4}) for which our curves show nearly complete wave confinement. Finally, we observe that thinner structures, such as dichromated gelatin, produce refractive index changes up to two orders of magnitude greater than those considered here. Thus, when spatial frequencies on the order of a few hundred cycles/mm are recorded, the guiding conditions are generally satisfied, even though the guiding effects are not observable, since the propagation distances are too short to reveal this phenomenon.

We thank the Office of Naval Research for their support of this work (contract number N 00014-67-A-0181-0058).

References

[1] R.L. Rosenberg and E.A. Chandross, Appl. Opt. 10 (1971) 1986.
[2] R.L. Rosenberg, J. Opt. Soc. Am. 62 (1972) 1175.
[3] H. Kogelnik, Bell. Syst. Techn. J. 48 (1969) 2909.
[4] R.C. Alferness, Appl. Phys., in press.

Propagation of spatial pulses in interferometrically produced guiding structures

G. C. Kung and E. N. Leith

Image transfer properties of interferometrically produced dielectric light guides are investigated. A general technique of analysis is developed. Computer calculations based on this approach are used to study the behavior of pulses traversing the guiding structures for various values of refractive index. Experimental results are obtained using photosensitized polymethyl methacrylate as the recording material. Computer results are compared with existing theory and found to be in close agreement.

Introduction

Optical wave confinement in dielectric slabs bordered by materials of lower refractive index has been widely treated. The general treatment of optical slab waveguides is usually based on the assumption that the cladding, the material of lower refractive index, extends to infinity. If several slab waveguides are placed parallel to one another in space, the assumption is usually made that the cladding is sufficiently thick that the presence of one guide does not distort the field of others, and there is thus no interaction between the waveguides. This is the treatment introduced by Tien.[1] However, in many practical cases, the assumption that parallel slab waveguides are independent of one another cannot be made; such waveguides must be considered to be coupled. This is the case when the slab waveguides are in close proximity and especially when there exists no discrete boundary between adjacent waveguides, as occurs when they are formed by recording of interference fringes in a thick dielectric medium. The coupled wave equations for this case become so unmanageably complicated that a different approach is in order.[2] A ray optics approach was used by Rosenberg in his analysis of the interferometrically produced fiber optics structures produced by Rosenberg and Chandross.[3,4]

Evidently, an array of slab waveguides formed in this manner can equally well be regarded as a volume phase grating, and we should expect that the various analyses that have been given for diffraction from volume gratings produced by recording interference fringes should also describe image transfer effects manifested by these gratings. We aim to develop a general theory that could, by no more than a change of parameters, describe Bragg diffraction, the image transfer effects that occur with sufficiently high index modulation, and the transition case where, with increasing index modulation, the Bragg diffraction effect becomes an image transfer or guiding effect.

Method of Analysis

We have adapted the thin-grating decomposition method of Alferness to the analysis of guiding in interferometrically formed slab waveguides.[5,6] This method is conceptually quite simple, yet it gives results that agree exactly with those of more complex theories such as given by Burckhardt,[7] Kogelnik,[8] and Kaspar.[9] The method consists of decomposing a thick grating into a stacked array of thin gratings and treating each thin grating component in terms of the well known thin phase grating theory. The diffracted orders of the ith thin grating forms the incident waves of the $i + 1$th thin grating. This process is continued until we reach the final plane, where the various plane waves emerge as the diffracted orders of the thick grating. These waves are just the ones that satisfy the Bragg angles, although no Bragg diffraction considerations were explicitly inserted into the theory. The various diffracted orders that do not satisfy the Bragg condition simply average to values near zero.

We have modified the Alferness method by using a narrow distribution of light (a spatial pulse) as the incident field (Fig. 1). We decompose this pulse into a spectrum of plane waves and propagate each one independently through the structure; each wave generates various diffracted orders. All waves are then

The authors are with the University of Michigan, Ann Arbor, Michigan 48107.

Received 3 June 1975.

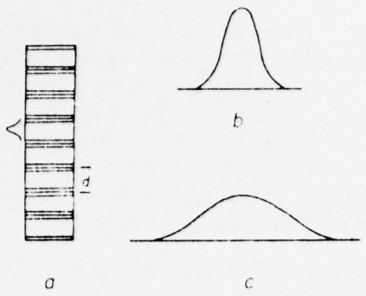

Fig. 1. Propagation of a pulse of light through a thick grating: (a) shows the grating structure, with spacing d; (b) shows the input pulse; and (c) shows the pulse emerging from the other surface.

summed at the output surface to yield the resultant intensity distribution. The theory as used here involves the same assumptions and conditions as imposed by Alferness. The polarization is with the E vector parallel to the surface of the recording material, and the diffracted waves are summed coherently at each successive thin grating, with the assumption of no polarization changes, following the earlier treatments of Burckhardt and Kogelnik. The intensity at the exiting plane is calculated without regard to propagation direction.

Although the method is not restricted to any specific profile of input pulse, we have assumed one with amplitude of the form

$$f(x) = \tfrac{1}{2}(1 + \cos 2\pi x/\sigma d)\ \mathrm{rect}\, x/\sigma d, \qquad (1)$$

where d is the grating period (10^{-2} mm in this paper), and σ is a constant that adjusts the width of the input pulse. Not only is this pulse spatially bounded, its spatial frequency spectrum is also nearly bounded. For computational purposes, we truncate the spectrum at $f_x = \pm 2/\sigma d$, thus ignoring the small secondary lobes lying outside this bound. This leads to only very small errors in the results because the secondary lobes are of the order of 10^{-3} that of the peak, as shown in Fig. 2. In our analysis, we represent $f(x)$ by a Fourier series; each term of the series represents a plane wave that we can propagate through the grating. This Fourier series representation results in additional pulses $f(x - nP)$, where P is the period of the fundamental component of the Fourier series. We must choose P sufficiently large, i.e., take many samples of the spectrum of $f(x)$ so that the various input pulses remain sufficiently separated that they do not interact as they travel through the grating.

A computer program developed by Alferness for his thin grating decomposition analysis was modified for the study of image transfer effects. The computer program, which assumes unslanted fringes and a sinusoidal variation of refractive index, allows for adjustment of input pulse width and grating thickness, lateral positioning of the input pulse, selection of refractive index modulation n_1, and adjustment of the grating period. The pulse spectrum is computed and sampled; each sample represents a plane wave. We can select the number of samples; the more we choose, the greater the separation of adjacent incident pulses and the thicker the grating that can be treated without errors from interaction between adjacent pulses. We can also choose the number of thin gratings into which the thick grating is decomposed. We follow two general guidelines in choosing the number of plane wave samples: the thickness of the thin gratings and the number of diffracted orders to be retained from each thin grating. First, the presence of fine oscillation patterns at the edges of the spreadout pulse indicates that adjacent pulses are interfering with each other, and therefore more plane wave samples are needed. The beginning of such overlap is evident in Fig. 3, curve a. Second, the total energy at the input and output planes should be conserved; conservation failure indicates that thinner sections are needed or that more diffracted orders should be kept. Throughout our analysis, we keep five diffracted orders (0, ±1, ±2 orders) and use a thin grating thickness of 0.03 mm. These values are generally adequate for index modulation n_1 up to 0.0015.

Computed Results

Using the theory thus developed, we have computed the behavior of pulses traversing the guiding structure. Figure 3 shows, for a representative configuration, the result of increasing the index modula-

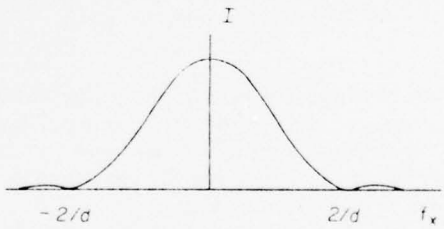

Fig. 2. Spatial frequency spectrum of the pulse. I is irradiance.

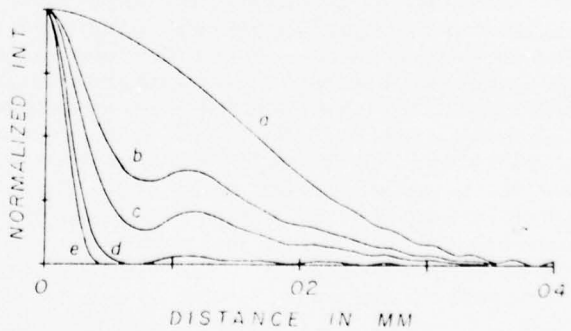

Fig. 3. Intensity distribution at output surface for various values of n_1: (a) $n_1 = 0$; (b) $n_1 = 10^{-4}$; (c) $n_1 = 2 \times 10^{-4}$; (d) $n_1 = 6 \times 10^{-4}$; (e) pulse incident at input surface. Grating thickness = 0.54 mm.

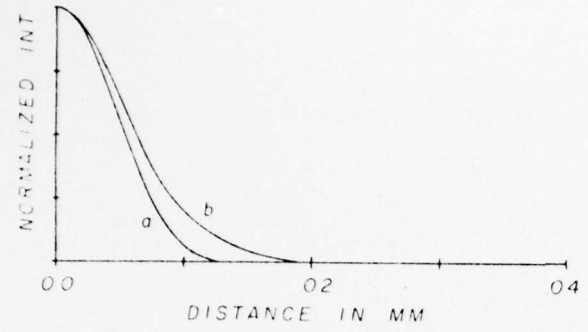

Fig. 4. Same as Fig. 3, except for a pulse width of 0.03 mm: (a) shows the incident pulse; (b) shows the output pulse for $n_1 = 0$.

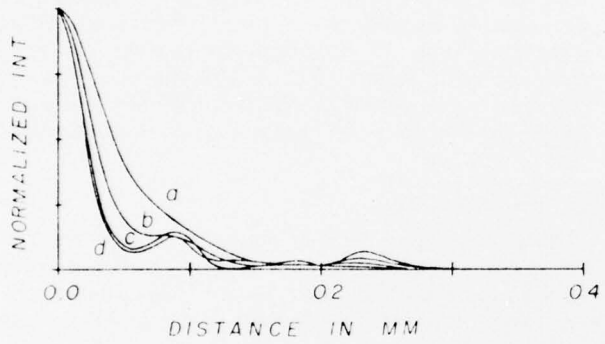

Fig. 5. Continuation of Fig. 4, showing output pulse for various values of n_1: (a) $n_1 = 10^{-4}$; (b) $n_1 = 3 \times 10^{-4}$; (c) $n_1 = 6 \times 10^{-4}$; (d) $n_1 = 10^{-3}$.

tion. As the index increases, the pulse width at the output approaches in width the input pulse, and the energy in adjacent channels diminishes. In Fig. 3, as well as in succeeding figures, the regions of maximum index are at 0, ±0.01 mm, etc.

Repeating the same experiment with increased pulse width produces the results shown in Figs. 4 and 5. The pulse width is now 0.03 mm, so that a portion of the pulse extends over the boundaries into adjacent channels. As n_1 increases, the output pulse is reshaped, dividing into several pulses occupying several adjacent channels, much as if the pulse, like an incompressible fluid, were being pressed into a mold, although it is seen that the reshaped energy distribution does not exactly conform to the mold. We note that the energy distribution in the various channels is not always centered at the center of the channel, which we take to be the points of maximum index, occurring at 0, 0.01, 0.02, . . . mm; such asymmetry is related to the asymmetry of the impressed irradiance across each channel input. Finally, we note that, despite the over-all confinement of energy to those channels upon which the energy was incident, there is, with increasing n_1, an increasing amount of energy in the outer channels, whereas, for $n_1 = 0$, there is negligible energy in this region.

Next we try a pulse of 0.005-mm width, which is half of the width of the guiding channels. Figure 6 shows the sequence at the output as a function of n_1. For sufficiently large n_1, the pulse width converges again, as in Fig. 3, to that of the input pulse. This result is representative of our findings; for a pulse narrower than a channel width, the output pulse width converges, with increasing n_1, to that of the input.

If the pulse is introduced at a position displaced from the center of a channel, the confinement decreases; the losses are greatest when the pulse is centered at a point of minimum index (Fig. 7). The dynamics of the off-centered pulse are further shown in Fig. 8, which traces the course of such a pulse. The pulse, as it progresses through the guiding structure, oscillates from one side of the channel to the other. As the pulse swings to one extreme, some energy surges across the refractive index barrier into the adjacent channel; this energy produces in that channel a propagating, laterally oscillating pulse, which in turn impels some of its energy into the next adjacent channel.

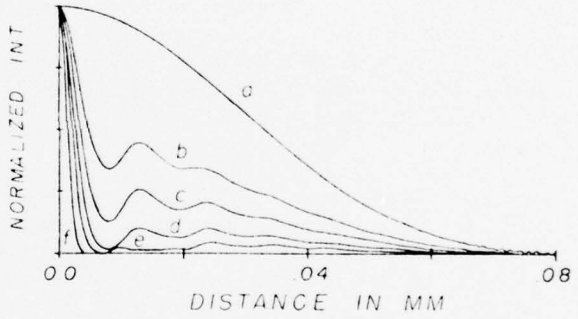

Fig. 6. Same as Fig. 4, except for a pulse width of 0.005 nm: (a) $n_1 = 0$; (b) $n_1 = 10^{-4}$; (c) $n_1 = 2 \times 10^{-4}$; (d) $n_1 = 4 \times 10^{-4}$; (e) $n_1 = 8 \times 10^{-4}$; (f) $n_1 = 2 \times 10^{-3}$.

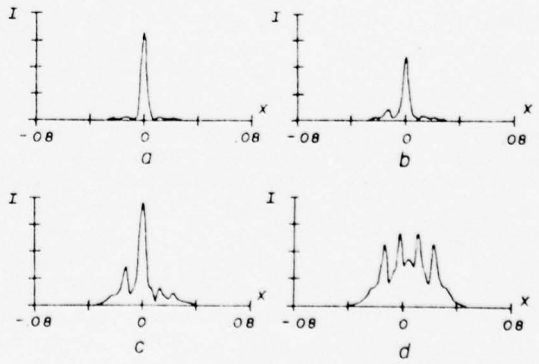

Fig. 7. Effect of introducing the pulse at an off-centered position: pulse width = 0.01; $n_1 = 6 \times 10^{-4}$; thickness = 0.54 mm. Displacement from center: (a) 0; (b) 0.002 mm; (c) 0.003 mm; (d) 0.005 mm. Vertical scale doubled for (c) and (d). Vertical scale is intensity, horizontal scale (x) is off-center displacement in mm.

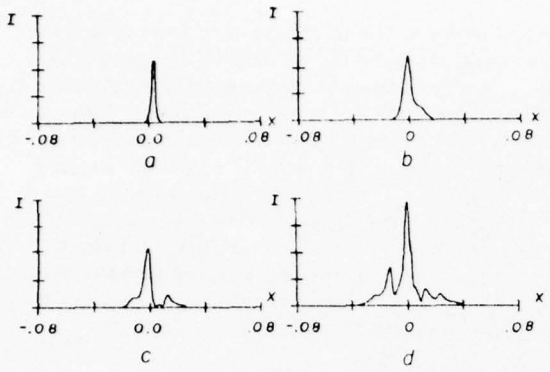

Fig. 8. Tracing an off-center input pulse through the guiding channel. Displacement at incidence, 0.003 mm; pulse width = 0.01 mm; $n_1 = 6 \times 10^{-4}$. I is intensity, x is displacement in mm. Depth at observation plane is (a) 0, (b) 0.18 mm, (c) 0.36 mm, (d) 0.54 mm.

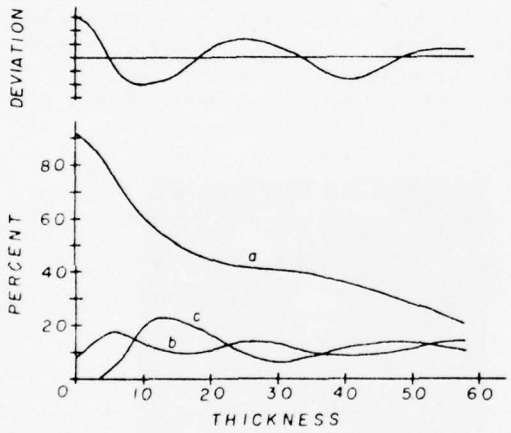

Fig. 9. Energy transfer between channels. The lower curve shows the percent decrease in energy in various channels with propagation distance: (a) is for channel 0 (the channel where the pulse was introduced); (b) is for the +1 channel; and (c) is for the −1 channel. Shown at the top, for reference, is the deviation of the pulse from the channel center.

The curves of Fig. 9 show that the greatest rate of energy flow into the adjacent channels occurs between the positions when the pulse has crossed the center of the channel and when the pulse reaches its maximum off-center displacement. The energy flow into the two channels adjacent to the 0th channel (the one where the pulse was introduced) is asymmetrical. Most notably, the energy buildup in the channel opposite to the direction of initial pulse displacement (the −1 channel) receives a bigger initial surge of energy than does the other (the +1 channel), evidently because the surge of energy into the +1 channel is aborted by the introduction of the pulse at a phase (maximum displacement) just past the position of maximum energy flow. Figure 10 shows the energy flow into other channels. In general, the pattern is the same as for the flow into the ±1 channels, and the previous observations apply. For comparison, we plot (Fig. 11) the energy flow out of the 0th channel for the case where the pulse is introduced at the channel center, the refractive index maximum. As expected, the energy loss is less oscillatory, although a transient occurs at the beginning. Also, the energy leakage is significantly lower.

Experimental Results

Experimental data supporting in a qualitative way some of the calculated results were obtained by preparing polymethylmethacrylate (PMM) casting sensitized with *p*-benzo quinone; at present we do not have sufficient control over the experimental process to produce quantitative results. Using the 0.488-μm line of the argon laser, unslanted fringes of 100-l/mm spatial frequency were recorded in 0.5-mm thick specimens. To demonstrate image transfer characteristics, scratches approximately parallel to the fringes were made on one face. The PMM was then illuminated with a green light of about 500 Å in spectral width, with the light impinging on the scratched

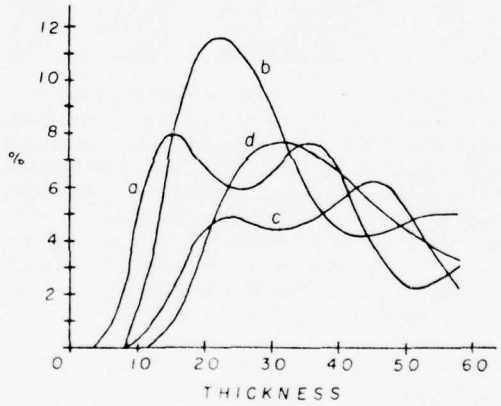

Fig. 10. Energy flow into other channels, showing energy in each channel as percent of incident energy: (a) is +2 channel; (b) is −2 channel; (c) is +3 channel; (d) is −3 channel.

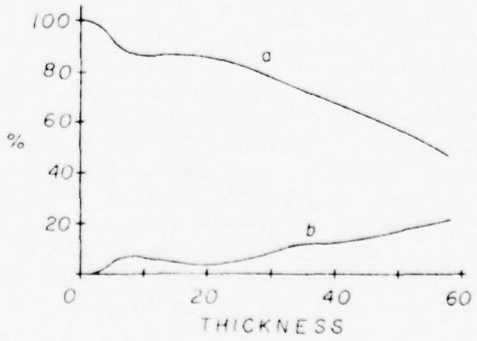

Fig. 11. Energy loss when the input pulse is introduced at the channel center: (a) shows the percent energy loss from channel 0; (b) shows the energy in the +1 or −1 channels.

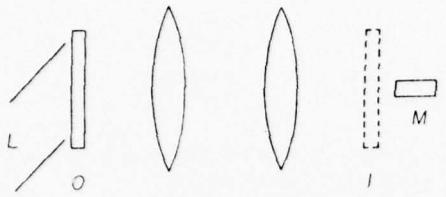

Fig. 12. Optical setup for observing guiding effects. 0 is the object, a PMM grating with scratches inscribed on the left surface. L is a light beam, introduced obliquely so that no direct light propagates through the system. I is the image of the PMM, and M is a microscope, which can be focused onto any part of the image.

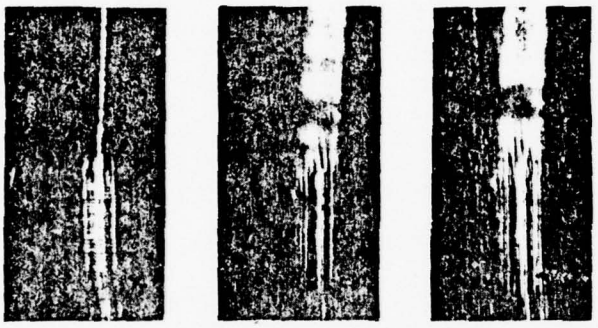

Fig. 13. Experimental results. The microscope is focused on a scratch at the incident surface. The upper portion of the photograph shows the scratch in sharp focus; in this region, no grating is recorded on the PMM. In the lower portion, the scratch is out of focus due to the presence of the grating waveguide. In the center, the microscope was focused on the exiting surface; here, in the region of the recorded grating, the pulse is sharply focused, thus demonstrating a strong guiding effect. At the right is the same image, overexposed so as to emphasize the side-lobes, i.e., the energy that has crept into other channels.

surface. This illumination was introduced obliquely, so that only scattered light entered the imaging system (Fig. 12). The recording camera could be focused on either the source or the observer side of the PMM. Results are shown in Fig. 13 (which is cropped to show only one scratch). At the left, the camera was focused on the source side. The recorded fringes are confined to the lower portion; thus, at the top, the scratches are clearly observed. In the center is shown the same image, but with the focus on the surface toward the observer, where a strong guiding effect is evident. The intensity irregularities result from nonuniformity of the scratch. At the right is the same image, using greater exposure on the recording film so as to emphasize the secondary or side-lobe structure of the image. The lobing region is of the same width as the unfocused beam, with the outer lobes being somewhat more intense than the inner ones.

Since the scratch is not accurately parallel to the recorded fringes, there is a continuous displacement as a function of the vertical coordinate between the input pulse and the guiding channels; this causes the pulse periodically to shift channels. This effect is shown in more detail in the magnified image of Fig. 14. Note that beginning at the center and continuing downward somewhat, the beam evidently falls in a region of lowest index (i.e., straddles the channels), and the light at the output is split between the two adjacent channels. The results of Fig. 14 were produced by imaging, using a He–Ne laser, a narrow slit onto the source-side surface of the PMM, and the recording camera focusing on the surface toward the observer. The result is essentially no different from the scratch method used for the previous results.

Comparison with Previous Results

Rosenberg, using a ray tracing analysis, has computed the efficiency of image transfer in interferometrically produced fiber optics structures.[3] Figure 4 of Ref. 3 shows guiding efficiency as a function of vertex angles of incident cones of light. However, there are two major differences between his case and ours. First, we treat only one-dimensional guiding structures, i.e., guiding slabs, whereas Rosenberg analyzes the properties of guiding columns. Second, our incident irradiance is a narrow pulse, having most of its energy concentrated at the middle of the guid-

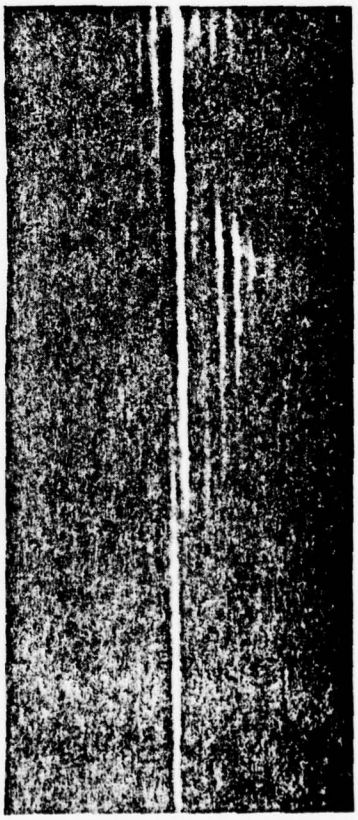

Fig. 14. Guiding of a slit image focused onto the PMM surface. The slit image is slightly nonparallel with the grating fringes. Somewhat below the middle, the pulse crosses over the channel boundary and is split into two nearly equal portions.

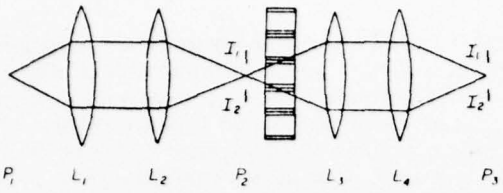

Fig. 15. Optical system for observing diffraction splitting. I_1 and I_2 are the broadened first order diffracted images. P_1 is the source plane. Source is imaged onto P_2 and finally onto P_3.

ing channel, where the guiding efficiency is highest, whereas Rosenberg considers rays of equal intensity in various directions. We define guiding efficiency as the percent of incident light that remains in the 0th channel after propagating through the guiding structure. For comparison of our results with Rosenberg's, we choose parameters identical to those of Rosenberg; we choose Δn ($= 2n_1$) = 0.0006, thickness of the guiding structure = 1.1 mm, and fringe spatial frequency = 100 l/mm.

From our computer result, we find that the guiding efficiency of a 0.01-mm wide pulse in the form of Eq. (1) is 42%. Since the spectral distribution of our pulse is not uniform, we cannot directly compare our result to that of Rosenberg. From the spectrum of our input pulse, we determine that 12% of the total energy lies between a wedge of 0.3°, 11.5% more lies within 0.6°, 11.2% more within 0.9°, 10.6% more within 1.2°, and so on. From the guiding efficiency curve of Rosenberg, we can estimate the guiding efficiency for the input irradiance lying within the various wedges. Multiplying these efficiencies by the percent of total input energy, we estimate the over-all guiding efficiency to be 45%, which is in close agreement with the result predicted by our analysis.

Diffracted Order Splitting

Another verification of the validity of the thin grating decomposition analysis is its success in predicting a phenomenon that is the optical counterpart of a well-known x-ray diffraction effect predicted by Kato[10]; namely, a plane wave incident at or near the Bragg angle of a sinusoidally stratified structure splits into four plane waves. We report some additional observations. Instead of using a narrow beam incident at the Bragg angle, as Forshaw[11] did, we illuminated the PMM sample by a spatially incoherent slit source with a beam divergence such as to include rays satisfying the Bragg condition for both first orders. The slit image was formed about 1 mm in front of the PMM surface. We then made observations on the slit image.

The experimental setup is shown in Fig. 15. The slit source was produced by a He–Ne laser beam passing through a rotating ground glass placed in front of a slit aligned parallel to the grating fringes. A unity magnification imaging system consisting of a lens pair L_1, L_2 was used to image the slit into the vicinity of the PMM. A second lens pair L_3,L_4 reimaged the PMM and slit image, and this final image was observed with a microscope, which could be focused on any plane in the vicinity of the PMM and slit images.

We illuminated first an area of the PMM sample on which interference fringes of low index modulation were recorded and which produced weak diffraction. We observed that the first order diffracted beams, as observed in the plane of the slit image, appeared as two uniform bands of light. As we changed the distance between the PMM plate and the slit image, while keeping the microscope focused on the slit image, the form of the light distribution remained the same, except for the increase in distance between the diffracted orders. For small source-plate distances, the orders overlapped; our observations here apply to distances sufficiently large that the orders are distinctly separated.

A simple model that explains the observed effects is shown in Fig. 16. The rays that satisfy the Bragg angle produce diffraction as they propagate through the plate. Rays diffracted at different planes in depth produce diffraction with different displacements from the zero order. For the weak diffraction exhibited by this exposure, the zero order is negligibly attenuated as it propagates through the plate, and subsequent diffraction produced by the diffracted waves is also negligible. These assumptions imply a uniform intensity distribution across the diffracted order, just as is observed. The width and position of the diffracted orders were measured and found to be just as predicted by this simple model.

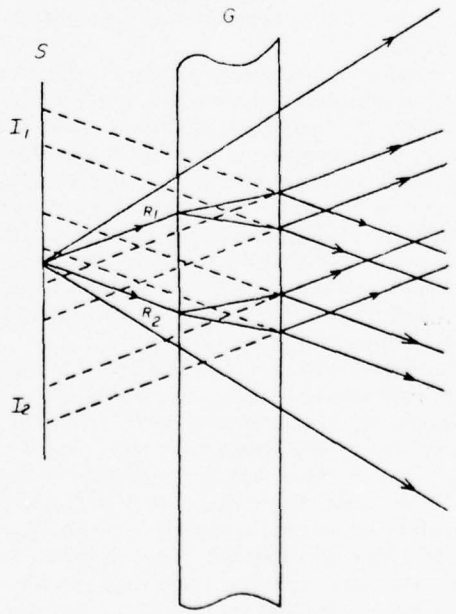

Fig. 16. Model for describing broadening of diffracted orders. R_1 and R_2 are the rays at the Bragg angle, I_1 and I_2 are the first diffracted orders. S is the plane of the source image, G is the grating.

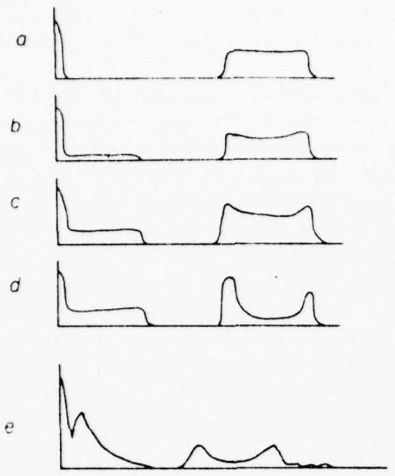

Fig. 17. Light distribution at the plane of Fraunhofer diffraction. (P_1 of Fig. 15), showing zero order (left) and one first order. Curves a to d represent increasing index modulation; e is a computer calculation for $n_1 = 0.0007$.

Illuminating regions of the PMM having larger index modulations, we observed that the images of the diffracted orders developed peaks at the edges (Fig. 17); also, a band of light appeared in the vicinity of the zero orders. These are the effects predicted by Kato. The latter can be explained as being produced by a secondary diffraction, whereby the light in the first order is rediffracted back into the zero order. The migration of first order light to the edges of the pattern is less easily explained in terms of an intuitive approach.

The computer analysis predicts exactly these results. The computer results also predict the width and position of the diffracted orders. However, the computer predicts symmetry about the center of the grating, whereas experimental results show an asymmetry that we presume is due to the absorption in the PMM; the absorption loss is about 30%. We find it quite interesting that an analysis based on nothing more than a continuing iteration of the quite simple thin grating diffraction theory should so readily predict these rather subtle effects.

If we observe planes other than the source plane, we find that the spreadout zero order contains two dark bands; these correspond to propagation directions that satisfy the Bragg condition, and the missing light is thus that which forms the first orders. Also, as we move from the source plane, the first order diffracted waves become broader and the edges less sharp; this is expected, since it is an angular band of light that satisfies the Bragg condition, the angle being determined by the Bragg angular selectivity, which depends on the grating thickness.

Simplified Approach

We suggest that approximate and useful results can be obtained for the sinusoidally profiled array of guides by comparing it, on a quite simplified basis, with the volume grating of sinusoidal profile. Despite the sinusoidal structure, we assume that in the Bragg diffraction process, all rays are reflected from discrete locations in the fringe contours; we take these locations to be at or near the regions of minimum refractive index; we assume one reflection per fringe period. A ray entering the material is thus partially reflected from each recorded fringe (Bragg surface) it encounters. Such a simplification has precedent, being the usual way of describing the Lippman method of color photography and a common way of describing holograms made by Denisyuk's method.

Confinement of rays between adjacent fringes occurs when an incident ray is entirely reflected from the first Bragg surface encountered. The depth of index modulation n_1 required to produce this condition can be obtained from the relation

$$Tn_1/\cos\theta_0 = \lambda_0/2 \tag{2}$$

as given by Kogelnik,[8] where T is the grating thickness, λ_0 is the free space wavelength of the light, n_1 is the magnitude of index variation ($2n_1 = n_{max} - n_{min}$), and θ_0 is the angle of the incident beam, measured within the material, assuming the Bragg condition is satisfied. When Eq. (2) is satisfied, the diffraction efficiency is 100%, that is, all the incident light appears in the diffracted wave. We consider a grating of thickness T_u such that each ray encounters only one Bragg surface in traversing the material; from simple geometry we find that

$$T_u = d/\tan\theta_0 \cong d/\theta_0. \tag{3}$$

Combining this relation with the Bragg diffraction law $2d\sin\theta_0 = \lambda_0/n_0$ yields

$$T_u = 2n_0d^2/\lambda_0. \tag{4}$$

where n_0 is the bulk index of the material. For guiding, we require 100% diffraction efficiency for the thickness T_u, that is, a single Bragg reflection placing all the incident light into the diffracted order. Thus, we combine Eqs. (2) and (4) and taking $\cos\theta_0 = 1$, we obtain

$$n_1 = (1/4n_0)(\lambda_0/d)^2 = n_0\theta_0^2 \tag{5}$$

as the minimum refractive index modulation required for guiding, where the third member of the equation is readily obtained from the second by application of the Bragg diffraction law. The reasonableness of this result is demonstrated by comparison with the comparable condition for guiding in slabs with sharp boundaries. At the boundary between an index $n_0 - n_1$ and a higher index $n_0 + n_1$, total reflection occurs for the condition

$$n_1 = \tfrac{1}{4}n_0\theta_0^2. \tag{6}$$

a relation readily derived from Snell's law and a small angle approximation. The two relations are nearly identical; the factor 4 between them suggests that the required index change is greater for sinusoidal variations than for discrete boundaries.

Substituting into Eq. (5) the values assumed in the

computed curves ($n_0 = 1.49$, $\lambda_0 = 0.6328\ \mu$m, and $d = 0.01$ mm), we obtain $n_1 = 6.7 \times 10^{-4}$, which is indeed about the value for which substantial wave confinement occurs (Fig. 3). Clearly, at one fourth this value, at which confinement occurs for the square-wave profile, there is decidedly incomplete confinement in the sinusoidal case.

We thank R. Alferness, J. Upatnieks, S. Case, and B. Hansche for their helpful suggestions. We also acknowledge the assistance of R. Zech, who so freely and patiently advised us on many technical aspects of this work. We thank the Office of Naval Research for its support of this work.

References

1. P. K. Tien, Appl. Opt. **10,** 2395 (1971).
2. S. E. Miller, Bell Syst. Tech. J. **33,** 661 (1954).
3. R. L. Rosenberg, J. Opt. Soc. Am. **62,** 1175 (1972).
4. R. L. Rosenberg and E. A. Chandross, Appl. Opt. **10,** 1986 (1971).
5. R. C. Alferness, Appl. Phys. **7,** 29 (1975).
6. E. Leith, G. Kung, R. Alferness, and B. Hansche, Opt. Commun. **14,** 229 (1975).
7. C. B. Burckhardt, J. Opt. Soc. Am. **56,** 1502 (1966).
8. H. Kogelnik, Bell Syst. Tech. J. **48,** 2909 (1969).
9. F. G. Kaspar, J. Opt. Soc. Am. **63,** 37 (1973).
10. N. Kato, Acta Cryst. **13,** 349 (1960).
11. M. R. B. Forshaw, Opt. Commun. **12,** 279 (1974).

V. W. Hughes—left—of Yale University and G. K. Woodgate of the Clarendon Laboratory during the July 1974 Fourth International Conference on Atomic Physics held at Heidelberg.

Reprinted from **APPLIED OPTICS,** Vol. 15, page 1800, July 1976

Nonlinear holographic waveguide coupler

B. J. Chang and S. K. Case

We have shown experimentally that for high exposure, higher order Bragg diffraction by volume holograms is dominated by the nonlinear refractive index modulation and proposed the application of nonlinear modulation to the construction of a high frequency volume-grating waveguide coupler.

Introduction

It is well known that first-order Bragg reconstruction of volume phase hologram gratings (in which the dielectric constant is spatially modulated in accordance with the exposure intensity distribution) can give diffraction efficiencies approaching 100%.[1] Higher order Bragg reconstruction of volume holograms is a lesser-known phenomenon, however. We have obtained strong second order diffraction, comparable in efficiency to the first order diffraction, from dichromated gelatin holograms. In this paper, we briefly discuss the mechanism of higher order Bragg reconstruction and propose a unique volume phase grating coupler whose construction is simplified over that of other grating couplers.

Higher Order Bragg Diffraction

Rose and Friesem observed strong higher order Bragg diffraction from dichromated gelatin holograms.[2] We found experimentally that for high exposure, higher order Bragg reconstruction is dominated by nonlinear modulation of the refractive index, an observation that is in agreement with the predictions made by Su and Gaylord[3] in their extension of coupled wave theory to nonsinusoidal gratings and to higher order Bragg angles.

Higher order Bragg diffraction can arise from two sources: first order diffraction from harmonic gratings created by the nonlinear response of the recording material to the exposure interference pattern and higher order diffraction from the fundamental and other lower order gratings.

B. J. Chang is with Environmental Research Institute of Michigan, Ann Arbor, Michigan 48107. S. K. Case is with Department of Electrical Engineering, University of Michigan, Ann Arbor, Michigan 48104.

Received 17 January 1976.

Although higher order Bragg diffraction is therefore the summation of all possible diffracted orders propagating at the appropriate angle, in the high exposure range the contribution of lower order gratings is small; thus the Bragg diffraction efficiency η_h of the hth order can be approximated by[3]

$$\eta_h = \sin^2[\pi n_h d/(\lambda_c \cos\theta_h)], \tag{1}$$

where λ_c is the reconstruction wavelength, d is the thickness of the hologram, n_h is the refractive index modulation of the hth harmonic grating when the refractive index profile of the hologram can be expressed as either a Fourier sine series or a Fourier cosine series, and θ_h is the Bragg angle of the hth order, determined by

$$\theta_h = \sin^{-1}(hf_1\lambda_c/2), \tag{2}$$

where f_1 is the fundamental spatial frequency of the hologram grating. Equation (1) is an accurate approximation under certain conditions[3]; otherwise, this is only a rough approximation. A detailed discussion of the mechanism responsible for higher order Bragg diffraction is beyond the scope of this paper.

To verify experimentally that higher order Bragg diffraction is dominated by harmonic grating diffraction we recorded plane wave holograms in dichromated gelatin derived from 649F plates. By slightly modifying the processing procedures,[4] we were able to vary the amount of nonlinearity in the hologram. If higher order diffraction by the fundamental grating is dominant, we would expect an approximately constant second order diffraction efficiency from holograms with different amounts of nonlinearity and the same first-order diffraction efficiency. We observed, however, that under these conditions, second-order diffraction efficiency varies over a wide range. In fact, with the appropriate nonlinear modulation, volume phase holograms can diffract nearly all the incident light into any desired order.

The angular bandwidth of the hth diffracted order of a volume grating having a sinusoidal index modulation is approximately proportional to $1/h$ times the ratio

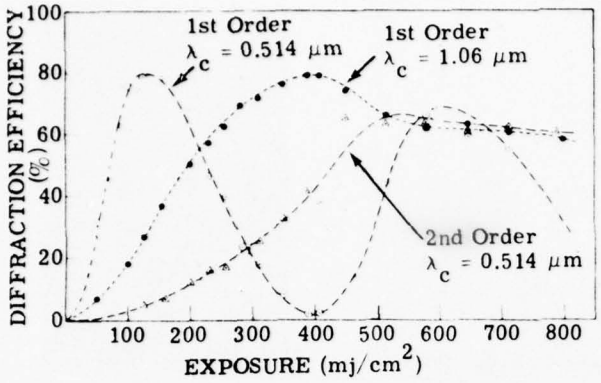

Fig. 1. Comparison between diffraction efficiency of first order at λ_c = 1.06 μm and second order at λ_c = 0.514 μm.

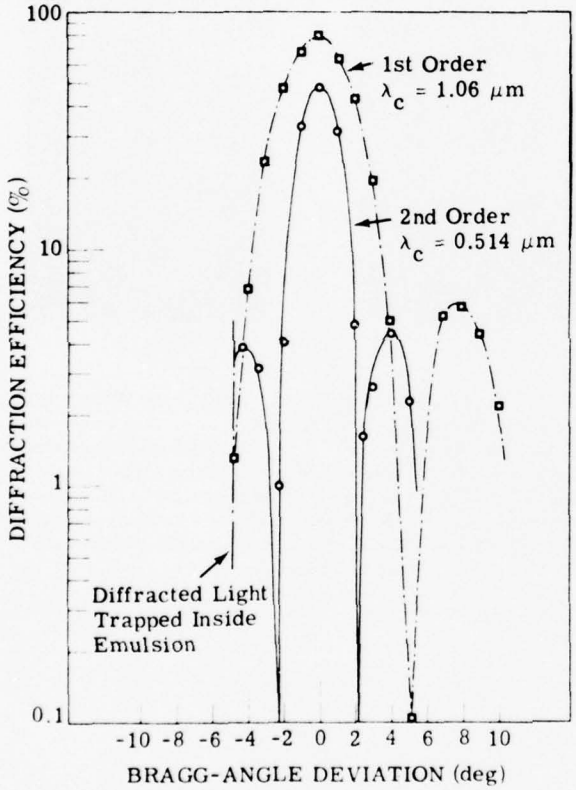

Fig. 2. Comparison between angular selectivity of first-order diffraction at λ_c = 1.06 μm and that of second-order diffraction at λ_c = 0.5145 λm; the solid and broken lines are the best fits of experimental data.

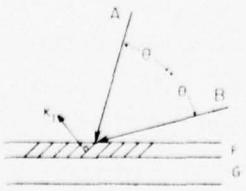

Fig. 3. Exposure of film F on glass substrate G by plane waves A and B.

of the fringe spacing and the hologram thickness; this is evident from an examination of the coupled-wave theory and k-vector diagram.[1] Therefore the angular bandwidth of the hth diffracted order is approximately the same whether it is the first-order diffraction from the hth harmonic grating or the corresponding higher order diffraction from the fundamental and other lower harmonic gratings, i.e., the angular bandwidth of hth diffracted order is approximately $1/h$ times that of the first order of the fundamental grating.

In Fig. 1, we show diffraction efficiency curves of the first and second orders reconstructed at their appropriate Bragg angles; the holograms were recorded at a wavelength of 0.514 μm and monitored at two wavelengths. The diffraction efficiency of the second order resulting from a large refractive index modulation of the harmonic grating can approach that of the first order; indeed, we have measured efficiencies that, corrected for reflection loss, are in excess of 95%.

Figure 2 shows experimental curves indicating the angular bandwidth of the first diffracted order at a reconstruction wavelength of 1.06 μm and of the second diffracted order at a wavelength of 0.514 μm. These diffracted orders have approximately the same Bragg angle. The angular bandwidth of the first diffracted order at a wavelength of 0.514 μm is of course similar to that of the first diffracted order at a wavelength of 1.06 μm, but the Bragg angles are different (assuming a constant ratio of refraction index modulation h_1 and readout wavelength λ_c). In Fig. 2, we see that the second-order curve is approximately half of the width of the first-order curve.

Nonlinear Grating Coupler

Kogelnik and Sosnowski describe a volume holographic coupler as a convenient means to feed light into a thin optical film.[5] For the construction of this volume holographic coupler, they use a prism coupler to introduce the construction beams at an angle greater than the critical angle for the waveguide. For some materials and devices, it may be undesirable to place a prism and index matching fluid in contact with either the photosensitive layer or the substrate. We alleviate this problem by exposing the film with one pair of external plane waves and using a nonlinear film response to generate a harmonic grating for which one of the readout waves will be a guided wave.

As shown in Fig. 3, exposure with plane waves A and B of wavelength λ forms a grating characterized by the grating vector $\mathbf{K}_1$, which is perpendicular to the fringe planes and has a magnitude $K_1 = 2\pi/\Lambda$, where Λ is the fringe spacing of the fundamental grating. The Bragg equation of the hth diffracted order is then given by

$$2\beta \sin\theta_h = K_h = hK_1, \tag{3}$$

where $\beta = 2\pi n_0/\lambda$ is the propagation constant in the recording medium, θ_h given by Eq. (2) is the angle in the recording medium, and n_0 is the bulk refractive index of the recording medium.

If the film has a nonlinear response to the incident illumination at high exposure levels, a second-order grating $\mathbf{K}_2 = 2\mathbf{K}_1$ of twice the fundamental spatial fre-

quency will be formed within the emulsion. The K-vector diagram in Fig. 4, for correct construction geometry and readout with wave A', indicates how we produce a Bragg diffracted wave B' at an angle greater than the critical angle for the guide (i.e., a trapped wave). Since the gelatin and the glass substrate have approximately the same refractive index, the trapped wave is guided in both the film and the substrate. Since the substrate thickness $t \gg \lambda$, our guide is multimode.

In order to verify the above theory, we constructed a grating coupler as shown in Fig. 3 with plane waves incident at 36° and 70° external angles with respect to the film normal. The polarization of light for both construction and readout is perpendicular to the plane of incidence. The readout geometry of this grating is shown in Fig. 5(a). A collimated beam of coherent light incident from the upper right passes through a 0.3-cm × 2-cm aperture and illuminates the 1-cm × 1-cm coupler grating. Light diffracted by the grating is removed from the incident beam while the undiffracted light falls on a piece of ground glass. Figure 5(b) shows the system with the coupler rotated away from the Bragg angle, so that there is no diffraction. Figure 5(c) shows the grating at its second-order Bragg angle and nearly 100% coupling efficiency, as is evident by the depletion of the incident wave in the coupler region. In this figure, however, the guided wave again strikes the coupler grating after its first guided bounce and, since it is at the complementary Bragg angle for the coupler grating, is uncoupled with nearly 100% efficiency. If the grating is translated so that the guided wave will miss the coupler grating after its first bounce, the light can be seen in this time exposure because the gelatin of the film scatters a small amount of light. Removal of the gelatin from areas of the guide where there is no coupler eliminates this scatter loss.

This coupler, of course, could also be used in conjunction with a thin film guide for single mode operation, but by having the thick guide, we have gained coupling efficiency[6] and have greatly relaxed the requirement on the sharpness of the grating coupler edge.

The authors thank E. N. Leith and W. S. Colburn for helpful discussions during the course of this work. We thank the Air Force Avionics Laboratory, the Office of Naval Research, and the National Science Foundation (grant GK 43148) for their generous support.

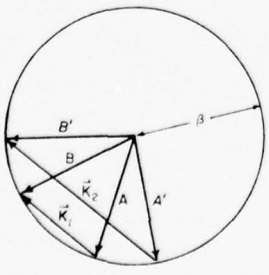

Fig. 4. Exposure with beams A and B produce fundamental grating $\mathbf{K}_1$ and harmonic grating $\mathbf{K}_2$. Readout at the second-order Bragg angle with wave A' produces guided wave B'.

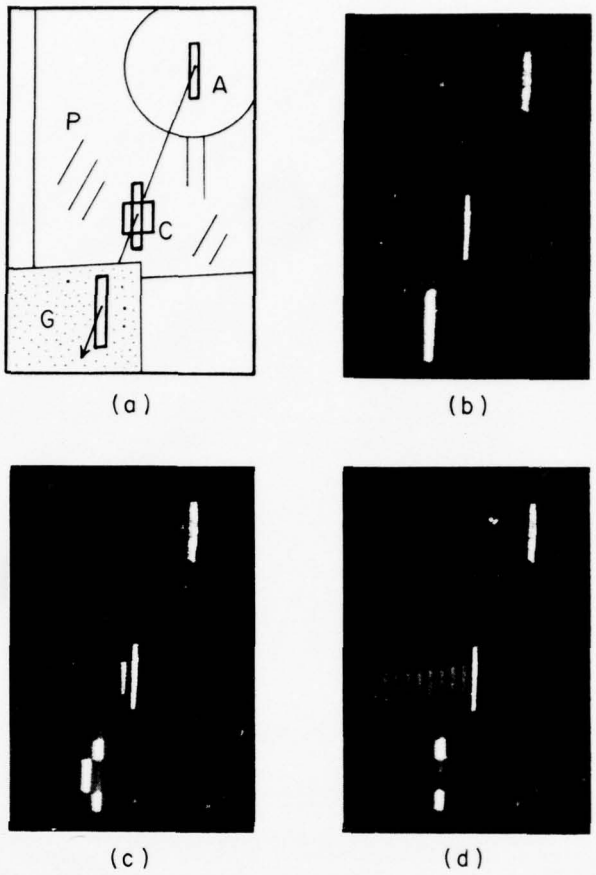

Fig. 5. (a) A collimated beam of coherent light passes through aperture A and illuminates the coupler grating C, which is supported by a 1-mm thick glass substrate P. The transmitted light illuminates ground glass G. (b) Illumination far from the Bragg angle of coupler grating C. (c) Bragg angle illumination near the center of the coupler. The incident wave is coupled into and back out of the guide after one bounce. (d) Bragg angle illumination near the edge of the coupler produces a guided wave.

References

1. H. Kogelnik, Bell Syst. Tech. J. **48,** 2909 (1969).
2. H. W. Rose, Ph.D. Dissertation, Ohio State University (1972).
3. S. F. Su and T. K. Gaylord, J. Opt. Soc. Am. **65,** 59 (1975).
4. M. Chang, Appl. Opt. **10,** 1550 (1971).
5. H. Kogelnik and T. P. Sosnowski, Bell Syst. Tech. J. **49,** 1602 (1970).
6. K. Ogawa and W. S. C. Chang, Appl. Opt. **12,** 2167 (1973).

MULTI-MODE HOLOGRAPHIC WAVEGUIDE COUPLER

S.K. CASE and M.K. HAN
Department of Electrical Engineering, The University of Michigan, Ann Arbor, Michigan 48104, USA

Received 23 June 1975

A double-exposure thick-holograhic-grating waveguide coupler is described in which two waveguide modes can be excited with a single incident beam. Single-grating decouplers are also designed to selectively remove one of the coupled waves.

1. Introduction

Present couplers for integrated optical circuits [1] have been restricted to coupling one external wave into one guided wave. We concern ourselves in this report with a thick holographic grating coupler designed to provide simultaneous excitation of more than one guided mode when illuminated by a single external beam. Once the guided waves have been processed within the guide, we will want to selectively decouple one of the guided modes without perturbing the other. A single grating decoupler is designed for this purpose.

2. Double-grating coupler

We have shown earlier [2] that it is possible to double expose a thick grating such that it acts like a double beam splitter to diffract 50% of the incident energy into each of two diffracted orders. We use this principle to construct a two-mode waveguide coupler as in fig. 1. A dichromated gelatin film is exposed through a prism first with plane waves A and B, and then with plane waves A and C. After development, readout with common wave A′ will produce both guided waves B′ and C′ (fig. 2) so that we can simultaneously excite two modes in the guide with a single incident beam.

We have also constructed two single-grating decouplers by exposing a piece of film through the prism with beams A and B, and by exposing another piece of film with beams A and C. Each single-grating decoupler is exposed and developed on its own 1 mm thick glass substrate and can now be mounted on a waveguide to couple or decouple beams of light. By choosing the construction waves B and C sufficiently far apart (in angle), we can construct the single grating decouplers such that they act independently on either of the two guided waves [3].

In fig. 3a, we show a double-grating coupler mounted on top of a $\frac{1}{4}$" Kodak Microflat glass guide (emulsion removed) using xylene as an index matching

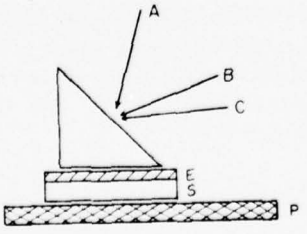

Fig. 1. Construction of a double grating coupler. A, B, C are incident plane waves; E is the dichromated gelatin emulsion on substrate S; P is an absorptive backing plate. Xylene is used as an index matching fluid between the components.

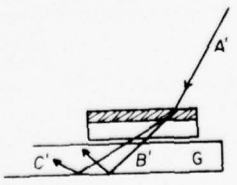

Fig. 2. Readout of the double-grating coupler with wave A′ produces guided waves B′ and C′ in guide G.

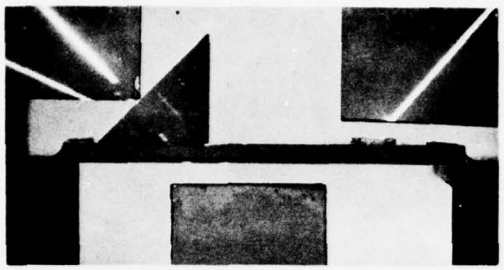

(a)

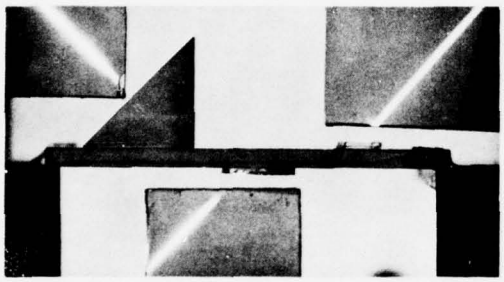

(b)

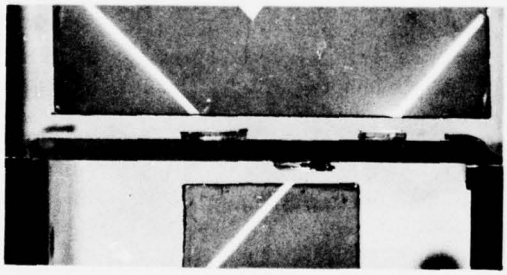

(c)

Fig. 3. Double-grating coupler: a) Two guided modes are simultaneously excited in the waveguide. b) One of the guided waves is decoupled by a single-grating decoupler. c) Both of the guided waves are decoupled by separate single-grating decouplers.

fluid. The collimated beam of light (beam A′) incident from the upper right is coupled with nearly 100% efficiency into the guided beams B′ and C′ as observed by the lack of transmitted light on the piece of ground glass below the guide. The two guided modes can be seen in this view after they have been uncoupled by a prism and illuminate a piece of ground glass held at grazing incidence. In fig. 3b, we attach a single-grating decoupler to the bottom of the guide. This grating was constructed with waves A and C so that on readout, it will decouple guided wave C′ and diffract it into the direction of wave A′. Guided beam B′ is not at the Bragg angle for this decoupler and remains trapped. In fig. 3c, we place the single grating constructed with waves A and B on top of the guide. This now decouples the energy from the remaining guided wave B′ into the unguided wave A′. The output beams can be diffracted in either an upward or downward direction by a suitable rotation of the decoupler gratings.

3. Extensions of the principle

This method of double-grating coupler construction (with common reference wave A) requires that the construction and readout wavelengths be the same so that the two gratings will have a common Bragg angle on readout. If the coupler is to be used at a wavelength different than that of construction, then the geometry of the construction beams must be adjusted so that the two gratings will have a common Bragg angle at the readout wavelength.

By making the mode-selective decoupler gratings sufficiently thick, their angular selectivity can be reduced so that they extract light over a very narrow angular range. In this way, the multi-mode coupler and decoupler system can be extended to include many more guided waves.

Acknowledgements

The authors wish to thank Professor Emmett Leith for helpful discussions during the course of this work. We thank the Office of Naval Research and the National Science Foundation (Grant #GK 43148) for their generous support.

References

[1] H. Kogelnik and T.P. Sosnowski, Bell Syst. Tech. J. 49 (1970) 1602.
[2] S.K. Case, J. Opt. Soc. Am. 65 (1975) 724.
[3] R.C. Alferness and S.K. Case, J. Opt. Soc. Am. 65 (1975) 730.

Reprinted from **Applied Optics,** Vol. 15, page 2307, October 1976

Modular optics mode converter

Steven K. Case and Robert A. Russell

University of Michigan, Department of Electrical Engineering, Ann Arbor, Michigan 48104.
Received 4 June 1976.

We advance here the concept of modular optics and its application to waveguide optical systems. We describe a modular optical element as an element constructed on its own small, thin substrate[1] and capable of being selectively attached to the surface of an optical waveguide and later removed. These optical elements can be mass produced and individually tested before use in an optical circuit. In addition, if the elements are holographically formed, they do not have to be developed while attached to the waveguide, thus saving the guide from possible chemical attack.

We previously used thick hologram optical modules to couple and decouple waves selectively from a thick waveguide.[2] After a coupler module was attached to the guide to excite two guided waves within the waveguide, thick emulsion modular decoupler gratings were selectively attached to the guide at positions where we wished to sample one of the guided waves. In a similar manner, Wei and Tan[3] have developed a thin plastic grating coupler that can be fixed to a guide and later removed.

In Fig. 1, we show a construction geometry for a holographic optical module. Wave A in Fig. 1 is nearly normal to the emulsion E of the module. Waves B and C are at angles such that they will produce guided waves. We first construct a coupler grating by exposing a film module with waves A and B. Readout of this module with wave A will produce a guided wave B. We also construct a mode converter by exposing another piece of film with waves B and C. When placed on a guide, this module will allow diffractive coupling between waves B and C.

After development, the coupler module is mounted on top of a planar glass guide using xylene as an index matching fluid. In Fig. 2(a) the beam incident from the upper left is diffracted into guided wave B by our coupler module. Wave B is later decoupled by a prism and strikes a card held at grazing incidence.

In Fig. 2(b) we attach a mode converter module to the surface of the waveguide. As wave B strikes the module, it is converted into wave C, as can be seen in the decoupled output. This mode converter was exposed so the module is 100% efficient in converting wave B into C.

In Fig. 2(c) we place a different converter module on the guide. This grating has index modulation such that half the incident energy in wave B is diffracted into wave C. This element could serve as a beam splitter for use as the first element of an intrawaveguide interferometer.

It should be noted that we have used a very thick optical waveguide (6-mm thick Kodak Microflat glass). Since the guide is thick and the surfaces produce a small amount of scattered light, we can observe the paths of individual guided waves (see the bright spots within the guide in Fig. 2). For this thick guide demonstration we also do not have to worry about waveguide modes[4] or substrate thickness of the module. Our modules have been constructed in thick dichromated gelatin films obtained from Kodak 649-F plates.[5] Thus, the emulsion and the glass substrate (1 mm thick) of this film comprise the module. Similar devices could be built for thin waveguides.

The modular optics principle can be extended in a number of ways. In addition to constructing the modules with external laser beams as in Fig. 1, we can also construct modules by exposing a piece of sensitized film (which has been temporarily attached to a guide) at the intersection point of the guided outputs from two other modules. We also need not restrict ourselves to plane wave devices, as modular lenses and other elements can easily be constructed. Active elements can be included to build up modulators and switching assemblies. By placing a series of different modular elements on a waveguide, entire optical circuits can be assembled. Each element may be repositioned and adjusted to optimize the performance of the entire waveguide optical circuit. The

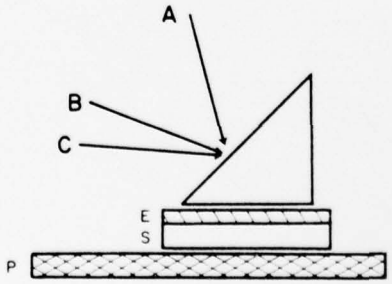

Fig. 1. A construction technique for modular optical elements. A, B, and C are incident plane waves; E is the thick dichromated gelatin emulsion on the module substrate S; P is an absorptive backing plate. Xylene is used as an index matching fluid between the components.

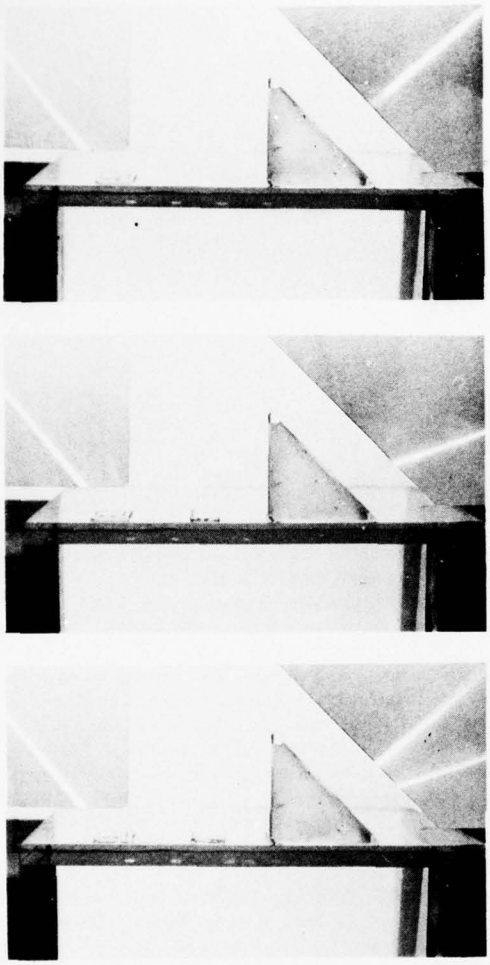

Fig. 2. Modular optical elements: (a) a coupler module is used to excite guided wave B; (b) a mode converter module converts guided wave B into guided wave C; (c) a beam splitter module converts half the energy in wave B into wave C.

elements may then be fixed in place. As it is presently difficult to construct an entire optical circuit via an integrated optics approach, the modular optics building-block concept appears to be quite useful.

The authors wish to thank Emmett Leith for discussions during the course of this work. The generous support of the Office of Naval Research and the National Science Foundation (Grant GK 43148) is appreciated.

References

1. If the material used to construct the element has sufficient mechanical strength, a substrate may not be needed.
2. S. K. Case and M. K. Han, Opt. Commun. **15,** 306 (1975).
3. J. S. Wei and C. C. Tan, Appl. Opt. **15,** 289 (1976).
4. R. P. Kenan, J. Appl. Phys. **46,** 4545 (1975).
5. S. K. Case, Ph. D. thesis, University of Michigan, 1976, Chap. 5.

ABSTRACT

Directional Coupling Properties of Interferometric Waveguides

by

G. C. Kung and W. Y. Wang

Directional coupling properties of sinusoidal grating waveguides are investigated. Our computer analysis which based solely on the diffraction theory of thin gratings predicts results that are in good agreement with those calculated in terms of coupled mode theory. The relationships between directional coupling efficiency and some parameters such as grating period, input pulse shape and guiding channel length are discussed. Our analysis predicts that we can substantially switch the input energy to adjacent channels with the proper choice of parameters.

When this work was done, all authors were with the University of Michigan, Electrical and Computer Engineering Department, Ann Arbor, Mi 48104; G.C. Kung is currently with General Dynamics, Pomona Division, Pomona, Ca 91766.

Introduction

The thin grating decomposition (TGD) method, developed by Alferness[1] and adapted to the analysis of guided wave propogation in parallel-channel planar waveguides[2,3] (Leith et al, Kung & Leith), has provided a very usual, intuitive, and simple basis for examining the propagation of spatial pulses of arbitrary shape optical waveguides of any arbitrary index cross-sectional profile. Insights are provided in situation where other techniques either are inapplicable or extremely difficult to apply.

These guides can alternatively be regarded as volume phase gratings of various index perturbation; the wave is guided along the contours of maximum refractive index. We consider grating of sinusoidal cross section, of the form

$$\tau(x,z) = \exp [jk \cos 2\pi x/d] \cong 1 + jk \cos 2\pi x/d \quad (1)$$

where d is the grating period.

The ability to confine energy within each guiding channel, or equivalently, the susceptibility to the coupling of light energy into adjacent channels is one of the most important characteristics of the array. We use the term guiding efficiency (η_0) to mean the fraction of energy that remains in the input channel after an input pulse of energy propagates through the structure, and the term coupling efficiency (η_1) to mean the fraction of energy that

is coupled from the i^{th} to the j^{th} channel over the interaction distance.

We consider the propagation of parallel-channel guides of sinusoidal profile, and we consider pulses primarily of the form of a simple cycle of a sinusoid. We report various observation which show the power of the technique in analogy a situation not easily treated other methods, and therefore not studied.

Effect of Guide Spacing

We examined the guiding and coupling efficiencies of guides with sinusoidal index variation spacing. The input pulse was introduced centered at a region of maximum index and has the form

$$f(x) = \cos^2(\frac{\pi x}{d}) \text{ rect } (x/d) \qquad (2)$$

where d is the pulse width. This pulse thus has the same shape and width as the guide.

The results are shown in Figures 1-3, we note as expected, that the guiding efficiency (η_0) in the input channel decreases monotonically with increasing quadrature, as plotted in Ref. 3.

Figure 2 shows the same informations plotted with guiding efficiency as a function of index modulation for various grating frequencies. In all cases, the input pulse is adjusted so as to be of the same width as the guide.

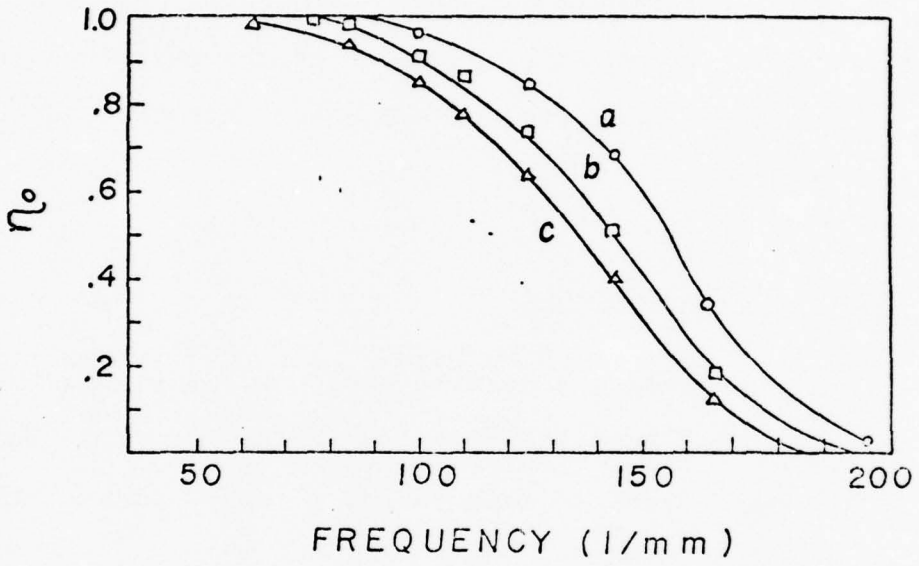

Fig. 1 Guiding efficiency versus grating frequency for a sinusoidal grating waveguide. Thickness = 0.54 mm. Input pulses are as wide as the grating periods. (a) n_1 = .0012; (b) n_1 = .0008; (c) n_1 = .0006.

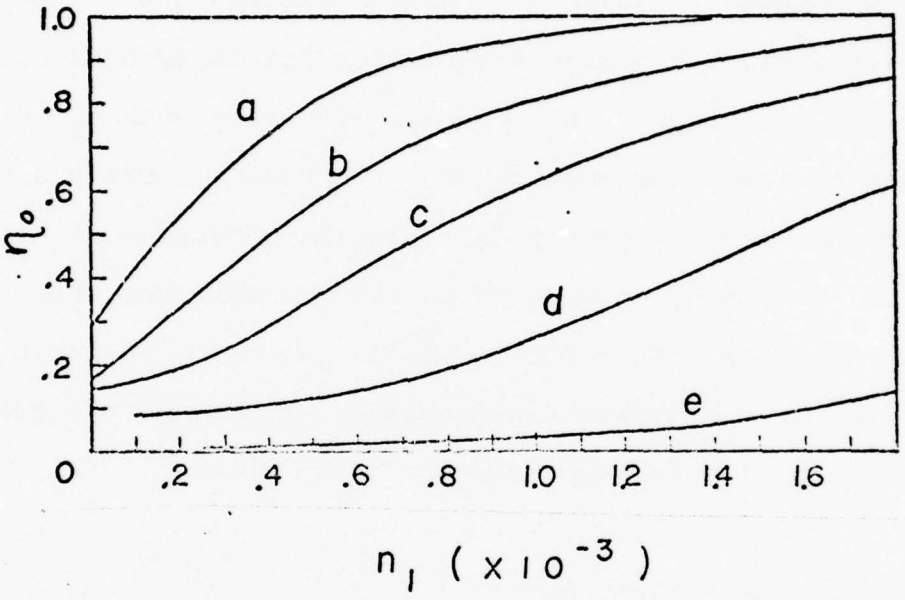

Fig. 2 Guiding efficiency versus index modulation for sinusoidal grating waveguides of various spatial frequencies: (a) 100 1/mm; (b) 125 1/mm; (c) 143 1/mm; (d) 167 1/mm; (e) 200 1/mm. Grating thickness = 0.54 mm. Input pulse widths are equal to grating period.

Also, we show (Fig. 3) the coupling efficiency η_1 is a function of n_1.

When there is little coupling to non-adjacent channels, the increase of energy confinement in the input channel with increasing n_1 corresponds to the continuous decrease of energy coupled to adjacent channels (curves a and b of Fig. 3). However, for higher frequency gratings such as curves c, d and e of Fig. 3, η_1 actually increases with n_1 in the region of low index modulation, this occurs because a significant amount of energy in a grating waveguide of high spatial frequency is coupled to the non-adjacent channels when the index modulation is small. With increasing n_1, the coupling to non-adjacent channels decreases. Therefore η_1 results in less leakage from the input channel.

Effect of Input Pulse Shape

The Alferness thin grating decomposition analysis is not restricted to any specific profile of input pulse. We have chosen, for simplicity, a sinusoidal pusle, as given by Eq. 2. Although sinusoidal grating waveguides cannot preserve the phase information (and hence the shape) of the input signal, we find that if the input pulse width is less than or equal to the grating period, then, with increasing n_1, the output pulse width converges to that of the input pulse. This phenomenon can be understood by consideration of the mode structure of the sinusoidal grating waveguides.

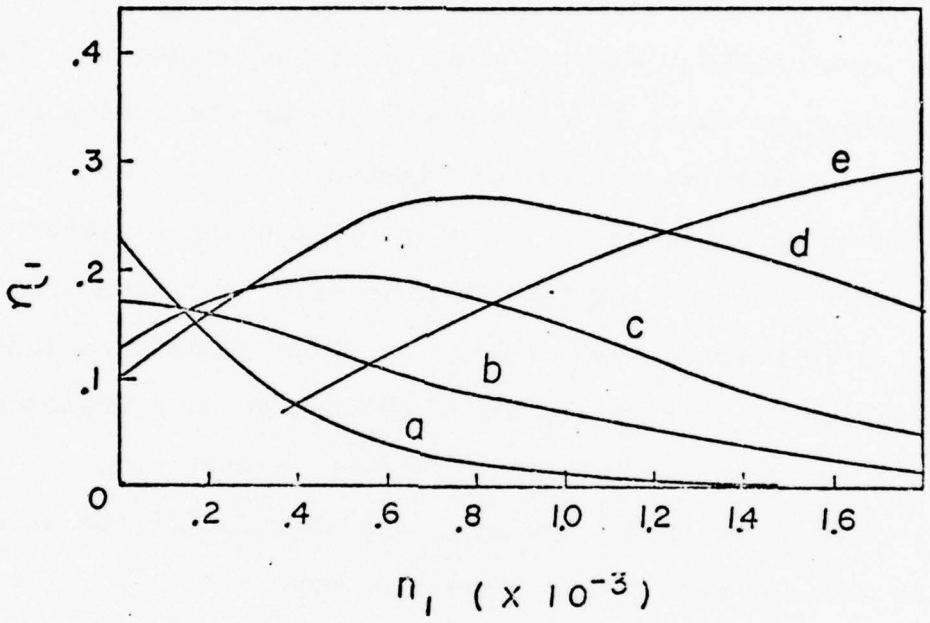

Fig. 3 Coupling efficiency to adjacent channel vs. index modulation for sinusoidal grating waveguides of various spatial frequencies: (a) 100 l/mm; (b) 125 l/mm; (c) 143 l/mm; (d) 167 l/mm; (e) 200 l/mm. Grating thickness = 0.54 mm. Input pulse widths are equal to grating period.

In general, when a signal is launched into a waveguide, it is coupled to the waveguide modes, some which are guided modes but most are not. The transmission of the input pulse depends entirely on the guided modes which are excited by the input field. What we observe at the output is a field distribution which is a superposition of the fields in the various guided modes; in most instances this distribution bears no resemblance to the shape of the input signal. Of course, the input coupling is most efficient when the input signal is matched with one of the guided mode distributions; otherwise, a part of the energy either becomes evanescent or simply propagates through the structure unguided.

For a sinusoidal grating, the solution of the wave equation for the TE modes has the form

$$E_n(x,z) = \exp(-j\beta_n z)\, F(x) \tag{3}$$

with F(x) satisfying

$$\frac{d^2F}{dw^2} + (a - 2q\cos 2w)F = 0 \tag{4}$$

where

$$w = \pi f x \tag{5}$$

$$a = \left(\frac{1}{\pi f}\right)^2 (n_0^2 k_0^2 - \beta^2) \tag{6}$$

$$q = -\left(\frac{1}{\pi f}\right)^2 n_0 n_1 k_0^2 \tag{7}$$

Eq. 4 is a Mathieu's equation whose solution may be expressed in the form

$$F(w) = \exp(pw) \sum_{h=-\infty}^{\infty} B_h \exp(j2hw) \tag{8}$$

where p is a constant. We consider a specific example of a grating with $n_0 = 1.49$ and $n_1 = .6 \times 10^{-3}$. From Eq. 7 q is found to be -0.893 when λ_0 is chosen to be 0.6328 μm. The relation between a, q, and p can be illustrated in the form of a stability diagram (Fig. 4), following the standard treatment of Mathieu's equation.[4] The a-q plane is divided into various stable and unstable regions; the unstable solutions correspond to complex values of p, which, are the guided modes of the structure. The operating line, q = -0.893 passes through several unstable regions. From the corresponding values of a and with the aid of Eq. 5, we can determine the z-directed propagation constant β of the guided modes whose transverse distributions have the form of Eq. 8.

From the a-q diagram, it is evident that for a fixed value of q, there are many continuous sets of "a" which correspond to many continuous sets of guided modes. However, for small values of q, the ranges of the guided modes are rather narrow. For the present case of q = -0.893, the values of "a" which give rise to guided modes lie in the following ranges: $a < -0.369$, $0.018 < a < 1.802$, $3.934 < a < 4.304$, $9.039 < a < 9.061$ and so on. The corresponding ranges of β, obtained from Eq. 5 are: $\beta > 14.7959$, $14.7944 > \beta > 14.7885$, $14.7814 > \beta > 14.7801$, $14.7643 > \beta > 14.7642$ and so on. Thus, even though the guided modes in theory form many continuous sets, the ranges of β, for small

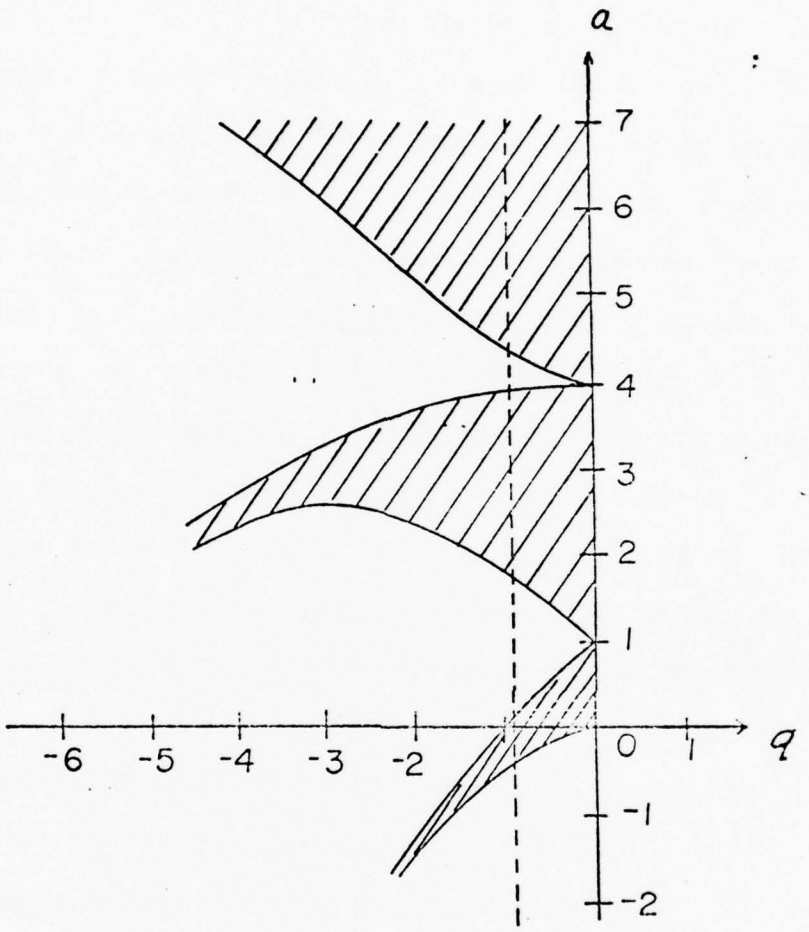

Fig. 4 Stability diagram of Mathieu's equation. The shaded areas are the stable regions. The dotted line corresponds to q = -0.893.

values of q, are so narrow that the modes of an interferometrically formed waveguide with index modulation typically in the order of 10^{-3} can be considered to be almost discrete. This would explain why the results of our computer analysis of a sinusoidal grating waveguide are in good agreement with those obtained from the conventional analysis of single mode coupled waveguides (i.e., those with discrete boundaries).

Pursuing the question of why a sinusoidal grating waveguide can preserve the shape of an input pulse of the form of Eq. 1, we consider a specific example by arbitrarily choosing a guided mode with a value of a = 1.5; resulting in a p value of approximately $\pm 0.3345 + j$. The transverse distribution of this mode consequently has the form

$$F(x) = \exp(-0.3345\pi fx) \sum_{h=-\infty}^{\infty} B_h \exp(j2\pi fhx)$$

$$= \exp(-0.105x) \sum_{k=0}^{\infty} 2B_k \cos 2\pi fkx \qquad (9)$$

which is a set of slowly damped standing waves. For an input pulse with the form of Eq. 9 and equal in width to the grating period, i.e., d = 1/f, we immediately see that the input pulse matches closely the fundamental space harmonic of the guided mode except for the slowly damped function, exp(-0.105x). Consequently, this is the mode which is principally excited; what we observe at the output plane is nothing more than this mode distribution; hence, the output pulse converges in shape to the input pulse. To further illustrate this point, we propagate a spatial pulse of a quite arbitrary profile through a sinusoidal grating of

thickness 0.54 mm. The distributions of the input and output pulses are shown in Fig.5. From these results and also those shown in Fig. 5 of Ref. 3 for an input pulse extended over three channels, it is quite evident that the output pulse distribution always has a nearly co-sinusoidal form within the guiding channels, regardless of what form the input pulse takes.

Effect of Channel Length

The continuous exchange of energy among guiding channels is illustrated in Fig. 6. An input pulse of 0.01 mm width is placed at the center of a guiding channel of the same width. The refractive index modulation of this thick grating is arbitrarily chosen to be 6×10^{-4}. As the pulse propagates through the structure, energy of the pulse is continuously coupled to the adjacent channels. The results shown in Fig. 6 are in qualitative agreement with that obtained from an optical discretely bounded single mode directional coupler.[5] Using the quantity guiding efficiency and the same parameters as before, we plot the fraction of energy in the 0 and +1 channels against propagation depths. The results (Fig. 7) show energy continuously leaking out to the adjacent channels. The close resemblance between interchannelized waveguides and directional couplers suggests a quantitative comparison of the two; although there are differences: one is a single mode device and the other is

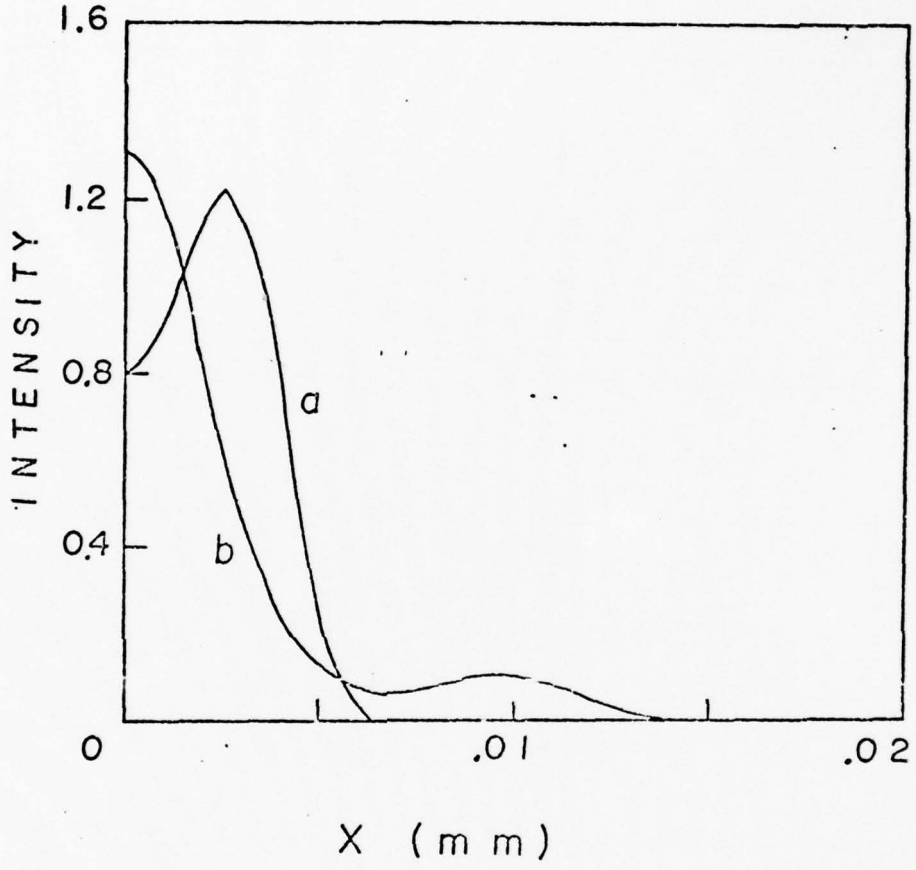

Fig. 5 Propagation of an input pulse of arbitrary shape in a sinusoidal grating waveguide of thickness 0.54 mm, frequency 100 1/mm, index modulation $.6 \times 10^{-3}$. (a) shows the input pulse; (b) shows the output pulse.

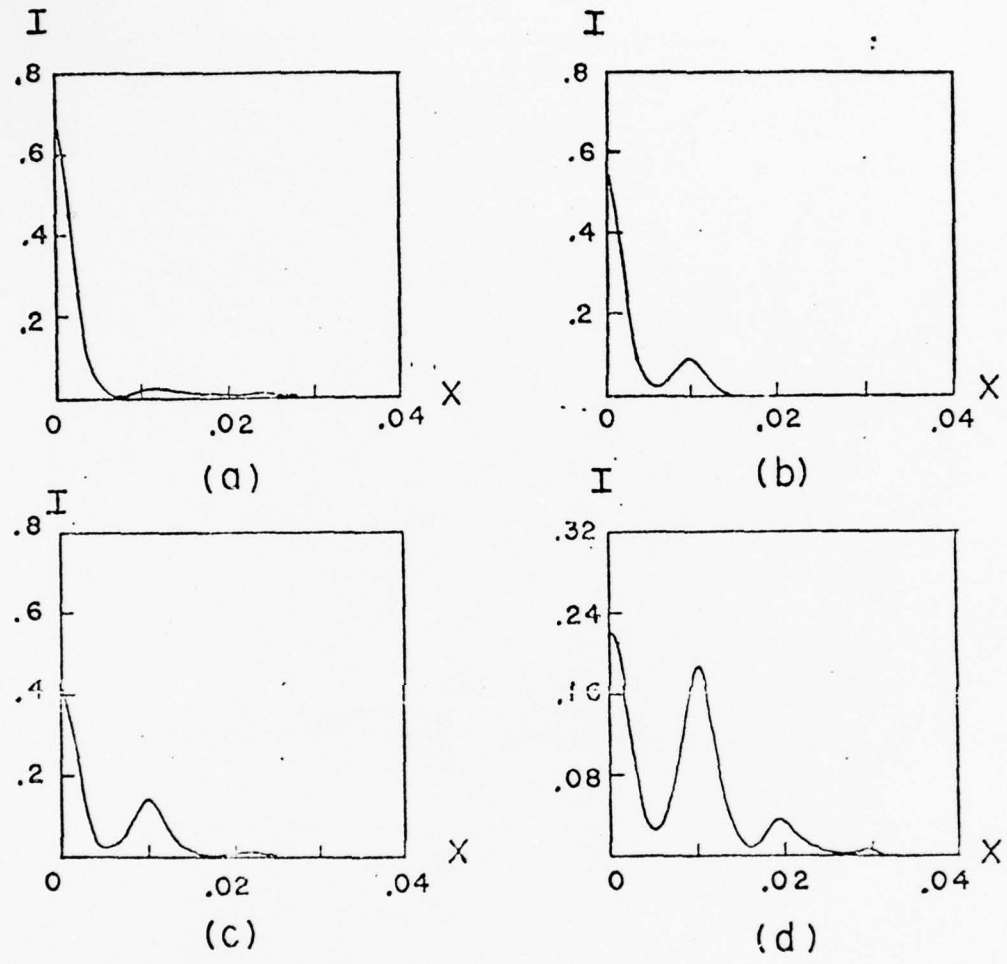

Fig. 6 Guided light intensity profiles for various channel lengths: (a) 0.54 mm; (b) 1.08 mm; (c) 1.62 mm; (d) 2.16 mm. Spatial frequency of the thick grating is 100 lines/mm; $n_1 = 6 \times 10^{-4}$.

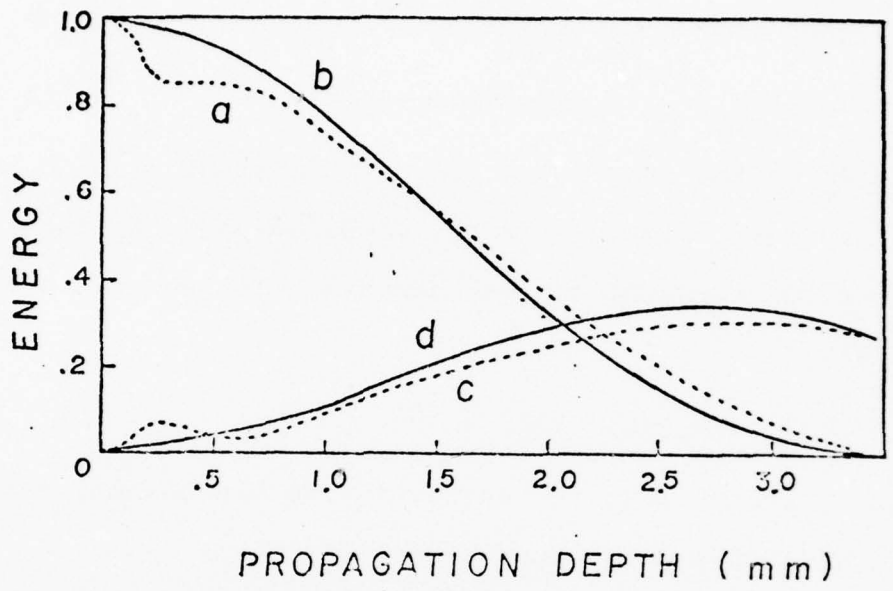

Fig. 7 Directional coupling of grating waveguides: (a) shows the energy that remains in the input channel at various propagation depths; (b) shows a function J_0^2 (.684z); (c) shows the energy directionally coupled to the adjacent channel; (d) shows a function J_1^2 (.684z)

multi-mode and in one there are two guides in parallel, whereas in the other there are many. The wave amplitudes, $a_k(z)$, in various channels of the single mode coupled waveguide when the energy is incident on the k = 0 channel is[5]

$$a_k(z) = (-1)^k J_k(2Cz)\exp(-j\beta k^2) \tag{10}$$

where J_k is the Bessel function of the first kind, C is the coupling coefficient, z is the propagation depth and k is an integer denoting the channel numbers. The energy in various channels is

$$E_k(z) = a_k^2(z) \propto J_k^2 \tag{11}$$

which indicates that the energy in the 0th channel varies as the square of a zero order Bessel function. We superimpose on Fig. 7 the functions $J_0^2(.684z)$ and $J_1^2(.684z)$. Note that, except for a small region of $z < 0.5$ mm, the computed results for the grating waveguides follow very closely the two Bessel functions; the coupling coefficient, C, of the grating waveguides is consequently found to be equal to 0.342.

Optical Directional Coupler Application

The results shown in Fig. 6, predict the directional coupling properties of a sinusoidally stratified structure; these results agree qualitatively to those calculated in terms of coupled mode theory. Some additional results illustrating the phase relation of the energy between the

coupled guides are shown in Fig. 8. By placing the input pulse of 0.01 mm width in front of the entrance surface of the guiding structure so that the pulse spreads over three channels (Fig. 8a), the light entering into the side channels suffers a time lag. Our analysis predicts (for properly chosen parameters) constructive interference of the light entering directly into the side channels and that directionally coupled into the side channels from the central one, because the directionally coupled light also suffers a time lag.[6] On the other hand, by placing the input pulse sufficiently behind the entrance surface (Fig. 8b), the interference in the side channels is destructive because now the direct lights entering the side channels have a time lead. Somekh has experimentally demonstrated such phenomenon. It is noteworthy that our analysis, which is based on nothing more than a continuous iteration of the quite simple thin grating diffraction theory, should so readily predict these rather subtle effects.

Our analysis indicates that we can substantially shift the input energy to adjacent channels of multichannel waveguides by using the proper choice of parameters. We can envision various applications, such as incorporation of this feature into an acousto-optical divice using the modulated medium as the guiding channels, which is possible provided sufficient index modulation is achieved.

Since the index modulation can be controlled, it would be possible to efficiently switch the input energy between

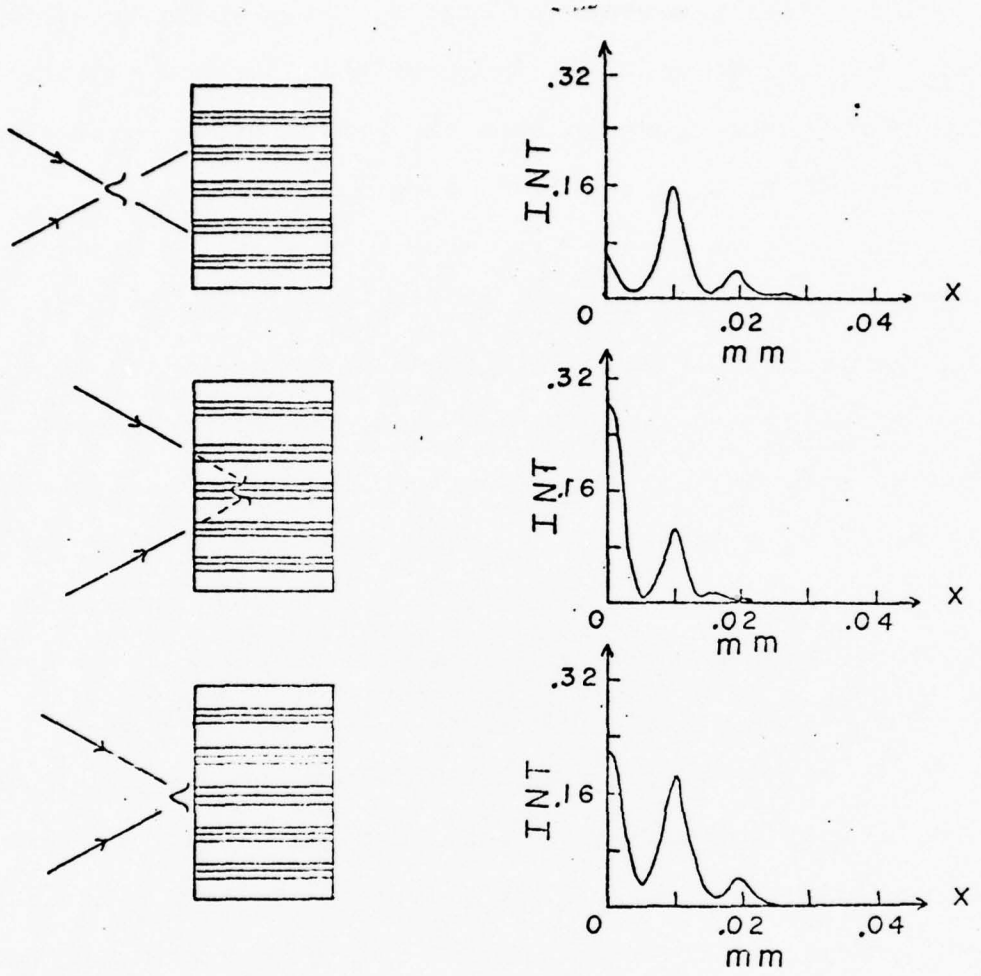

Fig. 8 Phase relation between directionally coupled modes in a sinusoidal grating waveguide. To the left are sketches illustrating various input conditions. The positions of the input pulse are: (a) 0.27 mm in front of the grating; (b) 0.27 mm behind the front surface of the grating; (c) on the front surface. To the right are the corresponding intensity distributions at the output plane. Thickness of grating is 2.16 mm, grating frequency is 100 1/mm and index modulation is 0.6×10^{-3}.

the 0th and 1st channels, thus forming a simple, yet versatile multi-mode switching device.

We are thankful to Professor Leith for his encouragement and valuable guidance on our work. We also want to acknowledge the support of Office of Naval Research under contract no. N000 14-67-A-0181-0058.

References

1. R. Alferness : App. Phy. 7,29(1975)

2. E. Leith, G. Kung, R. Alferness and B. Hansche : Opt. Commun. 14,229(1975)

3. G. C. Kung and E. N. Leith : Appl. Opt. 14,2614(1975)

4. N. W. McLachlan : Theory and Application of Mathieu Functions (Oxford University Press; London, 1947), Fig. 8(A)

5. S. Somekh, E. Garmire, A. Yariv, H. L. Garvin and R. G. Hunsperger: Appl. Phys. Lett. 22,46(1973)

6. S. Somekh : Introduction to Integrated Optics, ed. M. K. Barnoski (Plenum Press, New York, 1974), Chapter 11.

Modular Optics Interferometer

S. K. Case*
Virginia Polytechnic Institute and State University
Blacksburg, Virginia 24061

and

R. A. Russell
Department of Electrical Engineering
The University of Michigan
Ann Arbor, Michigan 48109

Abstract

A waveguide interferometer is assembled using holographically formed optical elements that are constructed as individual components and can be selectively attached to an optical waveguide. The interferometer is very rugged and easy to align.

*Work performed at The University of Michigan.

1. Modular Optical Elements

We describe modular optical elements as miniature optical components that are individually constructed and can be selectively attached to the surface of an optical waveguide.[1,2,3] These components can be individually adjusted to optimize system performance. In this paper, we describe the construction and use of modular optical elements to form a waveguide interferometer.

Our optical modules consist of holographic optical elements constructed in dichromated gelatin films that are coated on glass substrates. Each element serves as both a grating waveguide-coupler and a beam splitter, as shown in Fig. 1. The modular gratings are constructed by incoherently superimposing two thick gratings within a dichromated gelatin film such that the two gratings have a common Bragg angle, A.[1] Readout at the angle A will produce two diffracted waves each of which contains half of the incident energy.[4] The two diffracted waves are at angles such that they will both be trapped within the guide G.

2. The Interferometer

Having constructed our grating modules, we assemble our in-line interferometer by placing two of these modular gratings on the surface of the thick glass optical waveguide as shown in Fig. 2. Xylene is used as an index matching liquid between the modules and the guide. The first element (on the left) is used as the waveguide coupler and beam splitter while the second element acts as a beam-combiner and decoupler.

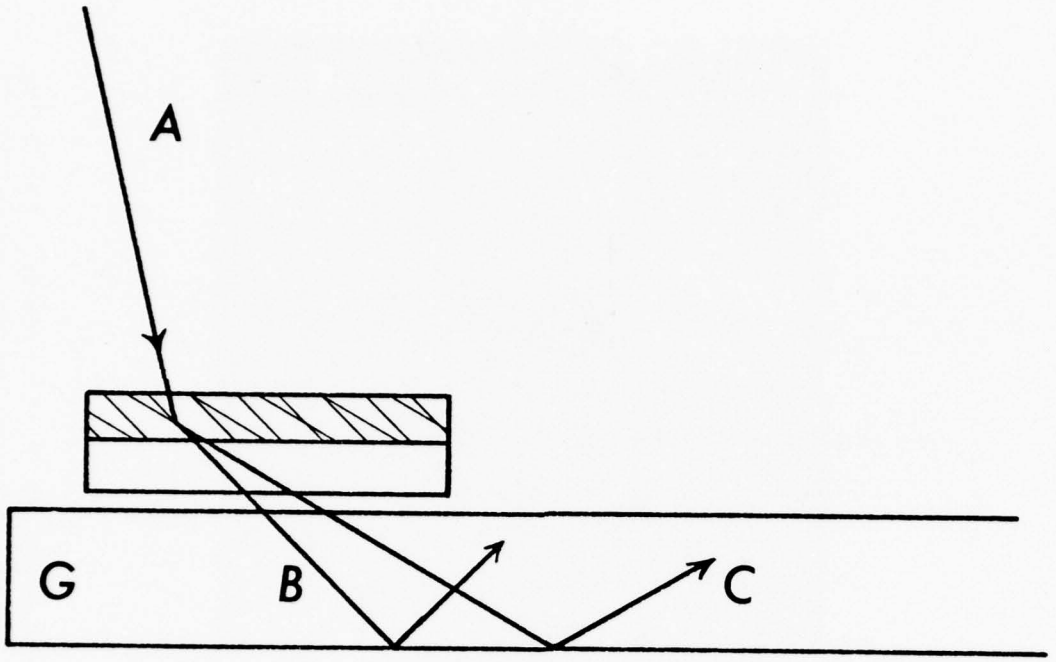

Fig. 1

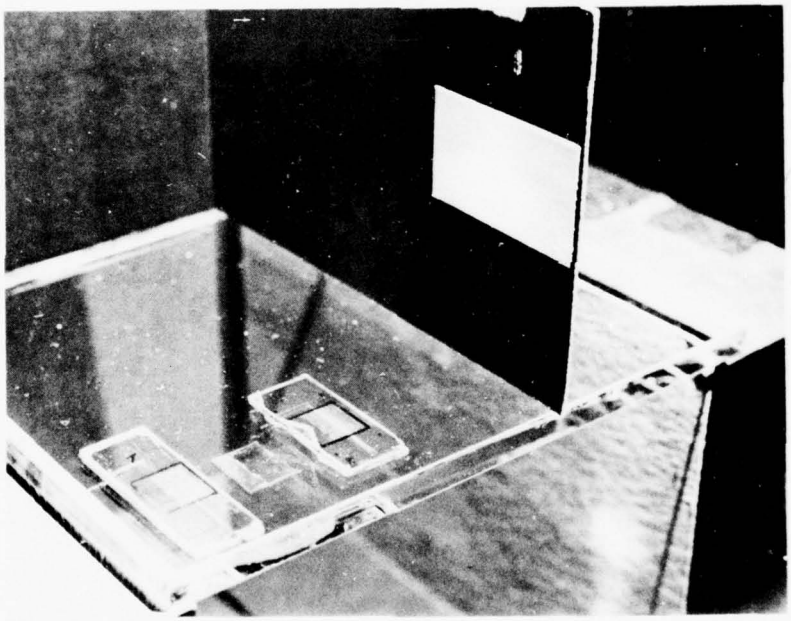

Fig. 2. The waveguide interferometer. Proceeding from left to right, one can see the coupler module, the test object, the decoupler module and the output beam which strikes the white card.

The interferometer is used by illuminating the coupler module with a coherent beam of light from the upper left in Fig. 2. Since the incident wave (A in Fig. 1) has a finite cross sectional area ($\simeq$ 1 cm^2), the waveguide is thick ($\simeq$ 6 mm) and the waves B and C propagate at greatly different angles ($\simeq 20^o$ difference), the areas at which the guided waves strike the surface of the guide are physically separated. Thus, we can insert a sample into the interferometer by laying it on the surface of the waveguide at a position where only one of the guided waves (e.g. wave C) strikes the surface. An index matching liquid (in this case, xylene) is placed between the sample and the guide. Thus, guided wave C leaves the guide, passes through the sample, and re-enters the guide as a modulated wave. A short distance later, where waves B and C again overlap, the beam combiner has been placed on the surface of the guide. This modular element in identical in construction to the beam splitter element and is merely rotated by 180^o (about a vertical axis in Fig. 1) before being placed on the guide. The two guided waves simultaneously enter the final grating, are combined, and are diffracted out of the guide.[4] The combined waves leave the guide at approximately 45^o as can be seen in Fig. 2 where they strike a white card after leaving the interferometer.

3. Experimental Results

The output of the interferometer is photographed by placing a camera in place of the white card in Fig. 2. With no sample in the interferometer, we see straight fringes present on the output (Fig. 3). The fringe frequency in Fig. 3 can easily be varied by small rotations

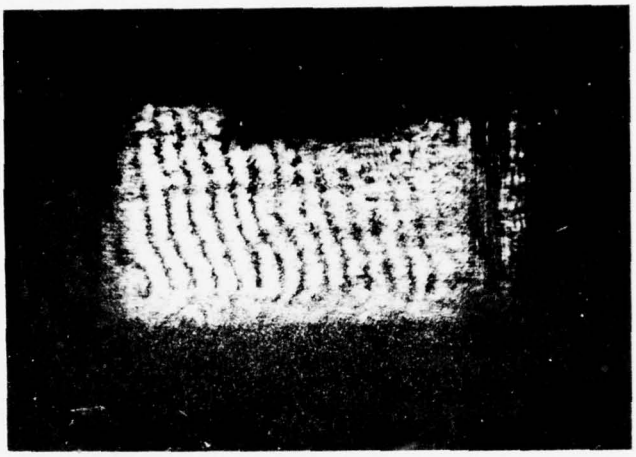

Fig. 3. The interferometer output showing straight fringes when no test object is in the interferometer.

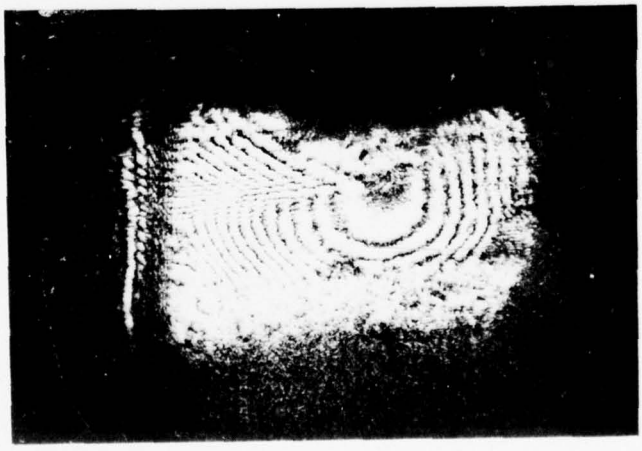

Fig. 4. Interferometer output when a piece of thin glass with a deep scratch is used as a test object.

of the final grating (about a vertical axis in Fig. 1). Because the angles between guided waves B and C are fixed during grating construction and cannot get out of alignment, the only adjustment that ever needs to be done is a slight rotation of the gratings.

In Fig. 4, we see the output when an object has been inserted into the interferometer. The test object is a small piece of glass (microscope slide cover-glass) in which we have put a deep scratch with a glass cutter. The scratch extends half way across our test object and shows up as dislocated fringes on the left side of the output.

4. Conclusions

The modular interferometer we have demonstrated is easy to adjust and is very rugged. Rapid changes in air temperature or air currents have little effect on the device.

The modular coupler elements can easily and quickly be placed on any piece of glass which we would like to interferometrically test for flatness or other optical properties.

Acknowledgements

The authors wish to thank Prof. Emmett Leith for discussions during the course of this work. We thank the Office of Naval Research and the National Science Foundation (Grant GK 43148) for their generous support.

References

1. S. K. Case and M. K. Han, Optics Commun. 15 (1975) 306.
2. J. S. Wei and C. C. Tan, Appl. Opt. 15 (1976) 289.
3. S. K. Case and R. A. Russell, Appl. Opt. 15 (1976) 2307.
4. S. K. Case, J. Opt. Soc. Am. 65 (1975) 724.

Analysis of Optical Propagation in Thick Reflection Gratings

W. Y. WANG

University of Michigan

Department of Electrical and Computer Engineering

Ann Arbor, Michigan 48109

Abstract

A method of analyzing optical propagation in thick holographic reflection grating by decomposition of the thick grating into thin slabs is investigated. The method is applicable to study higher order Bragg diffraction process in thick reflection grating. The method is shown analytically to be equivalent to the coupled-wave solution of Maxwell's equations for a thick sinusoidal reflection grating.

1. Introduction

A physically intuitive method for analyzing wave propagation in thick holographic transmission grating was developed by R. Alferness[1] in which the thick gratings are mathematically decomposed into a series of thin slabs, with each acting as a thin grating. For a readout plane wave of arbitrary spatial frequency, the total amplitude of the zero and dissracted orders is derived from computing the succesive effect of each thin grating is determined solely by thin grating theory. The thin grating decomposition method (TGD) for transmission grating has been widely used to study higher order diffraction and waveguide phenomenon. However, the coupling matrix does not apply to the case of reflection gratings. Recently, the use of reflection gratings has been considered for integrated, in such application as wavelength fibers and distributed feedback (DFB) and distributed Bragg reflector (DBR) lasers. In this paper, the TGD coupling matrix method is extended to the reflection grating case.

Our method for analyzing optical propagation in volume reflection grating offers, because of its conceptual simplicity and ease of implementation, advantages over the theory given by Burckhart[2] and Kasper[3]. Like the matrix theory the method is numerical; it requires only matrix multiplication and it proceeds to decompose the thick reflection grating into a series of thin slabs, each of which acts simply as a thin grating.

2. Description of the Method. We describe the method with a single reflection grating structure produced holographically, as shown in Fig. 1. The film emulsion of thickness of D is perpendicular to the z-axis and is assumed to be of infinite extent in the x and y directions. Plane wave R of amplitude a_1 incident at angle θ_1 (angle measured inside the emulsion) with respect to the z-axis, and plane wave S of amplitude a_2 at θ_2 interfere to produce a grating throughout the volume of the emulsion. The exposure $E = I\tau$ (I is the total intensity and τ is the exposure time) can be written as

$$E(x,z) = \tau I_o[1 + r \cos 2\pi f(z - z_x)] \quad ,$$

where $f = n_0(\cos \theta_1 + \cos \theta_2)/\lambda$ is defined as the spatial frequency in the z-direction, λ is the free space wavelength, $z_x = x \tan \theta$, $\theta = (\theta_1 - \theta_2)/2$ is the slant of the fringes, $I_o = a_1^2 + a_2^2$, and $\gamma = 2a_1a_2/(a_1^2 + a_2^2)$. For any plane x = constant with Δz as the thickness of the thin slab, the fringes are sinusoidally modulated with frequency f. However, because of fringe slant (when the construction geometry is not symmetrical about the x-axis) the fringes at z are shifted by z_x relative to those at x = 0, which introduce a relative phase shift of $-2\pi f z_x$.

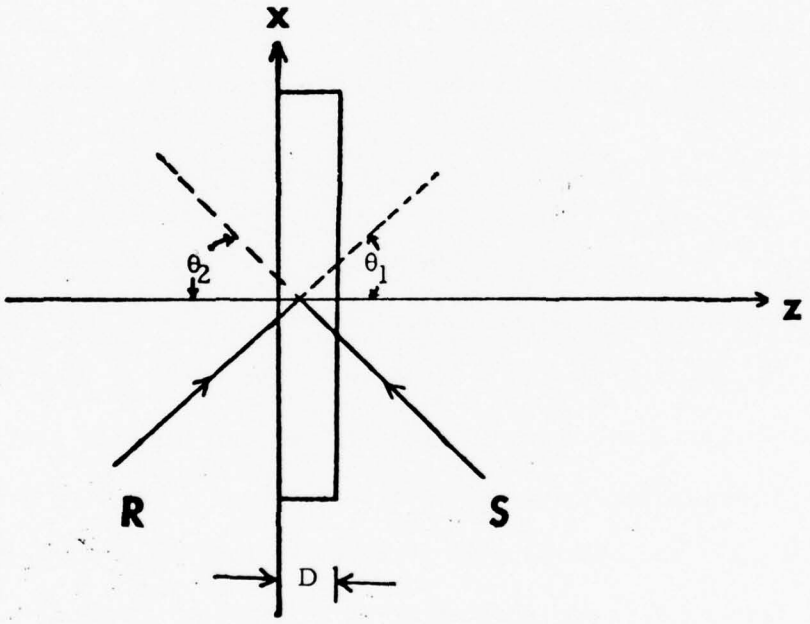

Fig. 1 Construction geometry of holographic reflection grating by interfering two plane waves R and S.

We examine the properties of optical propagation in the thick reflection grating of Fig. 1 by decomposing it into a series of thin slabs of thickness Δz which must be sufficiently small. The proper upper limit on Δz is that for a fixed readout wavelength and grating frequency, Kogelnik's[4] Q factor ($Q = 2\pi\lambda\Delta z f^2/n_0$) for the thin grating be less than one. Each of the thin gratings, therefore, exhibits no Bragg effects and its angular distribution of diffracted light is calculated based on the thin grating theory. We assume a pure phase reflection hologram in which the diffraction process takes place discretely at the plane $z = n\Delta z$, $n = 1,2,\ldots$. We also assume a linear relationship between the index of refraction and the exposure E: $n(x) = ME$. Therefore, the amplitude transmittance as a result from the exposure given by Eq. 1 for a plane wave at θ_i is expanded according to the method by Alferness[1]:

$$T_A(x,z) = \exp\left\{ 2\pi[n_0 + n_1 \cos 2\pi f(z - z_x)]\right\}\Delta z/\lambda \cos\theta_i \qquad (2)$$

and

$$T_A(x,z) = \exp\left\{\left[\frac{i2\pi n_0 \Delta z}{\lambda \cos\theta_i}\right] \sum_{q=-\infty}^{+\infty} (j)^q J_q(b) \exp\left[j2\pi q f(z - z_n)\right]\right\} \qquad (3)$$

where $J_q(b)$ is the q^{th} order Bessel function $b = (2\lambda\Delta z n_1/\lambda \cos\theta_i)$ and $z_n = x \tan\theta$. The n^{th} thin grating can be represented by an infinite superposition of amplitude gratings of spatial frequency qf with diffraction amplitudes equal to the qth order Bessel function. The terms with minus q portion in the summation sign correspond to the reflected diffracted waves and the terms with positive q portion correspond to the transmitted diffracted wave. The exponential outside the summation sign in Eq. 3 represents an unimportant common factor and can thus be neglected. The q^{th} frequency component is shifted in phase by $-2qf\ x \tan\theta$ because of the fringe slant. This phase determines the Bragg angle in the slanted reflection grating.

To find the effect of the thin slab upon an incident, a forward and a backward plane wave of arbitrary spatial frequency, we extend the thin grating theory to include the propagation factors of both forward and backward plane waves of arbitrary spatial frequency in the thin slab. First, propagation factors of the incident waves over the interval can be described by the free space transfer function. Then, the separation of incident forward or backward waves into the various diffracted waves at $z = n\Delta z$ is described by the amplitude transmittance function in Eq. 3. Therefore, for an input forward plane wave of x-spatial frequency f_i, amplitude A_{if} and phase θ_i at $z = (n - 1)\Delta z$, the field at $z = n\Delta z$ (i.e., out of the n^{th} grating) is

$$A_f(x, n\Delta z) = \exp(j\phi_i)\, A_{if} \sum_{q=-\infty}^{+\infty} (j)^q J_q(b) \exp(-j2\pi q f z_n)$$
$$\exp(jf_i x) \exp\left[j \frac{2\pi n_0}{\lambda} \sqrt{1 - (\lambda f_i/n_0)}\ \Delta z\right]$$
$$\exp(j2\pi q f z) \exp(jf_{iz} z) \quad , \qquad (4)$$

where $f_{iq} = f_i - 2\pi q f \tan\theta$ and

$$f_{iz} = \sqrt{1 - [(\lambda/n_0) f_{iq}]^2} .$$

Similar results can be obtained in an input backward plane wave except for a minus sign in the directional cosine. Therefore, each plane wave incident upon the n^{th} slab generates a countable number of plane waves with z-spatial frequency $(f_{iz} + qf)$. The amplitude of the q^{th} wave is the product of the input amplitude and the strength of the q^{th} grating frequency component.

The phase of each wave is given by three factors. The term $\exp(-j2\pi q f z_n)$ in Eq. 4. represents a phase shift resulting from the parallel shift of the n^{th} grating relative to the $(n-1)^{th}$ (a result of the fringe slant). The term

$$\exp\left\{\frac{jn_0 2\pi}{\lambda}\left[1 - \left(\frac{\lambda f_i}{n_0}\right)^2\right]^{1/2} \Delta z\right\}$$

gives the phase shift due to propagation through the distance Δz. In addition, because a phase material is used, there is the phase factor $(j)^q$. Then each plane wave output from the n^{th} slab is an input to the $(n+1)$ slab.

The thick grating is illuminated at $z = 0$ with a plane wave of z-spatial frequency f_{iz} and an amplitude R_i. We represent the amplitudes of each of the possible plane waves that exit from the n^{th} grating by

$$A_n = \begin{pmatrix} R_0 \\ S_0 \\ R_1 \\ S_1 \\ R_\ell \\ S_\ell \end{pmatrix}_n , \quad \ell \text{ integer} \geq 0 , \tag{5}$$

where R_ℓ is the total amplitude of the forward wave of z-spatial frequency $(f_{iz} + \ell f)$ while S_ℓ is the total amplitude of the backward wave of spatial frequency $[f_i - (\ell + 1)f]$. Because Eq. 4 is valid for an input plane wave of arbitrary spatial frequency, we can relate the total amplitude of each of the plane waves at $z = n\Delta z$ to its value at $z = (n - 1)\Delta z$ by

$$A_n = {}_nHA_{n-1} \quad , \tag{6}$$

where the matrix of coupling coefficients ${}_nH_{kj}$ determined from Eq. 2.19 describe the amplitude and phase shift effected by the n^{th} thin slab in diffracting the j^{th} plane wave into the k^{th} plane wave. The coupling matrix for the pure phase case appears in Appendix A.

If we use the initial condition at $z = 0$ to write

$$A_o = \begin{pmatrix} R_o \\ S_o \\ R_1 \\ S_1 \\ \vdots \end{pmatrix}_0 \quad , \tag{7}$$

the amplitude at $z = n\Delta z$ will be

$$A_n = {}_nH, \ldots, {}_1HA_o \tag{8}$$

The amplitude of each of the plane waves at the exit plane $z = D$ is given by Eq. 8 for $n = N = D/\Delta z$.

3. Results and Their Equivalence to Coupled Wave Approach. For a grating with sufficiently high Q factor it is assumed that only the zero and one diffracted order are significant for readout about the first order Bragg angle. Because only two orders are

important, the coupling matrix for the n^{th} thin grating in Eq. 4 can be truncated to a 2 x 2 matrix:

$$ {}^{n}H = \begin{bmatrix} e^{j\alpha_o} J_o(b_o) & je^{+j\alpha_1} J_1(b_1) e^{j\delta(n)} \\ -je^{j\alpha_o} J_{-1}(b_o) e^{-j\delta(n)} & e^{+j\alpha_1} J_o(b_1) \end{bmatrix} , \qquad (9) $$

where $b_\ell = 2\pi\Delta z n_1/\lambda \cos\theta_\ell$,

$\alpha_\ell = 2\pi\Delta z \cos\theta_\ell/\lambda$,

$\delta = 2\pi n f x \tan\theta$,

$\cos\theta_\ell = [1 - (\lambda/n_0)^2 f_\ell^2]^{1/2}$, $\ell = 0,1,\ldots$, (10)

$f_o = f_i$ = the x-spatial frequency of the readout wave,

λ = the free space wavelength of the readout wave,

θ = the slope of the fringes with respect to the x axis, and

n_1 = the index modulation of the grating.

To simplify we assume that the fringe slope angle θ is zero (i.e., unslanted fringes). For typical values of index modulation and Δz arbitrarily small, we can approximate the Bessel functions by their first order approximations,

$$ J_o(x) \simeq 1 , J_1(x) \simeq x/2 \quad \text{for} \quad x << 1 . $$

The coupling matrix for each thin slab can therefore be written as

$$ H = \exp\left(j \frac{2\pi n_0}{\lambda} \Delta z \cos\theta_o\right) \begin{bmatrix} 1 & -j \frac{\gamma}{\cos\theta_1} e^{j2\Phi} \\ \frac{Jr}{\cos\theta_o} & e^{j2\Phi} \end{bmatrix} , \qquad (11) $$

where $\gamma = \pi n_1 \Delta z/\lambda$ and

$$2\Phi = (2\pi n_0 \Delta z/\lambda)(-\cos\theta_c + \cos\theta_1), \tag{12}$$

in which $J_{-1}(x) = J_{-1}(x)$. All angles are internal,

$$2\Phi = 2\pi n_0 \Delta z/\lambda \quad \text{or} \quad 2\Phi = -2\pi n_0 \Delta z(\Delta\lambda)\cos\theta_o/\lambda \quad . \tag{13}$$

If the amplitudes of the zero and first order at the n^{th} thin slab are expressed by the elements of a column vector

$$A(n) = \begin{pmatrix} A_o \\ A_1 \end{pmatrix}_n , \tag{14}$$

then the value of A at the exit plane of the emulsion, z = D is

$$A(N) = H^N A(0) , \tag{15}$$

where $N = D/\Delta z$ and initial conditions

$$\text{at } z = D \ , \ R(0) = R \ , \ S(0) = 0 \rightarrow A(0) = \begin{pmatrix} R \\ 0 \end{pmatrix} \tag{16}$$

and

$$\text{at } z = 0 \ , \ R(N) = 1 \ , \ S(N) = S_N \rightarrow A(N) = \begin{pmatrix} 1 \\ S_N \end{pmatrix} , \tag{16}$$

can be obtained by performing the matrix multiplication of Eq.15 in the limit $N \rightarrow \infty$, $\Delta z \rightarrow 0$ such that $N\Delta z = D$.

As shown by the coupling matrix of Eq. 11 2Φ represents a relative phase shift between the two forward and backward waves that were produced by a thin slab when the reconstruction wave length or angle differ from their construction values. It is this phase shift that causes the decrease in diffraction efficiency for readout waves incident off the Bragg angle; Φ corresponds to the dephasing parameter of the coupled-wave theory.

The matrix multiplication of Eq. 15 is greatly simplified when H is represented in a basis such that it is diagonal. The diagonal elements are just the eigenvalues of H and the basis vectors are the associated eigenvectors. The eigenvalue of H can be easily shown to be

$$\psi_{1,2} = \exp(j\Phi) \exp\left[\pm \left(\frac{\gamma^2}{|C_o C_1|} - \Phi^2\right)^{1/2}\right] , \tag{17}$$

where we have used the limit $\Delta z \to 0$ to set $\sin^2 \theta = \theta^2$. Also, $C_o = -C_1 = \cos \theta_o$. The associated eigenvector E_1, E_2 are then

$$\begin{pmatrix} E_1 \\ E_2 \end{pmatrix} = \begin{pmatrix} 1 & a_1 \\ 1 & a_2 \end{pmatrix} \begin{pmatrix} A_0 \\ A_1 \end{pmatrix} \tag{18}$$

where $a_i = j(C_1/\gamma)(1 - \psi_i)e^{-j2\Phi}$.

From Eq. 11 and the initial condition on A (Eq. 16), we find the initial condition in the E basis; $E(0) = \begin{pmatrix} R \\ R \end{pmatrix}$. Therefore, in the diagonal representation,

$$E(N) = \begin{pmatrix} \psi_1^N & 0 \\ 0 & \psi_2^N \end{pmatrix} \begin{pmatrix} R \\ R \end{pmatrix} = \begin{pmatrix} Rx & \psi_1^N \\ Rx & \psi_2^N \end{pmatrix} . \tag{19}$$

We then use the inverse of the transformation of Eq. 18 to transform back to the original representation to find the amplitude of the diffracted order:

$$A_1(N) = \frac{R}{(a_2 - a_1)} (\psi_2^N - \psi_1^N) \tag{20}$$

and

$$A_o(N) = 1 = R(a_2\psi_2^N - a_i\psi_1^N)/(a_2 - a_1) . \tag{21}$$

Thus,

$$A_o(N) = Rxe^{j\Phi}x\left[j\Phi \sinh\left(\frac{N^2\gamma^2}{|C_0C_1|} - \Phi^2N^2\right)^{1/2} + \left(\frac{\gamma^2}{|C_0C_1|} - \Phi^2\right)^{1/2} x \cosh\left(\frac{\gamma^2N^2}{|C_0C_1|} - \Phi^2N^2\right)^{1/2}\right] x\left(\frac{\gamma^2}{|C_0C_1|} - \Phi^2\right)^{-1/2} = 1 ,$$

$$A_1(N) = Rxjx\left(\frac{\gamma}{C_1}\right)x \frac{\sinh\left(\frac{N^2\gamma^2}{|C_0C_1|} - N^2\gamma^2\right)^{1/2}}{\left(\frac{\gamma^2}{|C_0C_1|} - \Phi^2\right)^{1/2}} . \qquad (22)$$

From Alferness [5], we have $N^2\gamma^2/C_0C_1 \to \nu^2$ and $N^2\Phi \to \xi$ in Kogelnik's [4] notation, therefore

$$A_1(N) = \frac{-je^{j\Phi}\left(\frac{C_0}{C_1}\right)^{1/2}}{j\xi/\nu + (1 - \xi^2/\nu^2)^{1/2} \coth (\nu^2 - \xi^2)^{1/2}} , \qquad (23)$$

which is identical to Kogelnik's formula. The diffraction efficiency is

$$DE(N) = \frac{C_1}{C_0}|A_1(N)|^2 = 1/[1 + (1 - \xi^2/\nu^2)/\sinh^2 (\nu^2 - \xi^2)^{1/2}] . \qquad (24)$$

We have thus shown analytically the equivalence between the method of reflecting thin grating decomposition and Kogelnik's coupled-wave solution for wave propagation in a thick sinusoidal reflecting grating for which the assumption of the latter theory are valid. It is easy to write a computer program for solving any nonuniformly longitudinal index modulation cases.

Acknowledgments

We are thankful to Professor E. N. Leith for his encouragement and valuable guidance in our work. We are also grateful for the support of the Office of Naval Research (Contract No. N00014-67-A-0181-0058) and the National Science Foundation (Grant No. ENG 73-04166 A01).

References

1. R. Alferness, Appl. Phys. 7, 29 (1975).

2. C. B. Burckhardt, J. Opt. Soc. Am. 56, 1502 (1966).

3. F. G. Kaspar, J. Opt. Soc. Am. 63, 37 (1973).

4. H. Kogelnik, Bell Syst. Tech. J. 48, 2909 (1969).

5. R. Alferness, Optics Commun. 15, 209 (1975).

BRAGG EFFECT WAVEGUIDE COUPLER ANALYSIS

W. Y. Wang AND T. J. DiLaura

UNIVERSITY OF MICHIGAN
DEPARTMENT OF ELECTRICAL AND COMPUTER ENGINEERING
ELECTRO-OPTICS LABORATORY
ANN ARBOR, MICHIGAN 48109

ABSTRACT

We present an approach to the analysis of a holographically produced grating coupler, in which we separate the coupling problem into independent slab waveguide and diffraction grating problems. Considering the guiding structure as a slab waveguide, we obtain the paramenters of the propagating modes of the coupler through conventional analysis. The diffraction efficiency of the grating orders are then calculated by using the thin grating decomposition method (TGD). Utilizing the propagating mode angles of the waveguide and the calculated diffraction efficiencies of the grating, we are able to calculate the radiation loss coefficient and therefore the coupling efficiency of the holographic waveguide coupler.

Introduction

The basic component of an integrated optical circuit is the thin-film dielectric waveguide upon which a waveguide coupler is built. The waveguide coupler can be used to convert an incident light beam into a mode, or modes, of the waveguide. Couplers which are integral components of the waveguide are either corrugated surface gratings or holographic gratings above the waveguide. We suggest a third waveguide coupler configuration in which the grating is fabricated inside the waveguide structure. We initially adapted the first-order perturbation analysis of Ogawa[1] to this structure but obtained an excessively high radiation loss coefficient. Peng et. al[2] used the rigorous electromagnetic boundary problem to analyze the holographic grating coupler above the waveguide, but this method seems inapplicable to the case where the grating is inside the waveguide. We therefore develope a different approach, where we separate the analysis into a diffraction grating analysis and a slab waveguide analysis. We obtain guided and radiation modes as solutions of the unperturbed waveguide structure using a conventional slab waveguide

analysis. We then use the thin grating decomposition method of Alferness[3] to analyze the grating diffraction process which produces an exchange of energy among the guided and radiation modes as the guided wave propagates through the thickness of the grating waveguide. Combining the slab waveguide and diffraction grating results we then determine the radiation loss coefficient by accounting for the energy lost through radiation modes. From such a description of the waveguide coupler we then determine the corresponding coupling efficiency.

Problem Formulation

The coupler problem to be solved is described with reference to Fig.1. A plane wave (not shown) impinges on the grating from its air side, at an angle which satisfies the second Bragg condition for the grating in the waveguide. The grating is constructed so that the second diffracted order is a propagating mode for the planar waveguide structure containing the grating. As this diffracted wave propagates, a portion of its energy is diffracted into the first and second orders thus producing a coupler loss mechanism.

For purposes of analysis we find it convenient to reverse the process using the concept of optical reciprocity. We assume that a guided, propagating wave (represented in Fig.1 by Poynting vector $P^{(0)}$) is incident on the grating portion of the waveguide. As it travels it produces diffracted waves $P^{(-1)}$ and $P^{(-2)}$. By calculating the magnitude of these diffracted waves, we can obtain the amount of incident light remaining in $P^{(0)}$ and lost into $P^{(-1)}$ and $P^{(-2)}$. We can therefore obtain the radiation loss coefficient and the coupling efficiency which characterize the grating waveguide coupler.

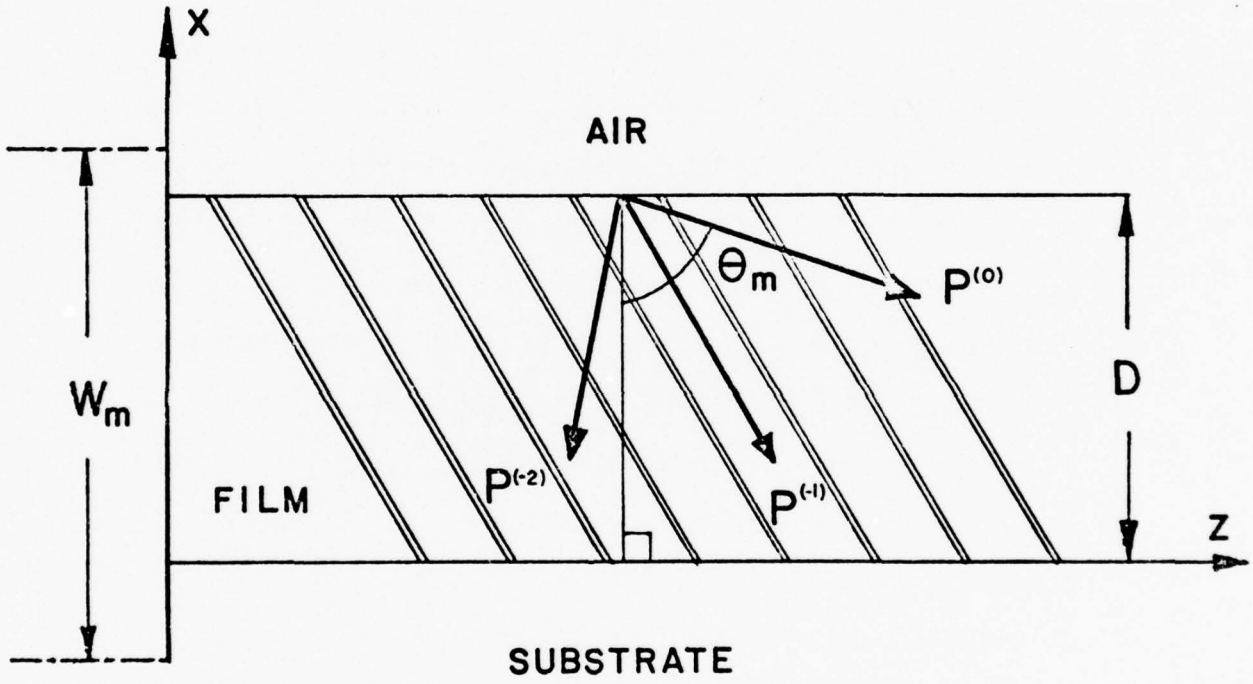

FIG. 1

Schematic diagram of grating waveguide configuration with guided mode (zeroth order) Poynting vector ($P^{(0)}$) and radiation mode (first and second order) Poynting vectors ($P^{(-1)}, P^{(-2)}$).

From a geometrical optics viewpoint we solve the planar waveguide problem for the mode reflection angle (θ_m), the effective guide width (W_m) and the Poynting vector ($P^{(q)}$) and also define a mode bouncing rate B_m. We assume that the guided wave with amplitude A is reflected back and forth between the waveguide boundaries at angles θ_m and $-\theta_m$. The effective guide width is obtained from the expression $W_m \simeq D + p_a^{-1} + p_s^{-1}$, where p_a and p_s are the exponential decay rates for mode m in the air and substrate regions with refractive indices n_a and n_s, respectively. The bounce rate for mode m in terms of θ_m and W_m becomes,

$$B_m = [2W_m \tan\theta_m]^{-1} . \qquad (1)$$

In Fig. 1 there are two diffracted wave orders with Poynting vectors $P^{(-1)}$ and $P^{(-2)}$. Using these Poynting vectors, a diffraction efficiency can be defined as the fractional amount of incident power diffracted into the various orders. Defining these ratios of power flow in the x direction in terms of amplitude ratios, we obtain

$$\eta_d^{(q)} = \frac{\cos\theta_e^{(q)}}{\cos\theta_m} \frac{|A^{(q)}|^2}{|A_i|^2} \qquad (2)$$

where ,

$\eta_d^{(q)}$ = diffraction efficiency of q^{th} order

$A^{(q)}$ = amplitude of q^{th} order wave after propagation through grating

A_i = amplitude of incident wave on grating

θ_m = angle of m^{th} propagating mode

$\theta_e^{(q)}$ = external angle of diffracted q^{th} order, where $n_g \sin\theta^{(q)} = n_e \sin\theta_e^{(q)}$

$\theta^{(q)}$ = internal angle of diffracted q^{th} order

n_e = index of external medium of q^{th} order

n_g = bulk index of grating .

It should be noted that the diffraction efficiency of a particular mode depends upon whether it remains in the waveguide or escapes to the substrate or air. This dependence is accounted for by setting n_e equal to the index of the material in to which the q^{th} order escapes or is trapped, θ_e being the external angle in this medium. By using the TGD method we can determine the amplitudes of the different Bragg diffraction output orders ($A^{(q)}$) for a given amplitude input (A_i).

The analysis of conventional bulk phase gratings is applicable to the thin film grating coupler. The basic difference between these two grating types is

that a bulk grating diffracts one free space propagation beam into another, whereas the Bragg thin film grating coupler transforms a free space propagation mode into a leaky guided mode of the waveguide. The leaky mode m is coupled into transmitted radiation modes via diffraction by the same grating orders which coupled the light into that leaky guided mode.

The power lost over the length of the grating coupler is characterized by the power loss coefficient, α_p or equivalently by the amplitude loss coefficient α_a. Because this loss is caused by diffraction of the guided wave by the grating, the loss coefficients become directly proportional to the diffraction efficiency of each diffracted order. We proceed to obtain the characteristic amplitude loss coefficient in terms of the diffraction efficiencies by considering a single section of the grating parallel to the x-axis. We then extend the results over the entire length of the grating to obtain a radiation (amplitude) loss coefficient and the coupling efficiency of the grating coupler.

Loss Mechanisms and the Coupling Coefficient

In the following approach we use the ray optics method to obtain an expression for the amplitude of the leaky guided mode and the radiation loss coefficient. Referring to Fig.2 we divide the total grating length into sections ($2W_m \tan\theta_m$) over which one bounce of the leaky guided mode occurs. We note that this is the distance in the z direction separating equi-phase points along the ray path. We qualify the loss over this section as the decrease in incident amplitude (A_i) diffracted out of the leaky guided mode as it satisfies the Bragg diffraction condition for the grating over one half of the section length. Therefore the guided wave amplitude after propagation through one section is,

$$A = [1-\eta_d^{(1)} - \eta_d^{(2)}]^{1/2} A_i. \qquad (3)$$

We now consider the field at some plane $z = \ell B_m^{-1}$. Allowing the guided wave to propagate through ℓ sections of the grating coupler and normalizing A_o to one, we obtain for the leaky guided mode amplitude,

$$A = [1-\eta_d^{(1)} - \eta_d^{(2)}]^{\ell/2}$$

$$\text{or,} \quad A \simeq \exp[-(\eta_d^{(1)} + \eta_d^{(2)}) \tfrac{\ell}{2}] \qquad (4)$$

$$= \exp[-(\frac{\eta_d^{(1)} + \eta_d^{(2)}}{2})(\frac{z}{2W_m \tan\theta_m})] \qquad (5)$$

$$= \exp[-\alpha_a z] \qquad (6)$$

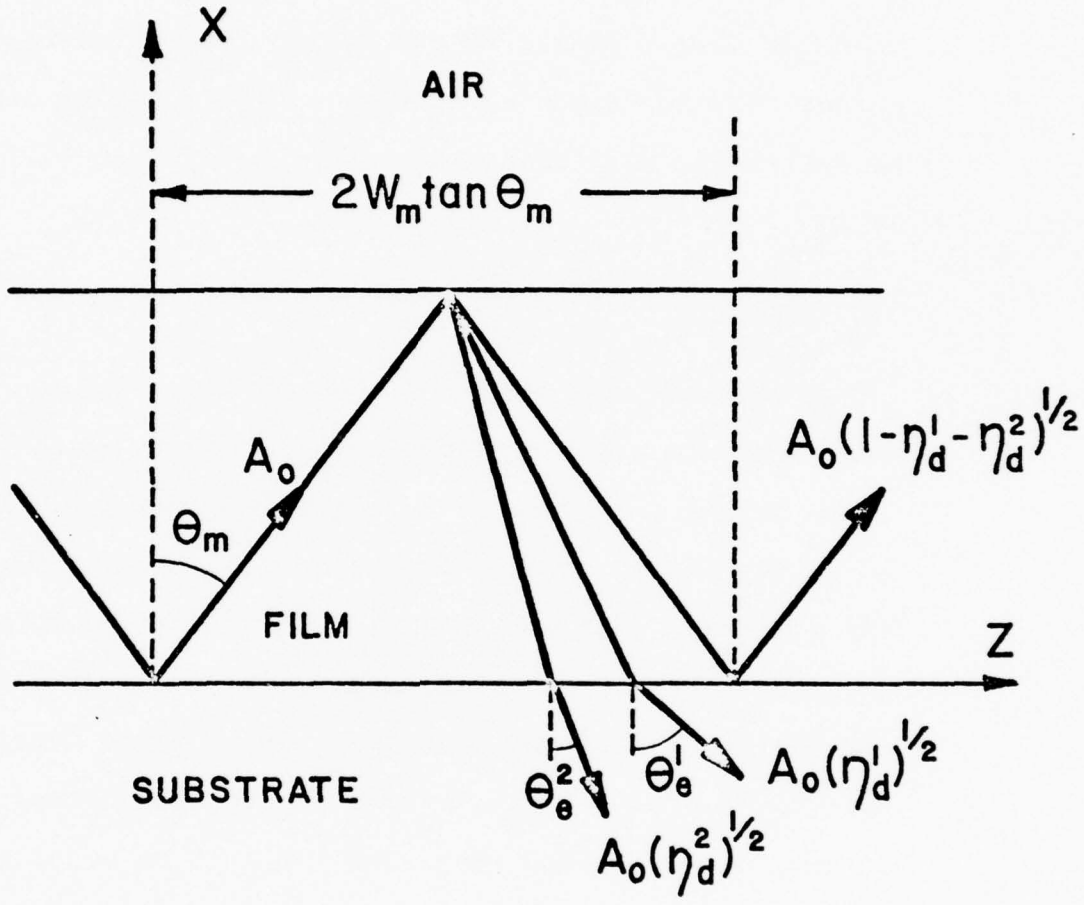

FIG. 2

One unit of the sectionalization of the grating structure, illustrating the decoupled energy, $A_o(\eta_d^1)^{1/2}$ and $A_o(\eta_d^2)^{1/2}$ with the remaining coupled energy. Loss occurs only over one half of the section where the guided mode satisfies the Bragg condition.

where we have obtained an expression for the leaky guided mode amplitude along the length of the coupler. We define the total radiation loss coefficient (α_a) to be,

$$\alpha_a = \frac{\eta_d^{(1)} + \eta_d^{(2)}}{4W_m \tan\theta_m} \quad . \tag{7}$$

The leaky mode amplitude therefore decays as $\exp(-\alpha_a z)$ for $z > 0$. Since the energy lost in the leaky guided mode must be gained by the radiation mode, the radiation mode in the near field outside the waveguide must have an exponential shape complementary to the guided leaky mode. The amplitude of the radiation mode can be calculated from the fact that for a semi-infinitely long grating the energy of an incident guided mode at $z = 0$ must be equal to the integrated energy in the radiation mode. The energy becomes,

$$1 = \int_0^\infty E_r^2(z)\,dx \tag{8}$$

where we set the integral equal to the initial normalized energy of one in the guided mode. The electric field of the radiation is then given by,

$$E_r(z) = E_o \exp(-\alpha_a z) \quad . \tag{9}$$

Substituting Eq.9 and evaluating Eq.8 gives,

$$E_r(z) = \sqrt{2\alpha_a}\ \exp(-\alpha_a z) \quad . \qquad (10)$$

This equation describes the near field directly adjacent to the grating waveguide. Using the optical reciprocity theorem we apply the above results, obtained through analyzing the decoupling process, to the coupling process to derive the coupling efficiency (η_c) of light diffracted into a guided mode.

For an infinitely long output grating waveguide characterized by α_a, all the initially guided light is coupled into a radiation mode and has an amplitude distribution $E_r(z)$ given by Eq.10. If the same grating waveguide is used as an input coupler, a 100% coupling efficiency can be obtained if the input amplitude distribution $E_i(z)$ has the field distribution $E_r(z)$ and propagates in the opposite direction. In most cases, $E_i(z) \neq E_r(z)$ so that some incident energy is either reflected or transmitted. Therefore the diffraction efficiency for light coupled into the waveguide (η_c) is equal to that fraction of the incident field that corresponds to $E_r(z)$. Therefore , where L is the coupler length,

$$\eta_c = \frac{[\int_0^L E_i(z)E_r^*(z)dz]^2}{\int_0^\infty E_i E_i^* dz \int_0^\infty E_r E_r^* dz} \quad . \tag{11}$$

Because the decoupling second order is the only order illuminated in coupling into the waveguide, for our coupler the factor $\eta_d^{(2)}/(\eta_d^{(1)}+\eta_d^{(2)})$ should appear in Eq.11. If α_a is constant and $E_i(z)$ is a uniform plane wave with length L then Eq.11 becomes,

$$\eta_c = \frac{\eta_d^{(2)}}{\eta_d^{(1)}+\eta_d^{(2)}} \left(\frac{2}{\alpha_a L}\right)[1-\exp(-\alpha_a L)]^2 . \tag{12}$$

Eq.12 indicates η_c has a broad maximum with a peak value of approximately 81% for $\alpha_a L = 1.25$ and zero first order efficiency.

Calculation of Distributed Diffraction Efficiency By TGD

Alferness[3] analyzed the wave propagation in thick holographic gratings by decomposing a thick grating into thin gratings. Such a method can be extended to analyze the optical propagation in the grating inside the waveguide if we consider the mode of the waveguide as consisting of two plane waves propagating at angle θ_m or $-\theta_m$[$\theta_m=\sin^{-1}(n_m/n_g)$]. The index profile of the grating inside the waveguide can be expressed as

$$n(z) = n_g(z)+n_1\cos(2\pi f(z-z_x))+n_2\cos(4\pi f(z-z_x)) \quad (13)$$

where f is the frequency of the fringes in any constant x plane (not the inverse of the perpendicular distance between fringe planes), $z_x = x\tan(\phi)$ where ϕ is the slant angle of the fringes, and n_1 and n_2 are the fundamental and second harmonic index modulation, respectively.

We examine the properties of the optical propagation in the waveguide of thickness D by decomposing it into a series of thin slabs of equal thickness Δx; where the magnitude of Δx is sufficiently small so that each slab acts as a thin grating. The amplitude transmittance resulting from a plane wave incident at

θ_m with input spatial frequency $f_i = n_g \sin(\theta_m)/\lambda$ is,

$$T_A(z,x) = \exp(j2\pi n(z)\Delta x/\lambda\cos\theta_m)$$

$$= \exp(j2\pi n_g \Delta x/\lambda\cos\theta_m) \sum_{q=-\infty}^{\infty} (j)^q J_q(b_1) \qquad (14)$$

$$\times \exp[j2\pi qf(z-z_n)] \sum_{p=-\infty}^{\infty} (j)^p J_p(b_2)$$

$$\times \exp[j4\pi pf(z-z_n)]\exp[j2n_g \Delta x\cos\theta_m/\lambda]$$

where $J_q(b)$ is the q^{th} order Bessel function, $b_i = 2\pi\Delta x n_i/\lambda\cos\theta_m$ (for i=1,2) and $z_n = n\Delta x\tan(\phi)$. The final exponential term is the propagator term of the incident wave over the slab thickness Δx.

As the plane wave propagates through the thickness Δx in the waveguide, it diffractes into an infinite set of plane waves of spatial frequency (2p+q)f and with amplitudes given by the product of Bessel functions of order q and p. Each diffracted wave then becomes the incident wave of the next thin slab and produces another set of diffracted waves according to Eq.14, and so forth. The process is continued until we reach the other boundary of the waveguide, where the original guided-wave undergoes total internal reflection with angle $-\theta_m$. Each diffracted wave will radiate

into the air or substrate region at an angle according to Snell's law.

Our application of thin grating decomposition to the analysis of a waveguide structure containing a slanted grating assumes input at the second order Bragg angle. The output amplitudes A(M) resulting from this initial condition are given by

$$A(M) = H^{M} \begin{bmatrix} 1 \\ 0 \\ 0 \end{bmatrix}, \qquad (15)$$

which is evaluated in the limit as $\Delta x \to 0$ and $m \to \infty$ such that $m\Delta x = D$, and where m is the number of thin film slices, the column vector is the initial input vector, and H is a 3x3 unitary matrix that describes the coupling between three plane waves over a thin slab of thickness Δx. We are then required to perform the multiplication indicated by Eq.15 with initial conditions corresponding to illumination at the second order Bragg angle. Referring to Fig.3 we define $C_o = \cos\theta_m$ and $C_q = \cos\theta_q$. By inspection of Eq.14 the 3 X 3 coupling matrix for each thin grating becomes,

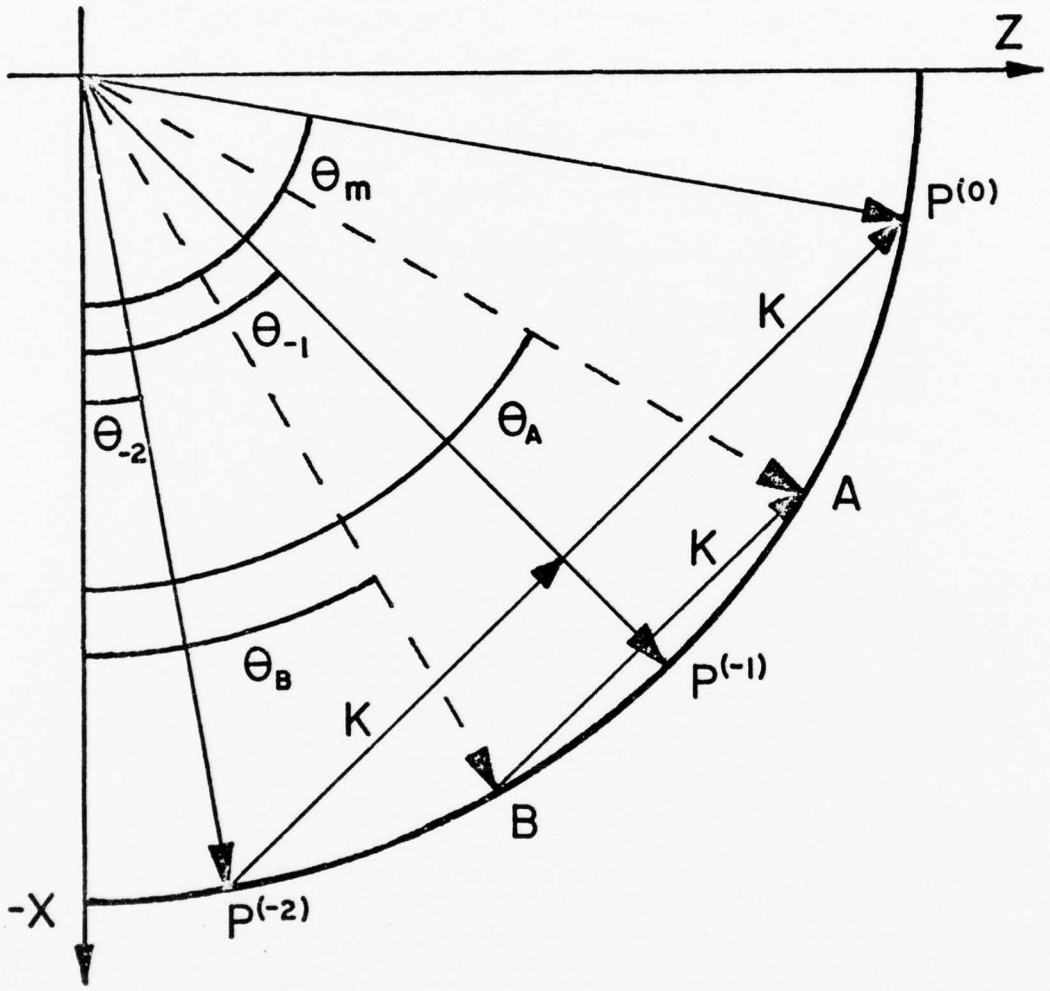

FIG. 3

The Bragg Diagram for the second order diffraction in a slanted grating (represented by grating vector K) which is constructed by interference of plane waves A and B.

$$H = \begin{bmatrix} 1 & j\frac{\delta_1}{C_1} e^{i\Phi_1} & j\frac{\delta_2}{C_2} \\ j\frac{\delta_1}{C_0} & e^{i\Phi_1} & j\frac{\delta_1}{C_2} \\ j\frac{\delta_2}{C_0} & j\frac{\delta_1}{C_1} e^{i\Phi_1} & 1 \end{bmatrix} \qquad (16)$$

where,

$$\Phi_1 = [C_1 - C_0 - \lambda f_z \tan\phi] \frac{2\pi \Delta x n_g}{\lambda}$$

$$\phi = \frac{\theta_1 + \theta_2}{2}$$

$$f_z = \frac{1}{\lambda}(\sin\theta_1 - \sin\theta_2) \qquad (17)$$

$$\delta_i = \frac{\pi n_i \Delta x}{\lambda} \quad (i = 1,2)$$

with θ_1 and θ_2 being the grating construction angles and n_1 and n_2 being the fundamental and first harmonic index modulation. To facilitate the matrix multiplication of Eq.16 we transform the coupling matrix into a diagonal matrix H' such that the M^{th} power of H becomes the M^{th}power of the diagonal elements of H'. The diagonal elements of H' (σ_i) are the eigenvalues of H and satisfy the matrix equation,

$$\det(H - \sigma_i I) = 0 \ . \qquad (18)$$

For convenience we adopt the form of the eigenvalues as, $\sigma_i = 1-j\psi_i \simeq e^{-j\psi i}$ (for small Δx). The eigenvalue problem is to find solutions ψ'_i which satisfy

$$\psi_i'^3 + p'\psi_i'^2 + q'\psi_i' + r' = 0 \qquad (19)$$

(a relationship derived from Eq.16 and 18)

where,

$$p' = \Phi_1$$

$$q' = \frac{-\delta_2^2}{C_0C_2} - \frac{\delta_1^2}{C_0C_1} - \frac{\delta_1^2}{C_1C_2} \qquad (20)$$

$$r' = \frac{2\delta_1^2\delta_2}{C_0C_1C_2} - \frac{\delta_2^2\Phi_1}{C_0C_2} \ .$$

The solutions of Eq.19 become,

$$\psi_o' = U' + V' + P'/3 \qquad (21)$$

$$\psi_1' = \frac{(U'+V')}{2} + \frac{(U'-V')}{2}\sqrt{-3} - \frac{P'}{3} \qquad (22)$$

$$\psi_2' = -\frac{(U'+V')}{2} - \frac{(U'-V')}{2}\sqrt{3} - \frac{P'}{3} \qquad (23)$$

where,

$$U' = \left[-\frac{b'}{2} + \left(\frac{b'^2}{4} + \frac{a'^3}{27}\right)^{1/2}\right]^{1/3} \qquad (24)$$

$$V' = \left[-\frac{b'}{2} - \left(\frac{b'^2}{4} + \frac{a'^3}{27}\right)^{1/2}\right]^{1/3} \qquad (25)$$

with,

$$a' = \frac{1}{3}(3q'-p'^2) \tag{26}$$

$$b' = \frac{1}{27}(2p'^3-9p'q' + 27r'). \tag{27}$$

The output amplitudes of the grating in terms of the diagonal matrix basis vectors become,

$$E(M) = [H']^M E(0) = \begin{bmatrix} e^{j\psi'_0} & 0 & 0 \\ 0 & e^{j\psi'_1} & 0 \\ 0 & 0 & e^{j\psi'_2} \end{bmatrix}^M E(0) \tag{28}$$

$$= \begin{bmatrix} e^{jM\psi'_0} & 0 & 0 \\ 0 & e^{jM\psi'_1} & 0 \\ 0 & 0 & e^{jM\psi'_2} \end{bmatrix} E(0)$$

$$= \begin{bmatrix} e^{j\psi_0} & 0 & 0 \\ 0 & e^{j\psi_0} & 0 \\ 0 & 0 & e^{j\psi_2} \end{bmatrix} E(0) \; . \tag{29}$$

The associated eigenvectors E_i satisfying the matrix equation,

$$(H - \sigma_i I)E_i = 0 \tag{30}$$

can be found in terms of the original basis vectors to be,

$$\begin{bmatrix} E_0 \\ E_1 \\ E_2 \end{bmatrix} = \begin{bmatrix} 1 & \mu_0 & \nu_0 \\ 1 & \mu_1 & \nu_1 \\ 1 & \mu_2 & \nu_2 \end{bmatrix} \begin{bmatrix} A_0 \\ A_1 \\ A_2 \end{bmatrix} \tag{31}$$

where,

$$\mu_i = \frac{-(\gamma_3\psi_i - \gamma_1\gamma_2)}{\gamma_1\gamma_3 - \gamma_2(\psi_i + 2\xi_1)} \left(\frac{C_1}{C_0}\right)^{1/2} \tag{32}$$

$$\nu_i = \frac{-C_2}{C_0} + \frac{(\psi_i + 2\xi_i)(\gamma_3\psi_i - \gamma_1\gamma_2)}{\gamma_1[\gamma_1\gamma_3 - \gamma_2(\psi_i + 2\xi_1)} \left(\frac{C_1}{C_0}\right) \tag{33}$$

with,

$$\gamma_1 = \frac{M\delta_1}{\sqrt{C_0C_1}} = \frac{\pi n_1 D}{\lambda\sqrt{C_0C_1}}$$

$$\gamma_2 = \frac{M\delta_2}{\sqrt{C_0C_2}} = \frac{\pi n_2 D}{\lambda\sqrt{C_0C_1}} \tag{34}$$

$$\gamma_3 = \frac{M\delta_1}{\sqrt{C_1C_2}} = \frac{\pi n_1 D}{\lambda\sqrt{C_1C_2}}$$

$$\xi_1 = \frac{M\Phi_1}{2} = [C_1 - C_0 - \lambda f_z \tan\phi] \frac{2\pi D n_g}{\lambda} .$$

ψ_i in Eq.32 and 33 are obtained from Eq.21-23 using Eq.24-27 by substituting p,q,r for p',q',r' where,

$$p = Mp' = 2\xi_1$$
$$q = M^2q' = -\gamma_1^2 - \gamma_2^2 - \gamma_3^2 \qquad (35)$$
$$r = M^3r' = 2\gamma_1\gamma_2\gamma_3 - 2\gamma_2^2\xi_1 \ .$$

Therefore in the diagonal representation of the coupling matrix H', the total amplitude after the M^{th} thin grating is,

$$E(M) = \begin{bmatrix} E_0 \\ E_1 \\ E_2 \end{bmatrix} = \begin{bmatrix} e^{j\psi_0} & 0 & 0 \\ 0 & e^{j\psi_1} & 0 \\ 0 & 0 & e^{j\psi_2} \end{bmatrix} \begin{bmatrix} 1 \\ 1 \\ 1 \end{bmatrix} \ , \qquad (36)$$

where the input column vector is the initial condition in terms of the eigenvector basis, obtained by the transformation relation of Eq.31 using the initial conditions of Eq.15. The final output amplitudes are obtained by transforming the output E(M) into the out-

put A(M) by using the inverse transformation from Eq.30. This procedure results in the amplitude of each diffracted order as being given by,

$$A_0 = \frac{1}{R_0}\left[\left(\frac{\nu_1 E_0 - \nu_0 E_1}{\mu_0\nu_1 - \mu_1\nu_0}\right) - \left(\frac{\nu_2 E_0 - \nu_0 E_2}{\mu_0\nu_2 - \mu_2\nu_0}\right)\right] \quad (37)$$

$$A_1 = \frac{1}{R_1}[(\nu_1-\nu_2)E_0+(\nu_2-\nu_0)E_1+(\nu_0-\nu_1)E_2] \quad (38)$$

$$A_2 = \frac{1}{R_2}[(\mu_1-\mu_2)E_0+(\mu_2-\mu_0)E_1+(\mu_0-\mu_1)E_2] \quad (39)$$

where,

$$R_0 = \left[\left(\frac{\nu_1-\nu_0}{\mu_0\nu_1-\mu_1\nu_0}\right) - \left(\frac{\nu_2-\nu_0}{\mu_0\nu_2-\mu_2\nu_0}\right)\right] \quad (40)$$

$$R_1 = \mu_0(\nu_1-\nu_2) + \mu_1(\nu_2-\nu_0) + \mu_2(\nu_0-\nu_1) \quad (41)$$

$$R_2 = \nu_0(\mu_1-\mu_2) + \nu_1(\mu_2-\mu_0) + \nu_2(\mu_0-\mu_1). \quad (42)$$

The amplitude of each diffracted order as given by Eqs.37-39 can now be inserted into Eq.2 to obtain the diffraction efficiency of each order ($\eta_d^{(1)}, \eta_d^{(2)}$).

The radiation loss coefficient (α_a) can then be determined for use in Eq.12 giving the coupling efficiency of our second Bragg order waveguide coupler.

Results and Discussion

Using the approach we have described we calculated the radiation loss coefficient for the following four representative holographic grating couplers:

a Slanted or unslanted holographic grating (with same periodicity in the z-direction) in the waveguide film utilizing the first order Bragg effect.

b Slanted or unslanted holographic grating on top of the waveguide film utilizing the first order Bragg effect which results from the interaction between the evanescent wave of the waveguide and the holographic grating.

c Slanted holographic grating in the waveguide film utilizing the pure double diffraction process ($n_2=0$), producing the second order Bragg effect.

d Nonlinear slanted holographic grating in the waveguide film utilizing second order Bragg effect ($n_2 \neq 0$).

In case b the interaction product of the evanscent wave of the waveguide and the holographic grating can be viewed as a plane wave incident with

mode angle θ_m upon the holographic grating of thickness Δx. Since the guided wave is incident upon a boundary of the waveguide, the reflected wave shifts along the propagation direction with respect to the position that one would expect from geometrical optics. Such a shift is known as the Goos-Hänchen shift (δz). Thus we should express the depth of the ray penetration (evanscent tail) $\Delta x = \delta z / 2\tan\theta_m$.

The diffraction efficiencies in cases a and b were calculated with the numerical analysis (Eq.14) and cases c and d were calculated with the closed form expressions (Eq.37-39). Comparing the radiated loss coefficient of the four generalized coupler configurations (Fig.4-9) it is apparent that the slanted grating of case a has the largest radiated loss coefficient (RLC) with the slanted coupler of case d having the next largest RLC. Approximately the same coefficient results for the unslanted grating of case a and the gratings of cases b and c .

In case a (Fig.4 and 5) the RLC is shown to be strongly dependent on grating slant angle, and the coefficient for the slanted grating is two orders of magnitude higher than that of the unslanted grating. We note that in this unslanted grating (Fig.5) that the

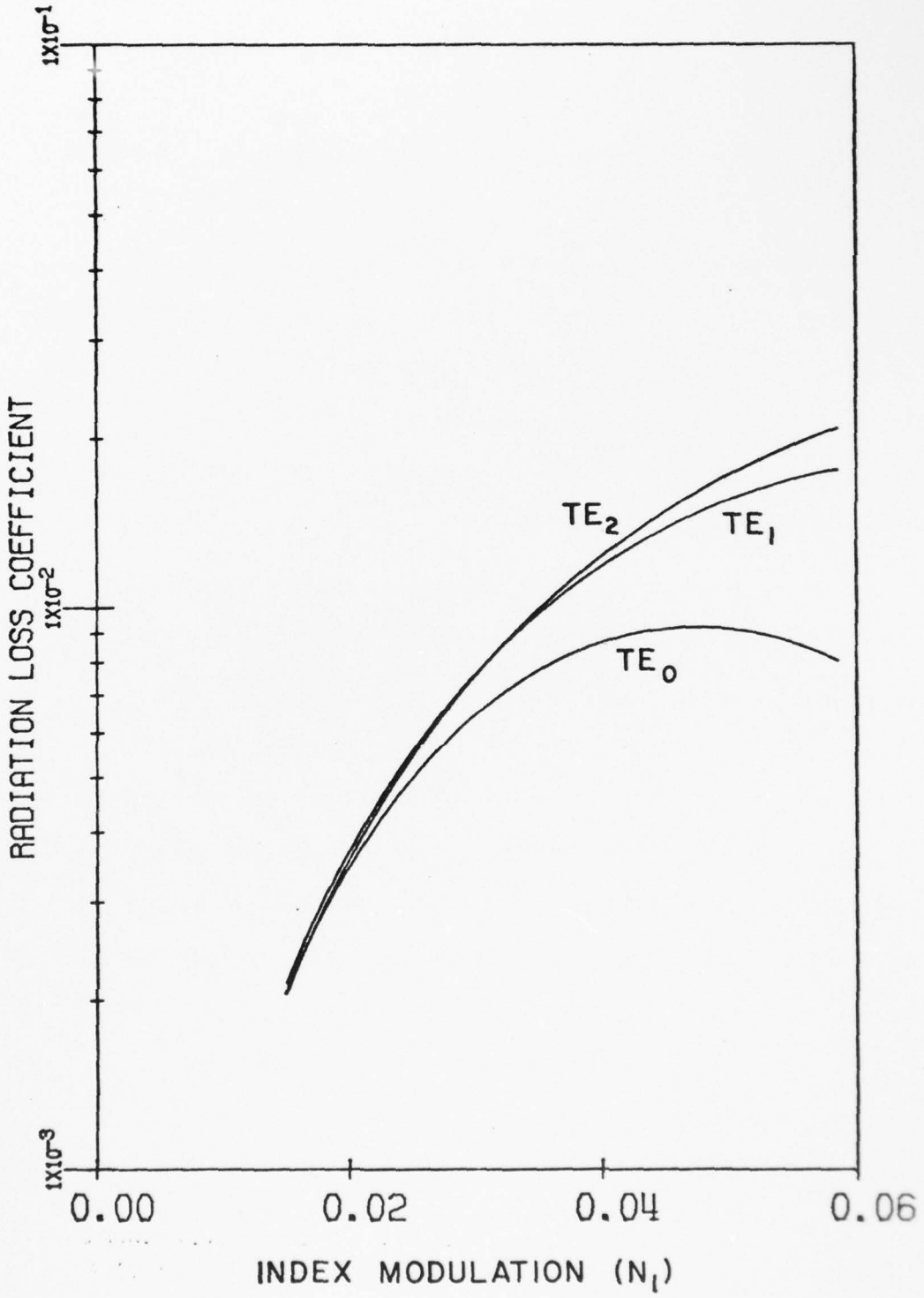

FIG. 4

Radiation loss coefficient (μm^{-1}) verses n_1 for the thickness $D = 2.0\mu m$ of a case a slanted grating.

AD-A041 213 MICHIGAN UNIV ANN ARBOR DEPT OF ELECTRICAL AND COMPU--ETC F/G 9/1
INVESTIGATION OF INTERFEROMETRIC WAVEGUIDES.(U)
MAY 77 E N LEITH, G C KUNG, S K CASE N00014-67-A-0181-0058

UNCLASSIFIED NL

2 OF 2
AD A041213

END

DATE FILMED
7-77

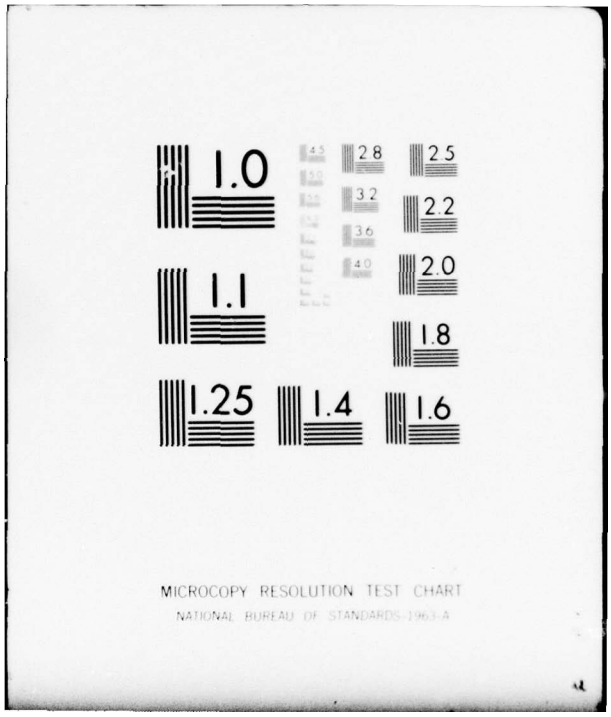
1.0
1.1
1.25
1.4
1.6
2.8
2.5
3.2
2.2
3.6
2.0
4.0
1.8
MICROCOPY RESOLUTION TEST CHART
NATIONAL BUREAU OF STANDARDS-1963-A

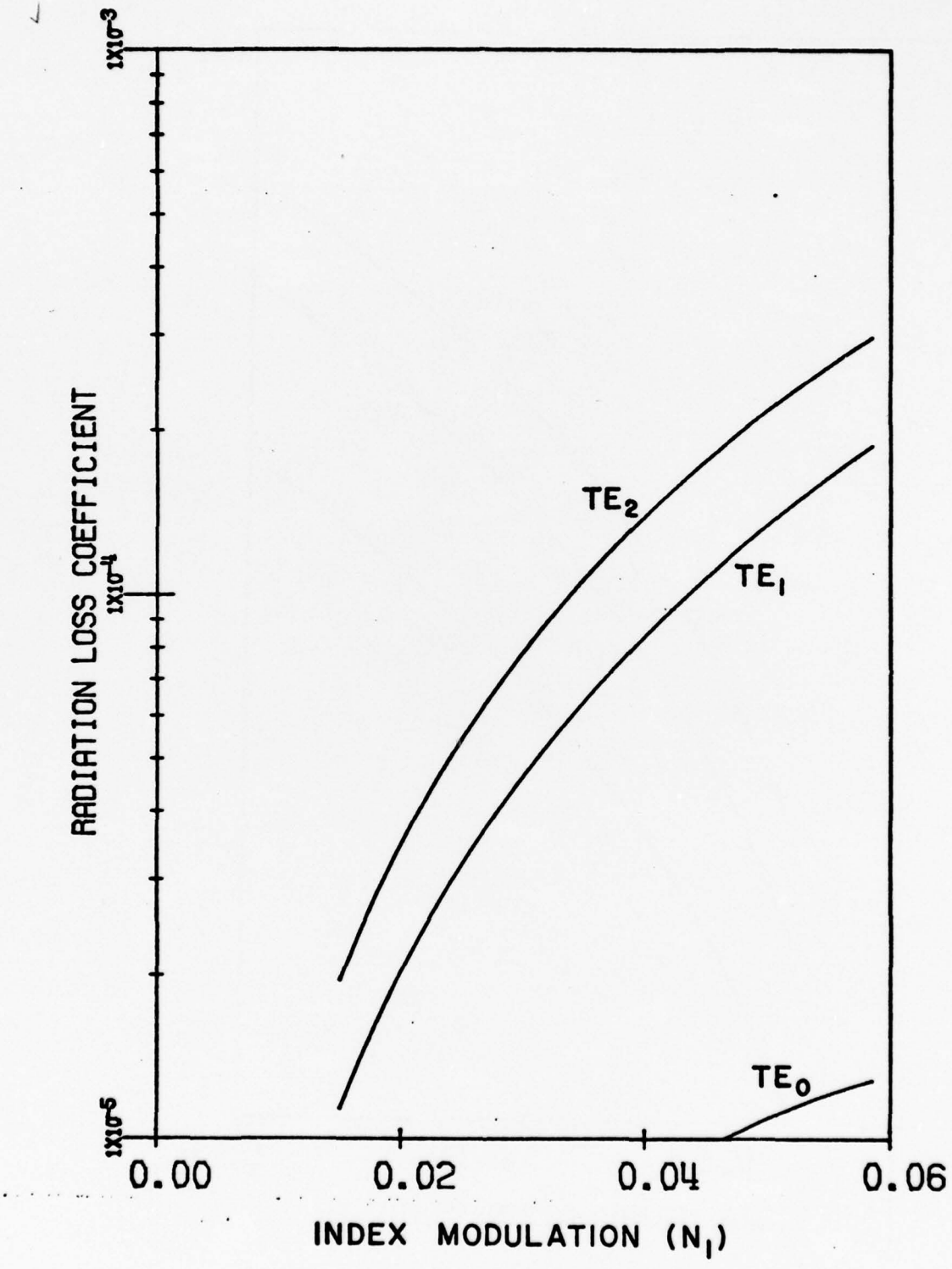

FIG. 5

Radiation loss coefficient (μm^{-1}) verses n_1 for the thickness D = 2.0μm of a case a<u>u</u>slanted grating.

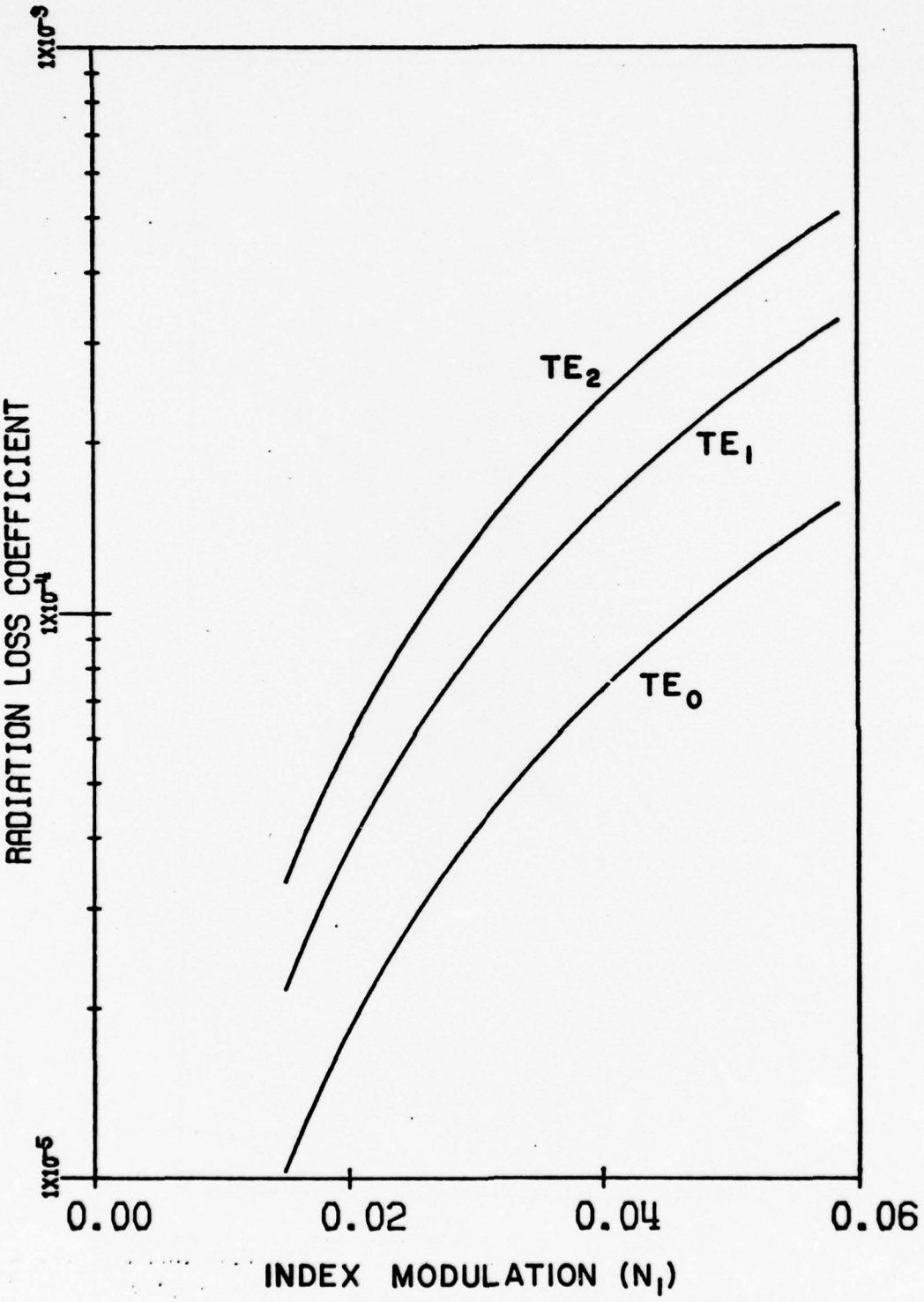

FIG. 6

Radiation loss coefficient (μm^{-1}) verses n_1 for the thickenss D = 2.0μm of a case b slanted grating.

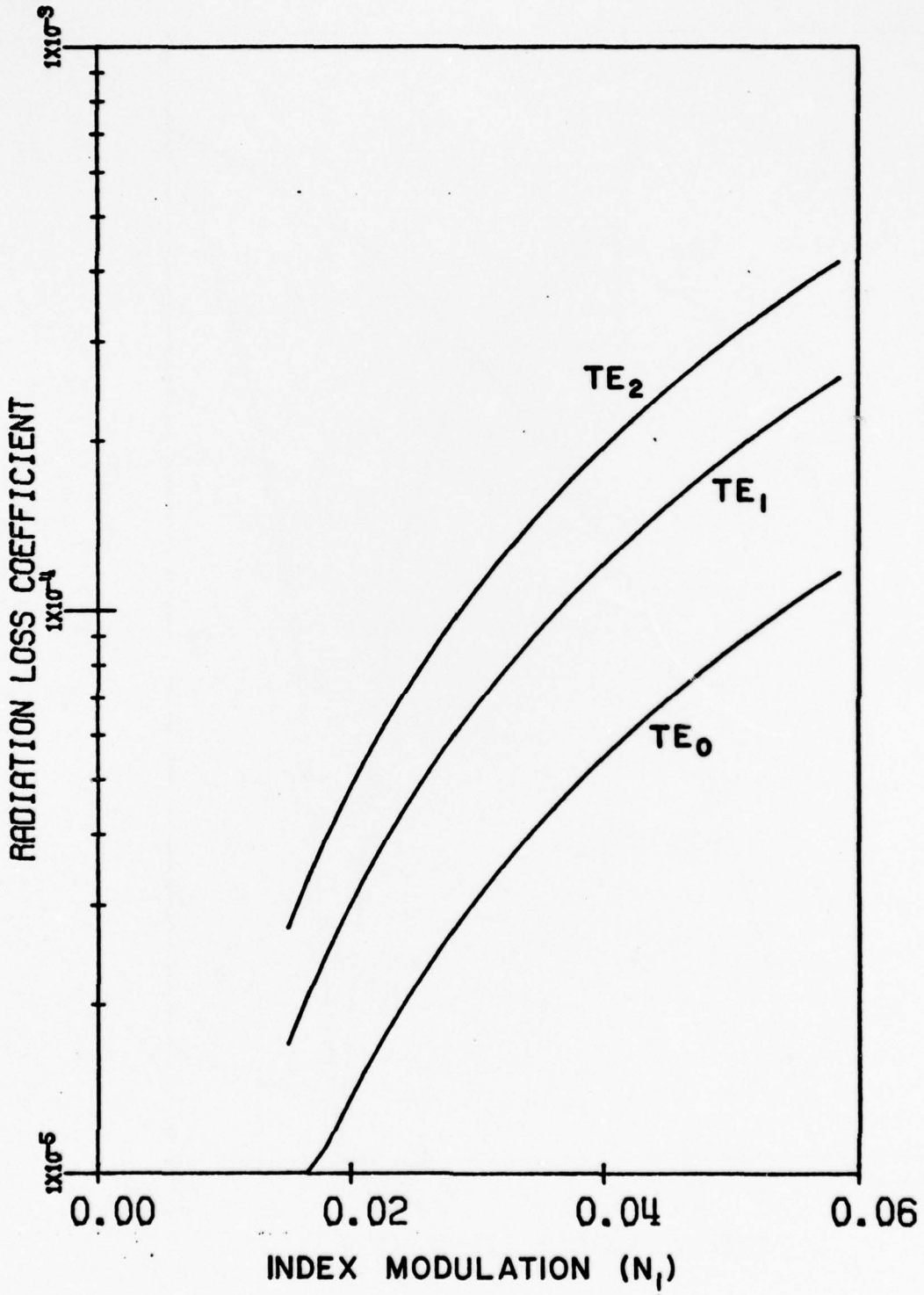

FIG. 7

Radiation loss coefficient (μm^{-1}) verses n_1 for the thickness D = 2.0μm for a case b unslanted grating.

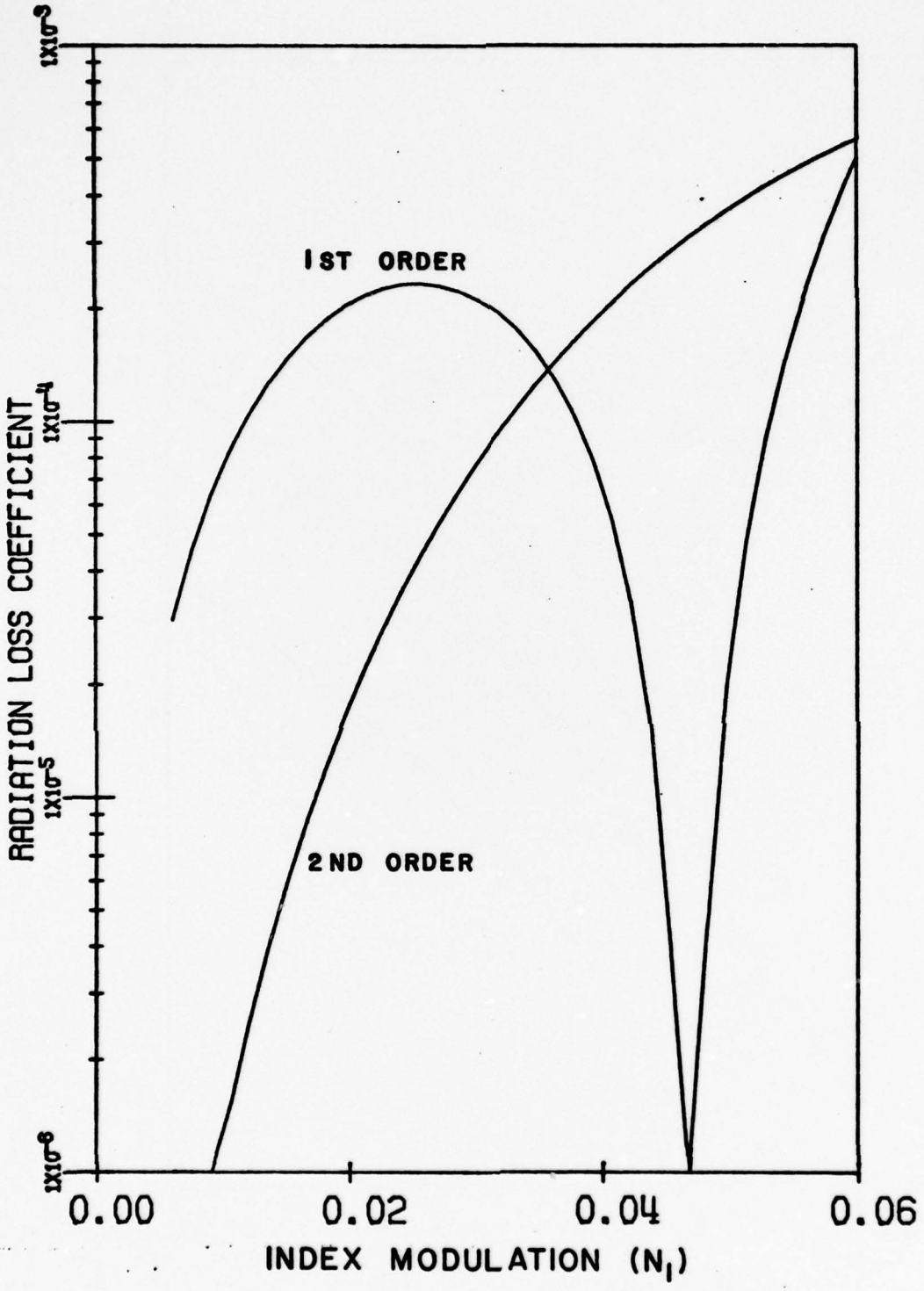

FIG. 8

TE_o radiation loss coefficient (μm^{-1}) verses n_1 with $n_2 = 0$ for the thickness D = 2.0μm of a case c slanted grating.

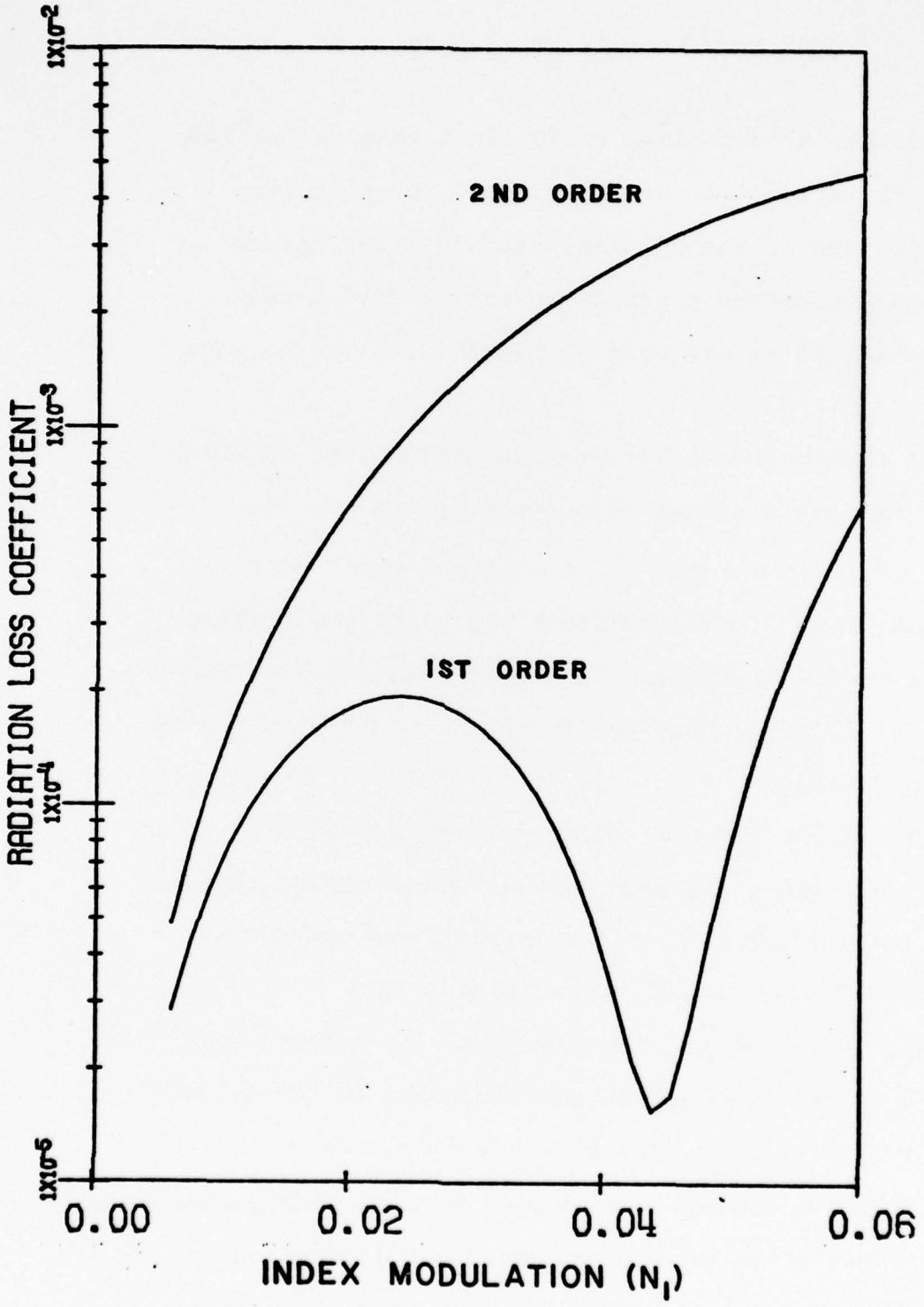

FIG. 9

TE_o radiation loss coefficient (μm^{-1}) verses n_1 with $n_2 = -n_1/3$ for the thickness D = 2.0μm of a case d slanted grating.

TE_1 mode has a lower loss coefficient than either the TE_0 or TE_2 modes. An examination of the electric field pattern of the TE_1 mode reveals a 180° phase shift and therefore a reduction in the diffracted field strength as the wave propagates across the waveguide.

In case b the radiation loss coefficient is observed to have a slight dependence on the grating slant angle (Fig.6 and 7), due to the small penetration depth of the evanscent tail into the grating. If the grating thickness is larger than the evanescent tail the radiated loss coefficient would be independent of the thickness.

In case c, (Fig.8) utilizing the double diffraction process the second order Bragg effect coupler can be constructed if the required index modulation can be achieved inside the waveguide film.
In case d (Fig.9) it is evident that an effective second order Bragg effect coupler could be constructed when a nonlinearity exists in the film ($n_2 \neq 0$).

Kogelnik and Sosnowski[4] used a thick dichromated gelatin holographic phase grating to achieve 70% coupling efficiency. Such high coupling efficiency can be attributed to the

first order Bragg diffraction process which redistributes the energy from various diffracted beams into the guided beam. Because it is difficult to construct a waveguide with a sufficiently high spatial frequency and fringe slant to provide for first order Bragg coupling we choose to employ the second order Bragg effect.

Alferness[5] has demonstrated that the second order diffraction process can result from both double diffraction through the fundamental grating frequency and single diffraction throught any existing second harmonic grating frequency. If the second harmonic component is negative relative to the fundamental, the two diffraction processes add, giving the highest level of second order diffraction. Utilizing this second order Bragg effect, we could produce in an optical waveguide a Bragg diffraction grating which couples light through its second order diffraction angle into a guided mode of the waveguide.

A practical and efficient grating waveguide coupler must: i) consist of a lossless and scatter-free material, ii) suppress unwanted diffraction orders and iii) possess a highly spatially modulated re-

fractive index to achieve strong waveguide coupling, with a thin or moderately thick (2-10μm) layer of phase material acting as a waveguide, our grating waveguide could meet all of the grating coupler constraints. This coupler would be fabricated with relative ease because of the low grating frequencies required for the second order effects, is completely integrated into the waveguide material and has the potential to achieve high coupling efficiencies from air to waveguide modes.

In summary, a simple geometrical optics concept is presented in which a grating waveguide coupler analysis is divided into independent planar waveguide and diffraction grating problems. The analysis of the grating is accomplished with a closed form solution of the diffraction efficiencies derived from the thin grating decomposition method. Using the conventional analysis of a planar waveguide the distributed radiation loss coefficient of any grating waveguide coupler can be determined from the separate grating analyses. The results of our analysis are completely compatible with those of the analyses utilizing the perturbation approach[1] and the electromagnetic boundary value approach[2]. However, our analysis has the advantages of being conceptually

simple, physically intuitive, with results obtained through minimal computation.

Acknowledgments

We are thankful to Professor E. N. Leith for his encouragement and valuable guidance in our work. We also are grateful for the support of the Office of Naval Research (Contract No. N00014-67-A-0181-0058) and the National Science Foundation (Grant No. ENG 73-04166 A01).

Bibliography

1. K. Ogawa and W.S.C. Chang, Appl. Optics 12, 2167 (1973).
2. S. T. Peng, T. Tamir, and H. L. Bertoni, "Theory of Periodic Dielectric Waveguides," IEEE Trans. Microwave Theory Tech. 23, 123 (1975).
3. R. Alferness, Appl. Phys. 7, 29 (1975).
4. H. Kogelnik and T. P. Sosnowski, Bell. Syst. Tech. J. 49, 1602 (1970).
5. R. Alferness, J. Opt. Soc. Am. 66, 533 (1976).

Third order Bragg diffraction in a periodic medium

W. Y. Wang
University of Michigan
Department of Electrical and Computer Engineering
Ann Arbor, Michigan 48109

Abstract

Algebraic experssions are derived for the diffraction efficiency of the first, second and third orders of a holographic grating recorded in a thick, pure phase material for readout at the third-order Bragg angle. The results demonstrate the importance of triple diffraction by the fundamental grating as well as diffraction by harmonic gratings. The method can be extended to analyze the first order Bragg diffraction at the first order Bragg angle with much greater accuracy. It is shown that strong cross coupling can be obtained from triply-incoherently constructed gratings.

In recent years, the thick grating has been studied extensively and a wide range of applications have been proposed, such as highly efficient diffraction gratings, narrow-band optical filters, thick-grating optical elements, grating deflectors and modulators, grating couplers in integrated optics, and distributed-feedback lasers and distributed Bragg-reflector lasers. The well-known applications of thick holograms include high capacity information storage, color holography, and white-light-reconstruction holography. In essence, the thick hologram can be regarded as recordings of a multiplicity of thick gratings.

The diffraction of a plane wave by a thick sinusoidal grating at or near Bragg incidence was studied by Kogelnik and by Burckhardt. Kogelnik obtained a closed-form expression for the diffraction efficiency at the first order Bragg angle by employing coupled-wave theory.[1] Burckhart[2] solved the exact electromagnetic boundary value problem and obtained numerical results by using the computer to find the eigenvalues of a matrix. His theory considered the energy exchange among higher orders so that no assumption of strong higher order Bragg suppression is required, which accoutns for it being used in gratings of arbitrary thickness. However, the drawback of such a method lies in its difficult implementation and lengthy computation. Recently, Alferness[3] introduced the thin grating decomposition method in a single grating case, which offers conceptual simplicity, general applicability and ease of implementation in the computer. His method has been used in analyzing second order diffraction and guiding effects in thick gratings. In this paper, his method is extended to analysis of third order

diffraction of thick, high index, sinusoidally modulated gratings which are assumed to be lossless. The surface reflections of such gratings can be neglected in the derivation, because, in practice, they can be eliminated by anti-reflection coatings. Even if there are surface and internal reflections, the transmitted diffraction efficiency can be corrected by a multiplicative transmittance factor.

Theory of Third Order Bragg Diffraction

Here we examine a grating constructed interferometrically in a thick emulsion, as shown in Fig. 1. The propagation vectors of each of the recording beams are in the xz plane and are symmetrical about the z-axis. Therefore, the fringe planes are perpendicular to the plate and there is no variation along the y axis. The thin grating decomposition method is valid for the incident readout wave polarized along the y axis. When we consider a pure phase material and the possibility of a film-generated nonlinearity, the refractive index inside the emulsion can be written as

$$n(x) = n_0 + n_1 \cos 2\pi fx + n_2 \cos 4\pi fx + n_3 \cos 6\pi fx \qquad (1)$$

where n_0 is the average bulk index and n_1, n_2 and n_3 are respectively the index modulations of the fundamental, second and third harmonics of spatial frequency f. In the thin grating decomposition method, we assume the thin vertical slab of the emulsion to be of thickness Δz. Since the fringe planes are along the z direction, the thin slabs are identical. The spatial phase shift caused by each thin slab

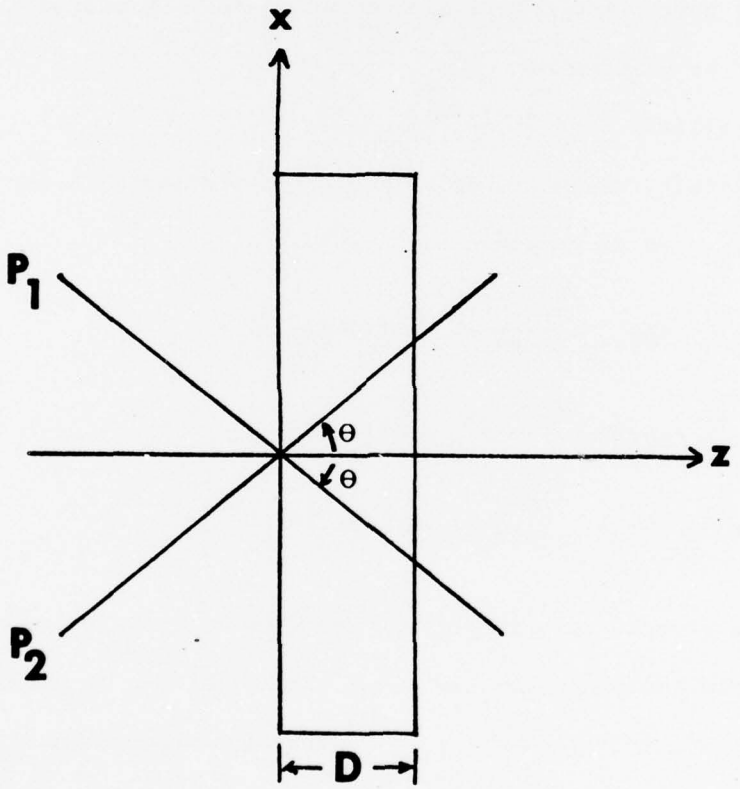

Figure 1. Construction geometry. P_1 and P_2 are plane waves with propagation vectors in the xz plane and symmetrically inclined about z axis. The fringe planes are out of the paper and perpendicular to the plane of the plate. The fundamental grating frequency is $f = 2(n_0/\lambda)\sin\theta$ and the emulsion thickness is D.

incident upon by a plane wave with direction cosine $\cos\theta_i$ (angle measured internally) is:

$$\phi(x) = 2\pi n(x)\ \Delta z/\lambda\cos\theta_i \tag{2}$$

where λ is the free-space wavelength of the readout wave. Since the emulsion is a pure-phase material, the amplitude transmittance of each slab can be written as

$$T_A = \exp(j\phi(x)) \tag{3}$$

The amplitude transmittance of each thin-grating slab for a wave incident at θ_i can be expanded as

$$\begin{aligned} T_A(x) = &\sum_{p=-\infty}^{+\infty} (j)^p J_p\left(\frac{2\pi n_1 \Delta z}{\lambda\cos\theta_i}\right) \exp(j2\pi pfx)\ x \\ &\sum_{q=-\infty}^{+\infty} (j)^q J_q\left(\frac{2\pi n_2 \Delta z}{\lambda\cos\theta_i}\right) \exp(j4\pi qfx)\ x \\ &\sum_{r=-\infty}^{+\infty} (j)^r J_r\left(\frac{2\pi n_3 \Delta z}{\lambda\cos\theta_i}\right) \exp(j6\pi rfx) \end{aligned} \tag{4}$$

where we have dropped an unimportant common multiplicative constant. The total field emerging from the first thin slab, due to an incident plane wave of spatial frequency $f_i = \frac{n_0}{\lambda}\sin\theta_i$ (the component of spatial frequency in the x direction), is the product of the input amplitude $A_{in} \exp(j2\pi f_i x)$ and the amplitude transmittance of the slab:

$$\begin{aligned} A_{out} = A_{in} &\sum_{p=-\infty}^{+\infty} (j)^p J_p\left(\frac{2\pi n_1 \Delta z}{\lambda\cos\theta_i}\right) x \sum_{q=-\infty}^{+\infty} (j)^q J_q\left(\frac{2\pi n_2 \Delta z}{\lambda\cos\theta_i}\right) x \\ &\sum_{r=-\infty}^{+\infty} (j)^r J_r\left(\frac{2\pi n_3 \Delta z}{\lambda\cos\theta_i}\right) \exp\left(j\frac{2\pi n_0}{\lambda}\Delta z\left[1 - \left(\frac{\lambda f_i}{n_0}\right)^2\right]^{1/2}\right) x \\ &\exp[j2\pi(f_i + pf + 2qf + 3rf)x] \end{aligned} \tag{5}$$

where we include the propagator of the incident wave over the slab thickness Δz.

In his coupled-wave analysis for readout near the first order Bragg angle, Kogelnik assumed that, for gratings with a Q factor greater than 10, [$Q = \frac{2\pi\lambda}{n_0} f^2 D$] only the zeroth (undiffracted) and one first diffracted order are important. Bergstein and Kermish[5] have shown that in a pure sinusoidal grating with $4n_0 n_1/(\lambda f)^2 << 1$, only the zeroth and mth orders are significant for the readout at the mth order Bragg angle; their condition implies that, in addition to a large Q factor, a correspondingly low index modulation is required if only two orders are to be significant. For typical gratings or special grating profiles (such as square, triangular, sawtooth profile) with a moderate Q factor, the necessary condition for only two orders does not apply to the readout at the higher order Bragg angle. Therefore, when we analyze diffraction at the third Bragg angle, we have to include four significant orders. For an incident wave at $z = 0$ of spatial frequency f_0, the spatial frequency of the first, second, and third orders are $f_0 - f$, $f_0 - 2f$, and $f_0 - 3f$. We write the amplitude of each of these plane waves as one component of a column vector:

$$A = \begin{bmatrix} A_0 \\ A_1 \\ A_2 \\ A_3 \end{bmatrix} \tag{6}$$

where the subscripts correspond to the order numbers. The result of

each thin-grating slab upon the propagating waves can be written as a coupling matrix which describes the multiplicative amplitude and phase change effected by the thin grating in diffracting the jth order into the ith. The i, j matrix elements can be found from Eq. 5, by choosing p, q, and r, such that,

$$f_i = f_j + pf + 2qf + 3rf \tag{7}$$

By inspection of Eq. 5, the coupling matrix of each thin-grating slab can be written as

$$H = \begin{bmatrix} e^{j\alpha_0} & j\frac{\delta_1}{c_1}e^{j\alpha_1} & j\frac{\delta_2}{c_1}e^{j} & j\frac{\delta_3}{c_0}e^{j\alpha_0} \\ j\frac{\delta_1}{c_0}e^{j\alpha_0} & e^{j\alpha_1} & j\frac{\delta_1}{c_1}e^{j\alpha_1} & j\frac{\delta_2}{c_0}e^{j\alpha_0} \\ j\frac{\delta_2}{c_0}e^{j\alpha_0} & j\frac{\delta_1}{c_1}e^{j\alpha_1} & e^{j\alpha_1} & j\frac{\delta_1}{c_0}e^{j\alpha_0} \\ j\frac{\delta_3}{c_0}e^{j\alpha_0} & j\frac{\delta_2}{c_0}e^{j\alpha_1} & j\frac{\delta_1}{c_1}e^{j\alpha_1} & e^{j\alpha_0} \end{bmatrix} \tag{8}$$

where

$$\delta_i = \pi n_i \Delta z/\lambda \qquad i = 1, 2, 3 \tag{9}$$

$$\alpha_l = 2\pi n_0 \Delta z \cos\theta_l/\lambda \qquad l = 0, 1 \tag{10}$$

$$c_l = \cos\theta_l \tag{11}$$

Since we can make Δz arbitrarily small, we can use the first order approximations of the Bessel functions, $J_0(x) \simeq 1$; $J_1(x) \simeq x/2$; and $J_q(x) \simeq 0$, $q \geq 2$ for $x \ll 1$, and J_1^2 is also neglected. We have also used $[1 - (\frac{\lambda}{n_0} f_l)^2]^{1/2} = \cos\theta_l$ and $J_{-1}(x) = -J_1(x)$. Since the output from a thin-grating slab is incident upon the next slab, the total amplitude after the Nth slab is

$$A_N = H^N A \tag{12}$$

Because the readout wave is a single plane wave of unit amplitude and zero phase, we have

$$A = \begin{bmatrix} 1 \\ 0 \\ 0 \\ 0 \end{bmatrix} \tag{13}$$

Here we analytically carry out the matrix multiplication of Eq. 13 of the readout wave incident at the third Bragg angle in the limit $N \to \infty$, $\Delta z \to 0$, such that $N\Delta z = D$, the emulsion thickness. The matrix multiplication of Eq. 12 is greatly simplified by transforming it to a basis in which H is diagonalized. The advantage of a diagonal representation is that the Nth power of H becomes simply the Nth power of each of the diagonal elements. The diagonal elements of H in this representation are the eigenvalues of H and the basis vectors are the associated eigenvectors. The eigenvalues σ_i of H satsify the matrix equation

$$\det (H - \sigma_i I) = 0 \tag{14}$$

where I is the identity matrix. It is convenient to make the substitution

$$\psi_i = -j\ (1 - \sigma_i)$$

The solutions of Eq. 14 are:

$$\psi_{1,2} = \frac{-A \pm \sqrt{A^2 + 4B}}{2} \tag{15}$$

$$\psi_{3,4} = \frac{-C \pm \sqrt{C^2 + 4D}}{2} \tag{16}$$

where

$$A = \phi_1 - \frac{\delta_1}{c_1} - \frac{\delta_3}{c_0} \tag{17}$$

$$B = \frac{\delta_1^2 - \delta_1\delta_3 + \delta_2^2 + c_1\delta_3\phi_1 - 2\delta_1\delta_2}{c_0c_1} \tag{18}$$

$$C = \phi_1 + \frac{\delta_1}{c_1} + \frac{\delta_3}{c_0} \tag{19}$$

$$D = \frac{\delta_1^2 - \delta_1\delta_3 + \delta_2^2 - c_1\delta_3\phi_1 + 2\delta_1\delta_2}{c_0c_1} \tag{20}$$

$$\phi_1 = \frac{2\pi n_0}{\lambda}(c_1 - c_0) \tag{21}$$

Since we can make Δz arbitrarily small, $\psi_i \ll 1$, therefore, the eigenvalues are $\sigma_i = 1 - j\psi_i \simeq \exp(-j\psi_i)$. The associated eigenvector E_i satisfies the matrix equation:

$$(H - \sigma_i I)E_i = 0 \tag{23}$$

and can be found in terms of the original basis.

$$\begin{bmatrix} E_0 \\ E_1 \\ E_2 \\ E_3 \end{bmatrix} = \begin{bmatrix} 1 & -\frac{c_1(\psi_1 - \frac{\delta_3}{c_0})}{(\delta_1 - \delta_2)}e^{-j\phi_1} & \frac{c_1(\psi_1 - \frac{\delta_3}{c_0})}{(\delta_1 - \delta_2)}e^{-j\phi_1} & -1 \\ 1 & -\frac{c_1(\psi_2 - \frac{\delta_3}{c_0})}{(\delta_1 - \delta_2)}e^{-j\phi_1} & \frac{c_1(\psi_2 - \frac{\delta_3}{c_0})}{(\delta_1 - \delta_2)}e^{-j\phi_1} & -1 \\ 1 & -\frac{c_1(\psi_3 + \frac{\delta_3}{c_0})}{(\delta_1 - \delta_2)}e^{-j\phi_1} & \frac{c_1(\psi_3 + \frac{\delta_3}{c_0})}{(\delta_1 - \delta_2)}e^{-j\phi_1} & 1 \\ 1 & -\frac{c_1(\psi_4 + \frac{\delta_3}{c_0})}{(\delta_1 - \delta_2)}e^{-j\phi_1} & \frac{c_1(\psi_4 + \frac{\delta_3}{c_0})}{(\delta_1 - \delta_2)}e^{-j\phi_1} & 1 \end{bmatrix} \begin{bmatrix} A_0 \\ A_1 \\ A_2 \\ A_3 \end{bmatrix} \tag{24}$$

From the initial condition of A (Eq. 13) and from the transformation of Eq. 24, the initial condition in the E_i basis is:

$$E = \begin{bmatrix} 1 \\ 1 \\ 1 \\ 1 \end{bmatrix} \tag{25}$$

Therefore, in the diagonal representation, the total amplitude after the Nth grating is

$$E(N) = \begin{bmatrix} e^{-j\psi_1} & & & \\ & e^{-j\psi_2} & & \\ & & e^{-j\psi_3} & \\ & & & e^{-j\psi_4} \end{bmatrix}^N \begin{bmatrix} 1 \\ 1 \\ 1 \\ 1 \end{bmatrix} = \begin{bmatrix} e^{-jN\psi_1} \\ e^{-jN\psi_2} \\ e^{-jN\psi_3} \\ e^{-jN\psi_4} \end{bmatrix} \tag{26}$$

To find the amplitude of the first, second and third order after the Nth thin grating, we transform back to the original basis via the inverse of the transformation in Eq. 24, thereby obtaining:

$$A_0(N) = \frac{1}{2}\left[\left(\frac{\psi_3 E_3(N) - \psi_4 E_2(N)}{(\psi_3 - \psi_4)}\right) + \left(\frac{\psi_2 E_0(N) - \psi_1 E_1(N)}{(\psi_2 - \psi_1)}\right)\right] \tag{27}$$

$$A_1(N) = \frac{\delta_1}{c_1} e^{j\phi} \frac{1}{2}\left[\frac{-(\psi_1 - \psi_2)(E_2(N) - E_3(N)) - (\psi_3 - \psi_4)(E_0(N) - E_1(N))}{(\psi_3 - \psi_4)(\psi_1 - \psi_2)}\right] \tag{28}$$

$$A_2(N) = \frac{\delta_1}{c_1} e^{j\phi} \frac{1}{2}\left[\frac{-(\psi_1 - \psi_2)(E_2(N) - E_3(N)) + (\psi_3 - \psi_4)(E_0(N) - E_1(N))}{(\psi_3 - \psi_4)(\psi_1 - \psi_2)}\right] \tag{29}$$

$$A(N) = \frac{1}{2}\left[\left(\frac{\psi_3 E_3(N) - \psi_4 E_2(N)}{(\psi_3 - \psi_4)}\right) - \left(\frac{\psi_2 E_0(N) - \psi_1 E_1(N)}{(\psi_2 - \psi_1)}\right)\right] \tag{30}$$

with $N\Delta z = D$, we define

$$\gamma_1 = \frac{\delta_1 N}{(c_0 c_1)^{1/2}} = \frac{\pi n_1 D}{\lambda (c_0 c_1)^{1/2}} \tag{31}$$

$$\gamma_2 = \frac{\delta_2 N}{(c_0 c_1)^{1/2}} \tag{32}$$

$$\gamma_3 = \frac{\delta_3 N}{c_0} \tag{33}$$

$$\gamma_1' = \frac{\delta_1 N}{c_1} = \left(\frac{c_1}{c_0}\right)^{1/2} \gamma_1 \tag{34}$$

$$\xi = \phi_1 N = \frac{2\pi n_0}{\lambda} D(c_1 - c_0) \tag{35}$$

$$x_1 = \xi - \gamma_1' + \gamma_3 \tag{36}$$

$$x_2 = \xi + \gamma_1' - \gamma_3 \tag{37}$$

$$\rho_1 = (x_1^2 + 4\gamma_{11}^2)^{1/2}; \quad \rho_2 = (x_2^2 + 4\gamma_{22}^2)^{1/2} \tag{38}$$

$$\gamma_{11} = \gamma_1 - \gamma_2; \; \gamma_{22} = \gamma_1 + \gamma_2 \tag{39}$$

$$x_1' = (x_1 - 2\gamma_3); \; x_2' = (x_2 + 2\gamma_3) \tag{40}$$

Physically, γ_1, γ_2, γ_3, are respectively, the total grating strength of the fundamental, second harmonic and third harmonic, and ξ is the total phase dispersion (difference in propagation factors) between the second and the third order. The diffraction efficiency $DE_i = \frac{c_i}{c}|A_i|^2$ of each order after grating thickness D can be found from Eq. 27 through Eq. 30 by using Eqs. 15, 16, and:

$$D_{1,2} = \gamma_1^2\left[\left(\frac{\sin\frac{\rho_1}{2}\cos\frac{x_1'}{2}}{\rho_1} \pm \frac{\sin\frac{\rho_2}{2}\cos\frac{x_2'}{2}}{\rho_2}\right) + \left(\frac{\sin\frac{\rho_1}{2}\cos\frac{x_1'}{2}}{\rho_1} \pm \frac{\sin\frac{\rho_2}{2}\cos\frac{x_2'}{2}}{\rho_2}\right)\right] \tag{41}$$

$$D_{3,0} = \frac{1}{4}\left[\left(\frac{x_1}{\rho_1}\sin\frac{\rho_1}{2}\cos\frac{x_1'}{2} - \frac{x_2}{\rho_2}\sin\frac{\rho_2}{2}\cos\frac{x_2'}{2}\right) + \left(\cos\frac{\rho_2}{2}\sin\frac{x_2'}{2} \quad \cos\frac{\rho_1}{2}\sin\frac{x_1'}{2}\right)\right]$$
$$+ \left[\left(\frac{x_1}{\rho_1}\sin\frac{\rho_1}{2}\sin\frac{x_1'}{2} - \frac{x_2}{\rho_2}\sin\frac{\rho_2}{2}\sin\frac{x_2'}{2}\right) + \left(\cos\frac{\rho_1}{2}\cos\frac{x_1'}{2} - \cos\frac{x_2'}{2}\cos\frac{\rho_2}{2}\right)\right]^2 \tag{42}$$

We readily find that

$$DE_0 + DE_1 + DE_2 + DE_3 = 1 \tag{43}$$

Therefore, the energy flow in the z direction is conserved--as indeed it has to be, since for a pure-phase material the coupling matrix of Eq. 8 is unitary.

PURE SINUSOIDAL GRATING $n_2 = n_3 = 0$

In the case $n_2 = n_3 = 0$, all the energy in the third order Bragg

diffraction results from multiple diffraction through the fundamental grating. An interesting property of the third order Bragg diffraction of a pure sinusoidal grating is that its maximum diffraction effiency is periodic with ξ. By inspection of Eq. 42, we can express the conditions for 100% DE_3 as either

$$\begin{cases} \rho_1/2 = m\pi & m = 1, 2, 3 \ldots \\ \rho_2/2 = (m+1)\pi & \\ r_1'/2 = n & n = 1, 2, 3 \ldots \\ \xi = (2m+1)\pi/2n & m \geq n \end{cases} \tag{44}$$

or

$$\begin{cases} \rho_1/2 = m\pi & m = 1, 2, 3 \ldots \\ \rho_2/2 = (m+2)\pi & \\ r_1'/2 = (2n+1) & n = 1, 2, 3 \ldots \\ \xi = 4(m+1)\pi/(2n+1) & m \geq n \end{cases} \tag{45}$$

The condition imposed on ξ implies that for a fixed thickness and readout wavelength, the third order diffraction efficiency can be 100% only for discrete grating frequencies. In Fig. 2, we plot DE_3 vs γ_1 for several values of $(c_0/c_1)^{1/2}$, with $\xi = \frac{5\pi}{2}$. The maximum value of DE_3 can be made 100% for proper choice of γ_1 and the ratio $(c_0/c_1)^{1/2}$.

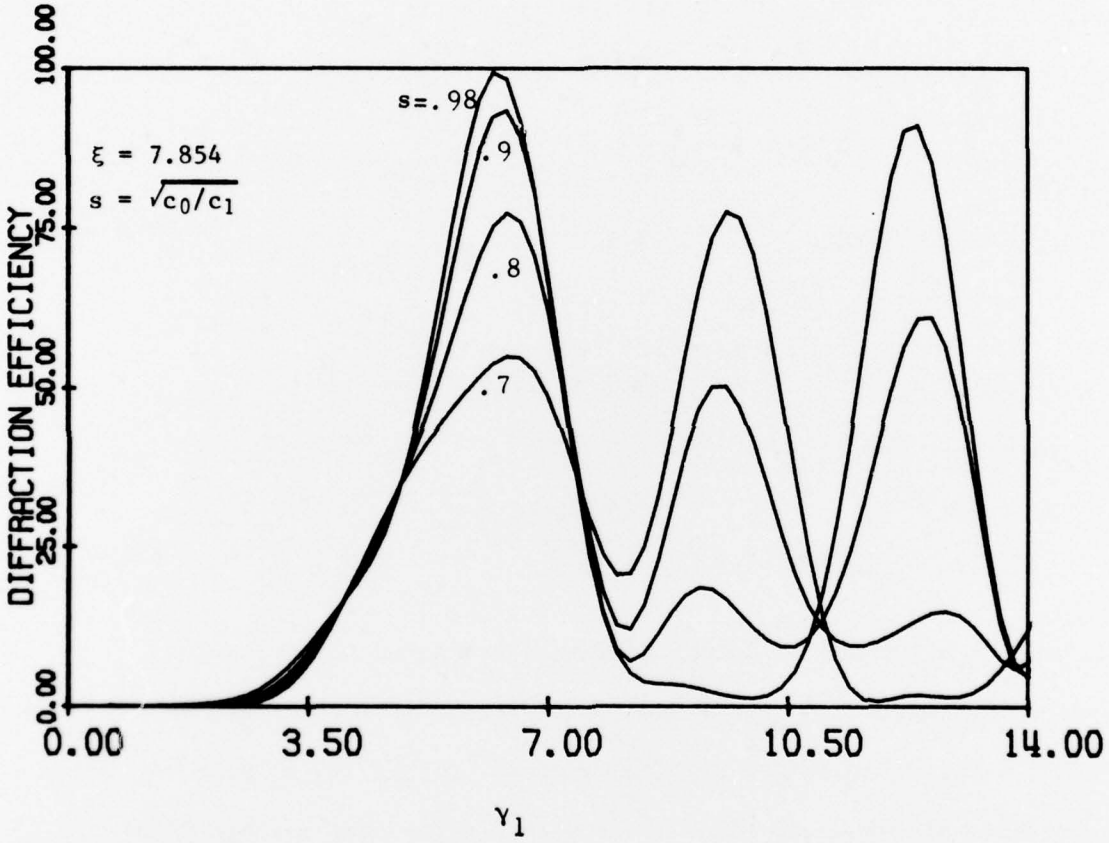

Figure 2. Diffraction efficiency of the third order at the third-order Bragg angle due to triple diffraction ($n_2 = n_3 = 0$) versus the fundamental grating strength $\gamma_1 = \pi n_1 D/\lambda(c_0/c_1)^{1/2}$ with $\xi = 5\pi/2$ for several values of $(c_0/c_1)^{1/2}$.

GENERAL CASE: $n_2, n_3 \neq 0$

In most cases of interferometrically constructed gratings of pure phase materials, the film response is nonlinear; therefore we must include all the terms n_1, n_2, and n_3. The necessary conditions for 100% diffraction efficiency in the third order are:

$$\begin{cases} x_1'' = 2n\pi = \gamma_1' + \gamma_3 \\ \rho_1/2 = m\pi;\ \rho_2/2 = (m+1)\pi \\ \rightarrow \xi = \dfrac{(2m+1)\pi^2 - 4\gamma_1\gamma_2}{[2n\pi - 2\gamma_3]} \qquad m \geq n \end{cases} \tag{46}$$

Because the condition on ξ include γ_1, γ_2 and γ_3, DE_3 can be as high as 100% for a fixed thickness and wavelength and for any arbitrary choice of spatial frequencies by proper choice of n_1, n_2 and n_3. In the case where n_1, n_2 are each zero, the result is identical to the coupled wave result at the first Bragg Angle.

RESULTS FOR γ_1/ξ, $\gamma_2/\xi \ll 1$

The general results of Eqs. 40 and 42 can be simplified under the assumption of index modulation small relative to $(\lambda f)^2$, or γ_1/ξ, $\gamma_2/\xi \ll 1$. The following small parameters are defined as:

$$t_1 = \gamma_1/\xi \simeq 2n_0n_1/(\lambda f)^2 \ll 1 \tag{47}$$

$$t_2 = \gamma_2/\xi \simeq 2n_0n_1/(\lambda f)^2 \ll 1 \tag{48}$$

$$t_3 = \gamma_3/\xi \simeq 2n_0n_1/(\lambda f)^2 \ll 1 \tag{49}$$

$$t_1' = \gamma_1'/\xi = \sqrt{\frac{c_0}{c_1}}\, 2n_0n_1/(\lambda f)^2 \ll 1 \tag{50}$$

We see that DE_3 from Eq. 42 is simplified to:

$$DE_3 \simeq \sin^2[\gamma_3 - \frac{2\gamma_1\gamma_2}{\xi} + (\frac{c_0}{c_1})^{1/2}\frac{\gamma_1^3}{\xi^2}] \tag{51}$$

The three terms in the bracket can be identified as three possible modes for achieving third order diffraction through the three Fourier components f, 2f, 3f; they are (1) triple diffraction through first harmonics, (2) combinations of diffraction through second harmonics and first harmonics, (3) diffraction through third harmonics. Eq. 51 shows the opposing effects of mode 2 against mode 1 and 3, if n_2 and n_3 are positive relative to n_1. Such results agree with those of D. L. Jaggard[6] in his extended coupled wave analysis of higher order Bragg coupling in a periodic medium; also with those of Su and Gaylord[7] on higher order diffraction by utilizing the Chu and Tamir[8] rigorous modal approach.

EXTENSION OF ANALYTIC RESULTS FOR THE FIRST-ORDER READOUT:

We can increase the accuracy of the analytical results for readout at the minus first Bragg Angle by including also the positive first and minus second orders. This is especially true for gratings of moderate Q factor or very high index modulation. At the first Bragg angle, the dephasing term associated with the conjugate first order is the same as that for the second order, and in general, these orders can be of comparable importance. The coupling matrix for the first order readout is the same as that for the third order readout, except for the modification of the initial condition:

$$A = \begin{bmatrix} 0 \\ 1 \\ 0 \\ 0 \end{bmatrix} \tag{52}$$

The minus first diffraction order of the results from the general four-waves analysis can be calculated. From the results we can see that as the Q factor increases, the first order diffraction efficiency gets closer to 100% when $\gamma_1 = \pi/2$, which means that as the Q factor increases, the higher orders can be neglected. The closed form solutions for diffraction efficiency of first positive, zeroth, minus first, and minus second orders can be obtained by changing the initial condition to those of Eq. 52.

The diffraction efficiency of such diffraction orders are:

$$DE_{+1,-2} = \left[\frac{\gamma_2}{\rho_2}\sin\frac{\rho_2}{2}\cos\frac{x_2}{2}' \pm \frac{\gamma_1}{\rho_1}\sin\frac{\rho_1}{2}\cos\frac{x_1}{2}\right]^2$$

$$+ \left[\frac{\gamma_2}{\rho_2}\sin\frac{\rho_2}{2}\sin\frac{x_2}{2}' \pm \frac{\gamma_1}{\rho_1}\sin\frac{\rho_1}{2}\sin\frac{x}{2}'\right]^2 \qquad (53)$$

$$DE_{0,-1} = \frac{1}{4}\left[-\left(\pm\frac{x_1}{\rho_1}\sin\frac{\rho_1}{2}\sin\frac{x_1}{2}' + \frac{x_2}{\rho_2}\sin\frac{\rho_2}{2}\sin\frac{x_2}{2}'\right)\right.$$

$$+ \left(\cos\frac{\rho_1}{2}\cos\frac{x_1}{2}' \pm \cos\frac{\rho_2}{2}\cos\frac{x_2}{2}'\right)\Big]^2$$

$$+ \left[\left(\frac{x_1}{\rho_1}\sin\frac{\rho_1}{2}\cos\frac{x_1}{2}' \pm \frac{x_2}{\rho_2}\sin\frac{\rho_2}{2}\cos\frac{x_2}{2}'\right)\right.$$

$$+ \left(\cos\frac{\rho_1}{2}\sin\frac{x_1}{2}' - \cos\frac{\rho_2}{2}\sin\frac{x_2}{2}'\right)\Big]^2 \qquad (54)$$

With small ξ, a grating can be considered as a thin grating: there is no Bragg effect on the diffraction efficiency and the maximum value of $DE_1 \simeq 33\%$ agrees very well with the first maximum of J_1^2.

With an intermediate ξ, the diffraction efficiency is strongly dependent on ξ and a rapid monotonic increase in DE_{-1} as the other orders are suppressed. In cases of very large ξ, DE_{-1} does not depend entirely on higher harmonic grating frequencies. The dependence of diffraction efficiency on higher harmonic grating frequencies is quite significant as we can see from Figure 3, where $\gamma_1 = 1.0$, $\gamma_2 = -0.5$, and various γ_3. For large ξ, the dependence of the diffraction efficiency on third harmonic grating frequencies is reduced drastically--almost independent. From Figure 4, where $\gamma_1 = 1.0$, $\gamma_3 = 0$, and various γ_2, we see that even for large ξ, at least a 10% increase in diffraction efficiency can be expected when the value of γ_2 increases

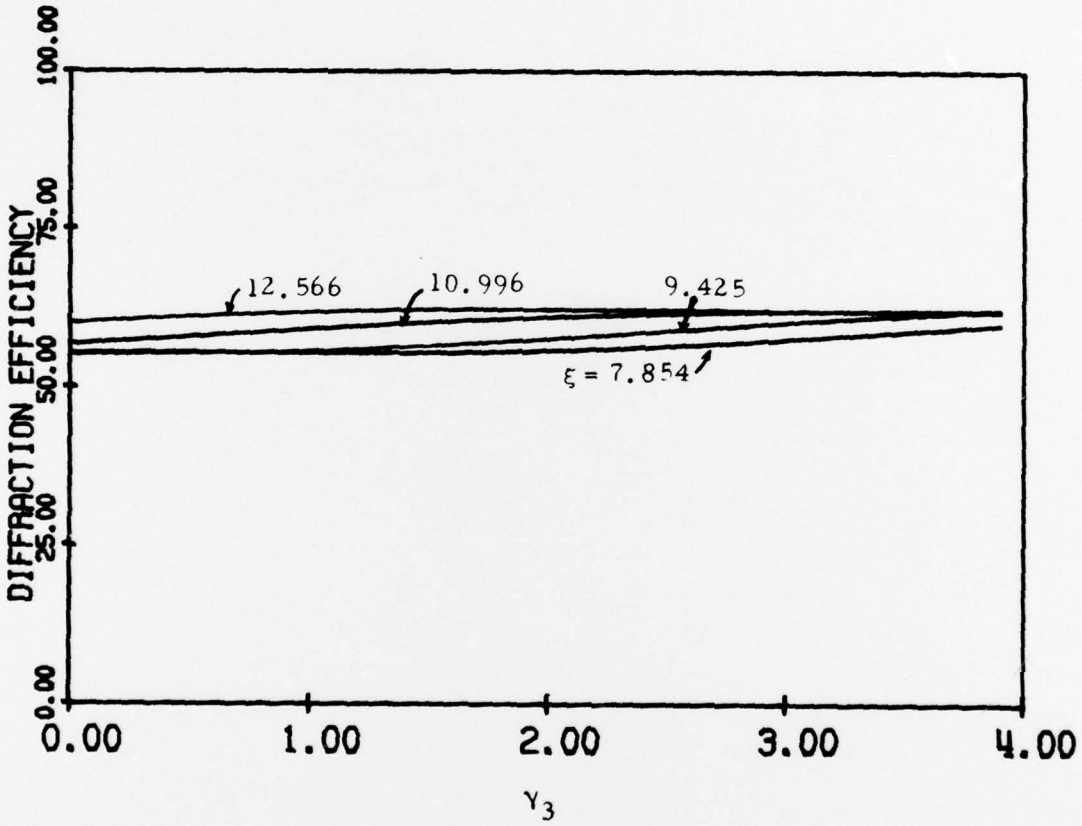

Figure 3. First order diffraction efficiency at the first Bragg angle versus γ_3 with a fixed $\gamma_1 = 1.$ and $\gamma_2 = -.5$ for several values of ξ.

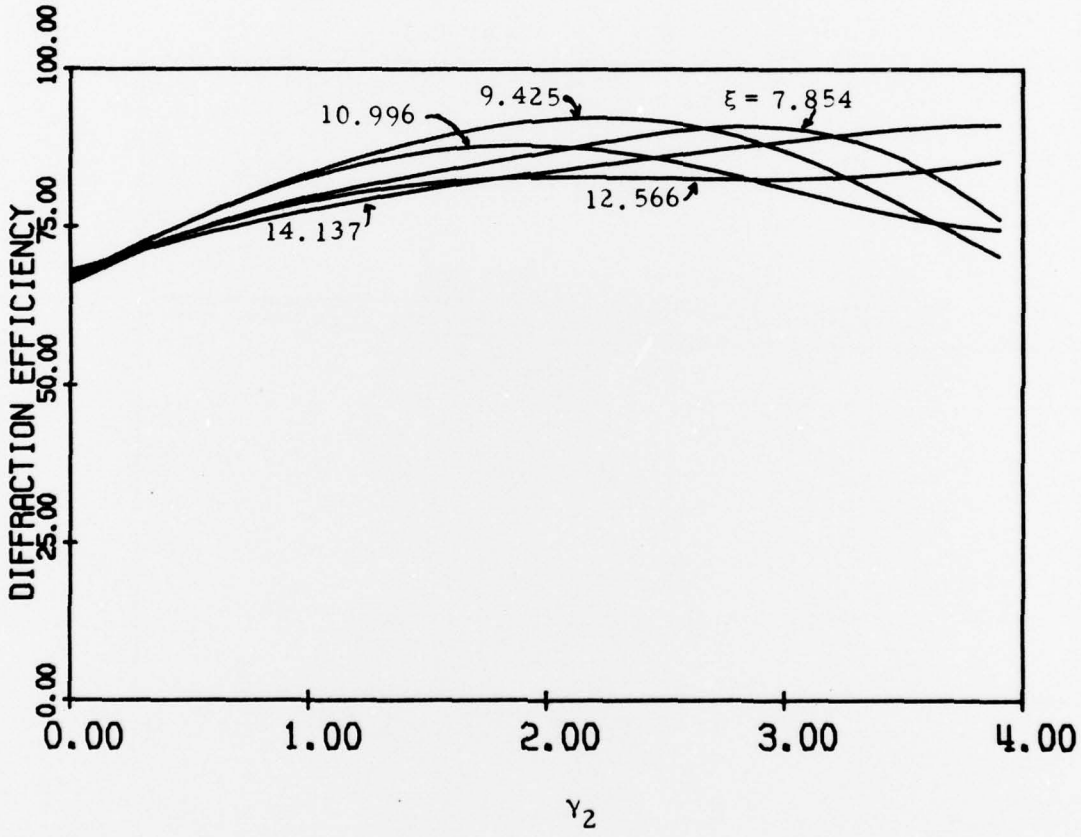

Figure 4. First order diffraction efficinecy at the first Bragg angle versus γ_2 with a fixed $\gamma_1 = 1.$ and $\gamma_3 = 0.$ for several values of ξ.

from 0 to 0.5. Therefore, it is evident that even for the first order diffraction it is necessary to include the higher order grating components in order to obtain accurate results.

ANALOGY WITH MULTIPLE GRATING $\xi = 0$

Figure 5 is a construction geometry for triply incoherently superimposed gratings. We first interfere plane waves P_1 and P_2, then P_2 and P_3, and finally P_3 and P_4. The incident wave at the Bragg angle of the first grating is strongly diffracted by it. This diffracted wave is at the Bragg angle of the second grating and is strongly diffracted again. And it finally is strongly diffracted by the third grating. The cross-coupled order via such triple diffractions is the same as the third order diffraction in the single grating of $n_2 = n_3 = 0$. It can be proved that the coupling matrix for the multiple grating described above is identical to Eq. 8, except that $\xi = 0$. The result for DE_3 will be the triple diffraction for a triple incoherently superimposed grating as illustrated in Fig. 5. The triple diffraction results are shown in Fig. 6 for different ratio of $(\frac{c_0}{c_1})^{1/2}$.

Acknowledgments

We are thankful to Professor Leith for his encouragement and valuable guidance in our work. We also are grateful for the support of the Office of Naval Research (Contract No. N 00014-67-A-0181-0058) and the National Science Foundation (Grant No. ENG73-04166 A01).

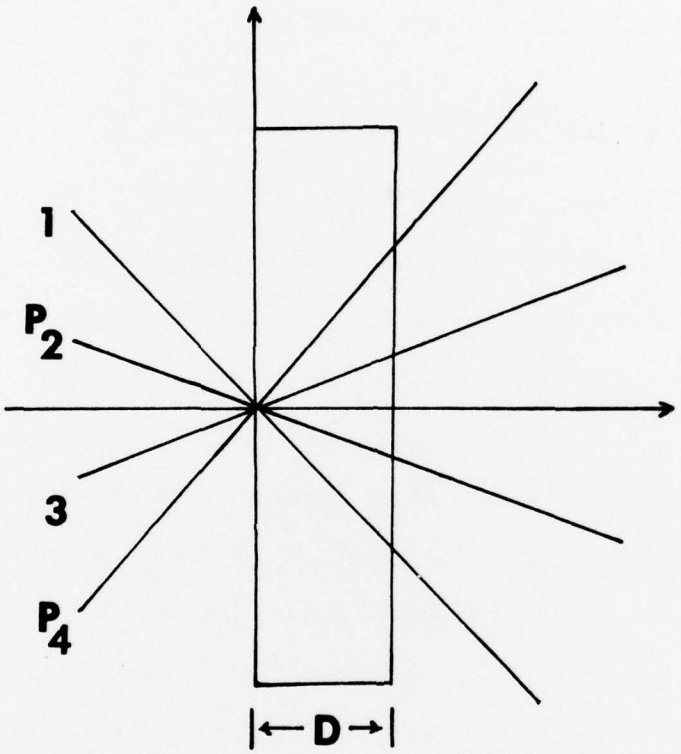

Figure 5. Construction geometry for multiple gratings. For the incoherent superposition, plane waves P_1 and P_2 are interfered first, then P_2 and P_3, and finally P_3 and P_4.

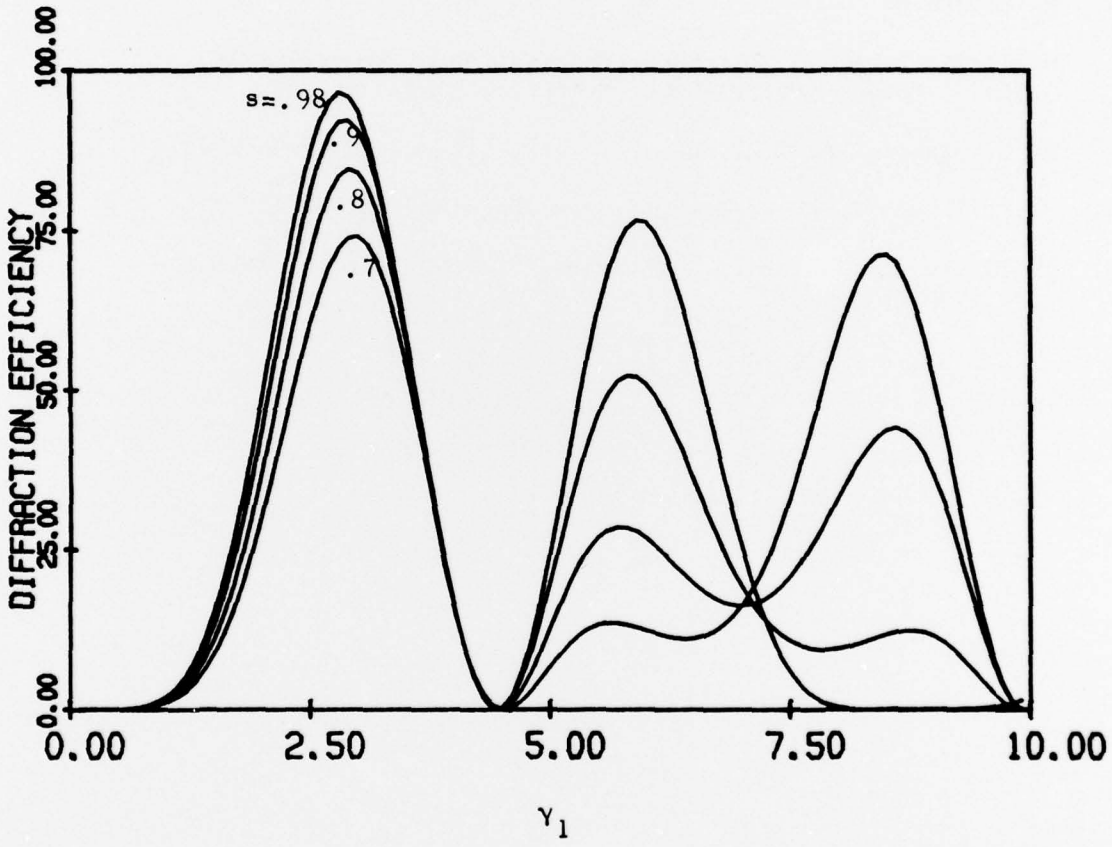

Figure 6. Diffraction efficiency of the cross-coupled order (P_4) versus the grating strength $\gamma_1 = \pi n_1 D/\lambda(c_0/c_1)^{1/2}$ for readout at the noncommon Bragg angle (P_1).

REFERENCES

1. H. Kogelnik, Bell Syst. Tech. J. 48, 2909 (1969).

2. C. B. Burckhardt, J. Opt. Soc. Am. 56, 1502 (1966).

3. R. Alferness, Appl. Phys. 7, 29 (1975).

4. R. Alferness, J. Opt. Soc. Am. 66, 353 (1976).

5. M. Bergstein and D. Kermisch, Proceedings of Symposium on Modern Optics (Polytechnic, Brooklyn, 1967), p. 655.

6. D. L. Jaggard and C. Elachi, J. Opt. Soc. Am. 66, 674 (1976).

7. S. F. Su and T. K. Gaylord, J. Opt. Soc. Am. 65, 59 (1975).

8. R. S. Chu and T. Tamir, IEEE Trans. Microwave Theory Tech. 13, 297 (1965).